ABSTRACT

Title of Thesis: CHARACTERIZATION OF PHYSICAL PROPERTIES OF MULTI-SCALE POLYMER COMPOSITES UNDER VARIOUS PROCESSING CONDITIONS

Anne Catherine Lederer, Master of Science, 2012

Thesis directed by: Associate Professor David I. Bigio
Department of Mechanical Engineering

There is a great interest in using micro and nano scale ingredients as fillers to create composites with enhanced physical properties. This thesis research explores the improvements these fillers offer with focus on combining both micro and nano ingredients to make multi-scale polymer composites. This investigation reveals the interplay of ingredient mixing, microstructural evolution, and processing conditions and characterizes the improvements of thermal and mechanical properties. This data is used to develop fundamental processing-structure-property relationships of these multi-scale composites across different concentrations of microscale and nanoscale ingredients and processing conditions in order to optimize their development.

CHARACTERIZATION OF PHYSICAL PROPERTIES OF MULTI-SCALE POLYMER COMPOSITES UNDER VARIOUS PROCESSING CONDITIONS

by

Anne Catherine Lederer

Thesis submitted to the Faculty of the Graduate School of the
University of Maryland, College Park in partial fulfillment
of the requirements for the degree of
Master of Science
2012

Advisory Committee:
Associate Professor David I. Bigio, Chair/Advisor
Professor Hugh A. Bruck
Associate Professor Guangming Zhang

Acknowledgments

I would like to start by extending my sincerest appreciation and gratitude to my advisor, Dr. Bigio. His support throughout this entire thesis, with not only technical advice, but with life goals in general, has proved to be invaluable. As the thesis developed more, I could tell that I was not only learning how to extrude and test a polymer composite, but also how to complete, acknowledge, and recognize other accomplishments. I also would like to offer a sincere thank you to my committee members. Dr. Bruck, your help in setting up the experiments, interpreting the results, and constant support throughout the entire process was most appreciated. Dr. Zhang, your encouragement throughout not only my graduate, but also my undergraduate degree helped me get to where I am today.

This thesis would not have been possible without all of the help from the team of students in the Advanced Manufacturing Lab. Graeme, your help in laying the ground work for this work was invaluable, along with your support throughout the thesis. Betel, your countless hours of processing and testing the composite was crucial to finishing this work, especially as we neared the end. Harry, your knowledge and experience benefited the entire group, and your mastery of optical work gave us great insight into the material. Hoyoung, Beserat, and Rushil, your hours spent running the extruder, laser cutting, and testing with such enthusiasm were much appreciated. Bunty, Jesse, and Roba, your support in the lab and future interests in the project will no doubt help with the continuation of this work.

I would like to thank Dr. Joe Golba and the PolyOne Corporation for supplying

the materials used throughout the thesis. I would especially like to thank Joe for his technical advice provided throughout the experiments. I would also like to thank Viorel Amariei and Jim Lochary at Adell Plastics for the local support with the extruder and vacuum pump.

Lastly, I would like to thank my friends and family, especially Mom, Dad, Graham, Allison, and Jon. Without your endless love, support, and encouragement, I would have never made it through the difficult and frustrating times so often seen with research.

Thank you to everyone who has helped me complete this thesis.

Table of Contents

List of Tables

List of Figures

List of Abbreviations

α	Thermal Diffusivity
ϵ	Strain
ν	Poisson's Ratio
ρ	Density
ρ_f	Density of Filler
ρ_m	Density of Matrix
σ	Stress
$\tau_{\frac{1}{2}}$	Rise time to 50% of Maximum Temperature
ϕ_m	Maximum Packing Factor
A_c	Cross Sectional Area
ASTM	American Society for Testing and Materials
c	Circumference
C_p	Specific Heat
CMF	Carbon Microfiber
CNF	Carbon Nanofiber
CNT	Carbon Nanotube
E	Young's Modulus
E_c	Composite Young's Modulus
E_f	Filler Young's Modulus
E_m	Matrix Young's Modulus
F	Force
h	Height of Channel
HDPE	High-Density Polyethylene
Hg	Mercury
k	Thermal Conductivity
k_1	Thermal Conductivity of the matrix
k_2	Thermal Conductivity of the filler
k_e	Einstein Coefficients
l	length
l_0	Initial length
l_n	Width of narrow kneading block
l_w	Width of wide kneading block

m	Mass
MWCNT	Multi-Wall Carbon Nanotube
n	Number of Screws
N	Screw Speed
PBT	Poly(butylene terephthalate)
PEEK	Poly(ether ether ketone)
PET	Poly(ethylene terephthalate)
PMMA	Poly(methyl methacrylate)
q	Orientation factor
Q	Flow Rate
Q_e	Energy
Q/N	Specific Throughput
SWCNT	Single Wall Carbon Nanotube
t	Thickness
ΔT	Change in Temperature
TSE	Twin Screw Extruder
v_f	Volume Fraction of Filler
v_m	Volume Fraction of Matrix
vol%	Volume Percent
VGCF	Vapor Grown Carbon Fibers
wt%	Weight Percent
W	Weight Fraction

Chapter 1

Introduction

Polymer composites have started to replace conventional materials because of their superior properties and processing abilities. Several types of fillers can be used to reinforce a polymer matrix, such as clay, glass, and natural fiber reinforced composites [1, 2].

This study examines the potential for a multi-scale polymer composite comprised of both carbon micro fibers (CMFs) and multi-wall carbon nano tubes (MWCNTs) in a polymer matrix of poly(butylene terephthalate)(PBT). While both nanocomposites and micro fiber reinforced composites have been thoroughly studied, the multi-scale composite must be fully characterized to see if the mechanical benefits from micro fibers and the thermal benefits from nanotubes can be combined and interact to form a more economical and property rich multi-scale polymer composite.

Furthermore, the conditions under which polymer composites are processed can have a significant effect on property performance. Variations in extrusion parameters yield various degrees of mixing and thus alter the resulting polymer composite.

1.1 Polymer Composite Fillers

Polymer composite fillers are used to enhance the properties of a homogeneous polymer. The base polymer, known as the polymer matrix, is mixed with a different material, known as the filler. The fillers are designed so that with a specified weight percentage of the filler in the polymer matrix, certain properties can be observed and are enhanced over the polymer without the filler. For this study, two fillers were examined: CMFs and MWCNTs.

CMFs are ideal for various applications. The fiber is a few micrometers in diameter, thus lending to its name. The micro-scale fiber allows for the superior mechanical strength to be observed while set in a much less expensive polymer. The fiber is layered graphene of either cones, cups, or plates.

MWCNTs are similarly named for their nanometer sized diameters. Carbon nanotubes, or more specifically single-wall carbon nanotubes (SWCNTs), are formed from a single layer of graphene rolled into a perfect cylinder, as seen in Figure 1.1.

Concentric cylinders can be layered to form multi-walled carbon nanotubes (MWCNTs). MWCNTs carry desirable properties such as high electrical and thermal conductivity, high mechanical strength, high adsorption, and low reactivity [3, 4, 5].

MWCNTs, however, are much more expensive than CMFs. Therefore, if the same property enhancement can be achieved with a combination of CMFs and MWCNTs as with solely MWCNTs, the cost will go down, making the polymer composite much more economical and applicable.

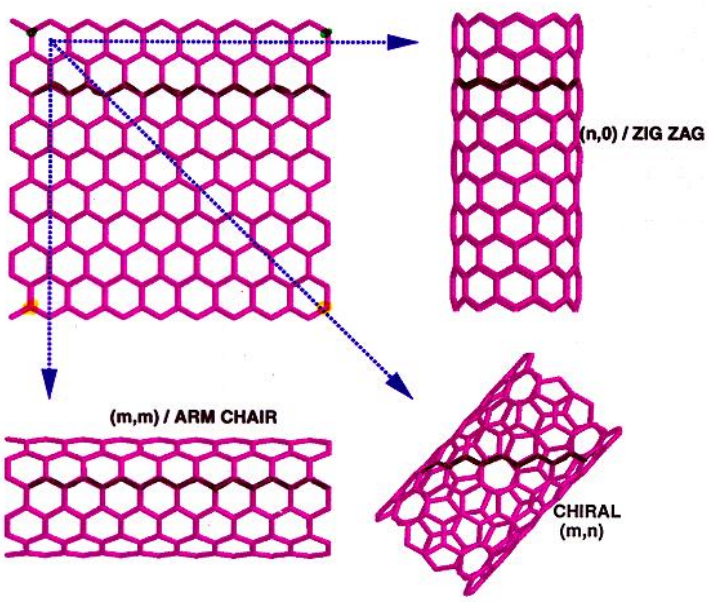

Figure 1.1: Diagram of a single-wall carbon nano tube [3].

1.2 Processing Polymer Composites

There are various methods available to process a composite. Polymer extrusion was selected to process the material for this research.

1.2.1 Extrusion

Twin screw extrusion was used to process the polymer composite. Extrusion is the process where material is forced through a shaped die [6]. It is a common manufacturing process typical in food, pharmaceutical, and polymer industries. In general, raw materials are heated to their melting temperatures, fed into an extruder, and can be mixed with other ingredients to form a new composite with a desired shape. The ingredients can be anywhere from the chocolate and toffee to make a heath candy bar to cement, water, and gravel to make concrete.

This process can be continuous or discontinuous. For this study, a continuous process with twin screw extrusion was explored for polymer processing. The extrusion process is considered continuous since the product will continue to exit the shaped orifice as long as there is material to push it though the extruder. Once the feed of material is stopped, the extrusion process is stopped. This method of polymer processing is ideal since it provides a consistent material throughout the process. Furthermore, upon start up, a functionally graded material can be collected as fillers are being added to the polymer.

Twin screw extruders (TSEs) offer a versatile method for continuous polymer processing. The extruder houses two screws comprised of several screw elements aligned on a shaft. The arrangement of these elements controls the motion and mixing of the polymer and its fillers. For example, there are forward and reverse conveying elements that push the material in the direction or against the direction of flow, respectively. Likewise, there are kneading blocks that aid in mixing the polymer with its fillers. With the ability to arrange the elements in any order, change the location for adding filler, and vary temperature of the heating elements, extrusion is an ideal processing method for polymer composites where aggressive or mild mixing can be selected depending on the application.

1.2.2 Mixing

The quality of mixing can be described with two adjectives: *dispersive* and *distributive*. The difference in these two types of mixing is best represented in

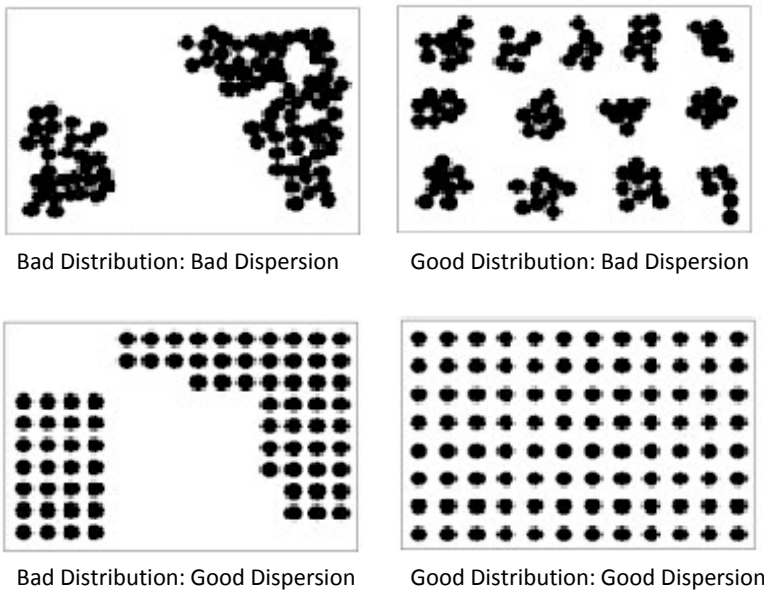

Figure 1.2: Diagram of different types of mixing [7].

Figure 1.2

Good distributive mixing means that the filler is arranged in a defined pattern. As seen in Figure 1.2, there is a clear grid of bundles of material. Good dispersive mixing means that the bundles of materials have been well broken up, but they are not necessarily in a defined pattern.

By changing screw geometries and operating conditions of the TSE, these different types of mixing can be achieved. In this study, good dispersion and distribution was the desired level of mixing.

1.3 Motivation for Research

Polymer composites are essential for moving forward and improving technologies. Their combination of strength, thermal and electrical conductivity, and weight

make them ideal for several applications. Likewise, their ease of manufacturing makes them much more versatile since they can be molded or formed directly into almost any shape. Additionally, polymer composites can be processed using extrusion which not only allows for a quick and reliable method, but also allows for functionally graded materials to be formed and the ability to analyze large ranges of filler loadings quickly.

Currently, cost is a limiting factor for the advancement of polymer composites, particularly for nano particle reinforced polymer composites. With a multi-scale polymer composite, the desirable properties can still be obtained; however, reducing the amount of carbon nano tube filler necessary will greatly reduce the cost of processing the material.

Furthermore, the processing techniques, filler loadings, and property relationships have yet to be fully characterized for this multi-scale polymer composite. Understanding the effects of processing conditions on the mixing and properties of the composite can lead to the ability to have materials-by-design. Materials can be made in order to accommodate the physical, environmental, and economical needs for each application.

1.4 Research Objectives

There are three main goals of this research. The first goal is to establish a relationship between filler loading and physical properties. A method for tensile tests and thermal conductivity tests is established in order to characterize this relation-

ship. The second goal of the research is to relate the physical properties back to the degree of mixing of the polymer. Optical images are obtained to observe the quality of distribution and dispersion in each sample. Lastly, the effects of the processing conditions of the TSE are to be mapped to the physical properties of the composite. By achieving these goals an initial processing-structure-property relationship could be established for the multi-scale polymer composite.

1.5 Thesis Outline

The thesis is an overview of the characterization of a multi-scale polymer composite through physical testing and results, and the development of a processing-structure-property relationship. The thesis is divided into five chapters. It begins with a summary of properties and processing conditions presently used for nano and micro composites in Chapter 2. Chapter 3 explains the experimental methods used in order to process and test the material. Chapter 4 reviews the mechanical and thermal results of testing the polymer under various filler loadings and TSE processing conditions, and compares the results to predictive models. Chapter 5 presents the conclusions and lays out future work that can come from this study.

Chapter 2

Literature Review

Several studies examine the effects of nanoscale and microscale fillers on a polymer matrix by studying the property enhancement of the resulting composite. Recently there has been a push to determine the actual changes in structure that occur within the composite to account for the changes in property. Furthermore, these changes in structure and property can be related back to the processing conditions of the polymer. This study focuses on this processing-structure-property relationship.

2.1 Property Enhancement

2.1.1 Mechanical Properties

CMFs and carbon nanotubes (CNTs) have been used as fillers to enhance physical properties of a base polymer because of their superior strength and properties [4, 8, 9]. CNTs and CMFs should be mixed well enough in the polymer matrix in order to transfer the loading from the polymer to the much stronger filler [10, 11].

Mechanical properties in fiber reinforced composites are primarily dominated by interfacial adhesion and dispersion [12, 13]. For polymer composites to yield improved properties, there must be considerable load transfer between the polymer matrix and filler, which in this case is PBT with chopped CMFs and MWCNTs.

When the adhesion between the fillers and matrix is bad, the filler acts more as a defect. The defects create stress concentrations, leading to premature failure [14, 15]. Furthermore, poor dispersion means there are agglomerates. These agglomerates then begin to fail before the actual individual fibers, a phenomena known as pull-out, once again reducing properties [16, 17].

These two concepts are very important when dealing with CNTs and often times additives are required in extrusion to maintain a high level of adhesion and dispersion [18, 19]. However, since CMFs are on a larger length scale, a high degree of adhesion and dispersion is easier to achieve with extrusion, and does not always require these additives [20, 21].

Several people have reported a significant improvement in mechanical properties when adding micro and nano scale fillers. Cho and Paul increased the loading of organoclay in a nylon 6-organoclay nanocomposites, and found improvements in strength and modulus and a loss in ductility as the loading increased [22]. Carneiro et al. found that more vapor grown carbon fibers (VGCF) increased the modulus and yield stress, but decreased the impact strength when varied from 0-20 wt% VGCF [23]. Bekyarova et al. studied multi-scale carbon nanotube-carbon fiber reinforcement in an epoxy resin. The multiscale hybrid composite had enhanced out-of-plane mechanical and electrical properties over the neat resin [24]. Sandler et al. observed an increase in tensile and bending stiffness, and an increase in tensile yield stress and strength for carbon nanofiber loadings up to 15 wt%. Ductility was able to be maintained up until 10 wt% carbon nanofibers in poly(ether ether ketone)(PEEK), and above that loading, the composite became more brittle as the

others had reported. They speculated that as the size of the filler decreases, the more pronounced the influence is on the polymer matrix during crystallization [20].

Andrews et al. found that good dispersion without breakage is key for achieving better properties for a nanofiber and MWCNT polymer composites. At low concentrations (less than 15 vol%) of nano fillers, the modulus increases and the tensile strength decreases. At higher concentration, both the modulus and tensile strength increase. Overall, the removal of defects increased the properties, and surface treatment improved interfacial bonding. Bad adhesion led to pull out, which reduced mechanical properties [17].

While many reported improved tensile strength with reduced ductility, there have also been cases where little improvement was observed. Lozano and Barrera found that with the addition of nanofibers, the ultimate strength did not improve significantly. However, increased brittleness was shown which could be attributed to the inability for the matrix to further crystallize when subject to deformation because of the molecular restrictions of dispersion [25].

Lee et al. claimed that a reduction of properties due to nano scale fillers indicates poor adhesion and dispersion. They used the process of electrophoretic deposition to deposit the nanoscale reinforcements and found that good homogeneity was achieved, ultimately improving properties [26].

Lastly, there have been reports where fillers improve properties up until a certain loading, and then begin to hinder the composite. Broza et al. found that the Youngs modulus, tensile strength, and strain to failure increased when increasing the amount of CNTs in a PBT matrix from 0.01 to 0.1 wt% CNT. However, when

increased from 0.1 to 0.2 wt% CNT, the strength and the strain of the nanocomposites decreased slightly [27]. Zeng et al. added carbon nanofibers (CNFs) to poly(methyl methacrylate) (PMMA) and found that there was an optimum loading of CNFs between 5 wt% and 10 wt% since beyond a 10 wt% CNF loading, the modulus began to decline. The authors recognize, however, that this optimum level would be a function of the diameter of the filler and quality of dispersion [28].

Yesil et al. studied microfiber reinforced high-density polyethylene (HDPE), poly(ethylene terephthalate) (PET), and MWCNT composites. They found that after an initial increase in tensile strength, the addition of microfibers and MWCNTs decreased the performance since there was a lack of compatibility with the polymer phase beyond 30 wt% loading of PET [29].

Overall, the mechanical properties are definitely altered when adding micro and nano scale ingredient to a polymer matrix. Most have reported improved properties, but recognize that sometimes there is either a minimum loading or a maximum loading that yields the best properties.

2.1.1.1 Small-Scale Mechanical Testing

To characterize the mechanical properties, sub-scale dogbone specimens were primarily used for tensile testings. This size specimen not only offers the ability to repeat several trials for minimal cost, but also has been shown to yield accurate results.

Zhang et al. used sub-scale specimens to characterize the mechanical proper-

ties with digital image correlation [30]. Although errors were detected when benchmarking with specimens of known properties, the error was due to the measurement system, not the scale of the dogbone.

Bruck and Gershon also used sub-scale specimens for tensile tests [31, 32]. They used the specimens to test various polymers and CNT combinations with digital image correlation. Again, the specimens were producing results with little error.

2.1.2 Thermal Properties

There have been very high predictions of thermal conductivity for polymer composites with CMF and CNT filelr [33, 34]. Thermal conductivity in polymer composites is dominated by the number of interfaces achieved within the composite. Heat conduction is the transfer of energy from more energetic to less energetic particles through particle interactions [35]. The energy level is related to the translation motion, internal rotation, and vibrational modes of the molecules. In solids, conduction is mostly attributed to the lattice vibrations and translational motion [35]. To achieve good thermal conduction, a network of fibers needs to be created within the polymer matrix, meaning good dispersion needs to be achieved [36, 37].

There have been several reports where high thermal conductivity was achieved using fillers. Hone et al. found that a loading of 1 wt% SWCNT in epoxy increases the thermal conductivity of by 120% [38]. Berber et al. developed a molecular dynamics model to predict the thermal conductivity of cabon nano tubes [33]. The

predicted value of thermal conductivity was reported as 6600 W/m-K at room temperature, which matched experimental data [39]. This was unusually high, however when considering the strong bonds and the nearly perfect atomic structure, the value is not surprising for an isolated nano tube [33].

Agarwal et al. found that when the carbon nanofibers are aligned in the direction of the heat flow, thermal conductivity is increased. Composites with a hyrbid of both microscopic carbon fibers and CNFs showed the best thermal conductivity since the contacts between the CMFs were aided with contacts from CNFs, especially when the CMFs are aligned. Thermal conductivity, however, did not increase as much as expected because of interfacical resistances between the polymer and the fibers. The best thermal conductivities were obtained with 10 vol% CMF and 30 vol% CNF and when both CMF and CNF were at 20 vol% [40].

Frusteri et al. examined carbon micro fibers of different lengths and loadings mixed with inorganic phase change materials [41]. The results showed that thermal conductivity increased linearly with loading, however the different lengths changed the thermal conductivity, where the shorter length yielded a higher thermal conductivity. They speculated that this was because of the degree of homogeneity achieved in the samples, where the micro carbon fibers of 7μm in diameter and 0.2mm in length were better dispersed than the micro carbon fibers of 3mm and 6mm in length. They also found that at a 7 wt% loading, the thermal conductivity quadrupled.

Zhou et al. examined surface treatment on micro and nanonano-SiC/DGEBA/EMI-2,4 composites to see how thermal conductivity was affected [42]. The results showed

that composites with nano-SiC and various surface treatments increased thermal conductivity significantly; however, even with surface treatments, the micro-SiC did not enhance the thermal conductivity significantly.

While many have reported higher thermal conductivity, others have found little improvement. Gojny et al. concluded that relatively low interfacial area and weak interfacial adhesion promote thermal conductivity, almost opposite of what aids mechanical properties. Thus they found that CNTs, which provide large interfacial areas, are not suitable for an enhancement of the thermal conductivity of polymer-based composites. [43]. Likewise, there have been reports of a decrease in thermal conductivity due to nanofiller, but this may be because of breakage during processing [44, 45, 46].

2.1.3 Electrical Conductivity

The electrical conductivity of the samples strongly depends on the network the filler is able to form within the polymer matrix. In order to achieve an adequate matrix, the filler must be well dispersed and distributed within the polymer, as with mechanical properties. Additionally, it has been shown several times that there is a certain percolation level that must be met, meaning under a certain loading of filler, no electrical effects will be observed.

Pedroni et al. were able to achieve electrical conductivity in MWCNTs and styrene-butadiene-styrene block copolymers with loadings as low as 0.25 wt%. They also found that MWCNTs act as a reinforcing agent, with an overall improvement

in mechanical properties [47].

Bai and Allaoui found that when the MWCNT length was increased from 1 to 50 μm in epoxy resin, the electrical conductivity threshold decreased significantly. Well dispersed nanotubes generally have higher aspect ratios than nanotube aggregates, so the percolation threshold decreases with better dispersion [48].

In general, it has been shown that higher loading yield higher electrical conductivity, as long as the initial loading is above the percolation level.

2.2 Processing Conditions

The processing method for this experiment was extrusion. This versatile method of melt-mixing materials lends itself to being able to achieve the desired level of mixing, and it produces a continuous product, thus making it ideal for this since many tests had to be performed for each sample. However, with such versatility, the conditions under which the material is processed is very important. As mentioned previously, there are plenty of options for processing conditions that change the outcome of the material.

The shear stress seen by the material in the extruder is strongly dependent on the screw speed. Chen et al. found that at higher shear rates, which in his case related to higher screw speeds, electrical properties are observed at a lower loading of 1.5 wt% CNT versus 2.5 wt% CNT when processed at a lower shear rate. However, while the higher shear rates leads to better dispersion and properties, it also reduces the alignment of the CNTs, reducing other properties. [49].

Villmow et al. found that with an increased screw speed, the filler was more dispersed in the material [5]. They found that at a constant flow rate of 5 kg/hr, a screw speed of 500 rpm yielded better dispersion of MWCNTs in a poly(lactic acid) matrix when compared to 200 rpm and 100 rpm.

Vera-Agullo et al. did an extensive study on the dispersion of carbon nanotubes. They found that more aggressive the mixing sections led to better dispersion, however breakage of the filler occurred. This aggressive mixing was necessary to remove the agglomerates, which enabled effective reinforcement of the matrix for mechanical properties. With less aggressive mixing, adequate dispersion could be achieved for an effective electrical conductive network [50].

Gao et al. presented work that showed that the degree of mixing is dependent on both the screw speed and flow rate, or in other words, the specific throughput (Q/N) [51, 52]. Pappas further explored this concept and characterized the stress seen by the ingredients in an extruder. He found that specific throughput and screw speed control the imparting stress on the filler, where higher values mean higher stress on the filler, leading to a higher percent break-up of the filler [7].

Overall, by varying processing conditions, the end structure and properties of the composite can be altered significantly.

2.3 Structure Observations

The structure of the composite is very important for understanding the relationship between processing and properties. Upon examining the structure of a

sample, variations in performance can be explained.

One structural aspect that is very important is the quality of mixing of the filler within the polymer matrix. Dispersion of the filler plays a significant role in the properties. In addition to the reports of authors previously discussed, Rong et al. concluded that the optimum nanoparticle loading depends on the best distribution of the particles [53]. Gong et al. examined surfactant aids to help the interfacial interaction between carbon nanotubes in epoxy. They found that the better dispersed and distributed the CNTs were in the epoxy, the better the thermal and mechanical properties [54].

Additionally, the alignment of the fibers should be observed since the orientation of fibers can cause anisotropic effects within the composite [55]. Du et al. did an extensive study on the alignment and dispersion of SWCNT in PMMA and related it to mechanical, thermal, and electrical properties. While all the composites showed improvement over neat PMMA, the electrical conductivity was greatly influenced by the alignment, where the aligned samples were 5 orders of magnitude lower in electrical conductivity when compared to unaligned samples [56].

Thostenson and Chou found that extrusion indeed creates alignment of carbon nanotubes, and this alignment yields a higher modulus, especially when compared to a random orientation of CNTs. Furthermore, the improvement in yield and ultimate strength indicates that they are achieving a load transfer between the CNTs and polystyrene matrix [57]. Kuriger et al. found that the alignment of the fibers improves with a longer time in the extruder, having a significant effect on properties. They tested the thermal conductivity in the longitudinal and transverse

direction with respect to the orientation of the fiber to observe how orientation changes properties. They found the most improvement in thermal conductivity was seen in the longitudinal direction [58].

Contrarily, Zeng et al. and Potschke et al. found that nanofillers were not necessarily aligned after using an extruder [28, 59]. Sandler et al. found that the alignment of carbon nanofibers further decreases when injection molding parts [20].

Lastly, the homogeneity of the composite can be quantified when observing the structure. Defects, such as voids, and contaminants, such as moisture and volatile organic compounds, ultimately reduce property performance [60]. At higher nanotube loadings, the extent of improvement in mechanical properties might be limited by the high viscosity of the composite and the resulting void defects [14]. Kota found that with the addition of a vacuum port while processing polymer composites on a TSE, the porosity of the polymer is significantly reduced, and physical and electrical properties are greatly increased [3]. Kuriger et al. found that the number of voids increased with the weight percent of the fiber loading [58].

Developing a processing-structure-property relationship is very important when dealing with composites. After examining each individually, it is evident that they are very much related to one another where improvements and adverse effects in one area usually means a change in another.

Chapter 3

Experimental Procedures

The following sections describe the materials, equipment, and procedures used to process and test the polymer composite in order to characterize the mechanical and thermal properties.

3.1 Materials

There were three main ingredients for this polymer composite: the polymer matrix, the microscale filler, and the nanoscale filler.

3.1.1 Polymer Matrix

Poly(butylene terephthalate) (PBT) was used as the polymer matrix for the composite. PBT is a semi-crystalline thermoplastic that offers a good combination of thermal and mechanical properties when compared to other polymers [61]. It is in the polyester resin family and is similar to polyethylene terephthalate (PET). PBT is often used as an insulator for electrical components in various industries and it is durable under harsh environments, making it ideal for some applications. It is used in applications like electrical appliances, car grilles, switches, car body panels, coffee makers, and bicycle gears [62, 63].

For this application, it allowed for a structure that crystallized quickly, mak-

ing collection easier, and it allowed for the thermal properties of the fillers to be examined without aid from the polymer matrix. The molecular weight of PBT is 28,000 and it has a melt temperature of 224°C [60]. PBT requires three hours of pre-drying at 140°C before processing.

3.1.2 Fillers

Toho Tenax America, Inc. provided C493 Chopped Carbon Fibers. This type of CMF was recommended for use with PBT because of the chemistry of the polymer and this fiber mixing best.

The PolyOne Corporation supplied a pre-compounded mixture of PBT and 15 wt% MWCNTs. In general, other additives are used when processing polymer with MWCNTs to improve the adhesion between PBT and the MWCNTs. Therefore receiving a pre-compounded mix was a more consistent way to ensure that the MWCNTs were properly distributed and dispersed within the polymer matrix. The pre-compounded mixture of MWCNTs and PBT as well as the CMFs were used as the fillers. The manufacturer specified properties for these materials and the polymer matrix are listed in Table 3.1.

The PBT and pre-compounded MWCNT and PBT mixtures were received in pellet form, and the CMFs were received as fibers. With the state of these materials, a master-batch was used to feed in the PBT and MWCNTs and the CMFs were added further downstream in the extruder.

Table 3.1: Manufacturer specified properties of materials.

Property	PBT	CMF	CNT
Density (g/cm^3)	1.31	1.82	1.5
Length (μm)	–	6000	1.3-10
Diameter (nm)	–	7000	11
Tensile Strength (MPa)	57	4412	–
Young's Modulus (GPa)	2.7	226	–
Cost ($/kg)	3.31	24.25	85

3.2 Equipment and Settings

The following sections describe the equipment used for each step of the procedure along with the settings used for the equipment.

3.2.1 Processing Composites

The polymer composite was processed using a TSE. Extrusion is a melt mixing process that is commonly used in food and pharmaceutical industries, among many others. Extrusion is a continuous process as long as there is a product being fed into the extruder. This allows for a consistent and well-mixed product. Additionally, extrusion serves as a safe, economical, and flexible type of manufacturing.

The polymer composite was processed on a Coperion ZDSK-28mm co-rotating,

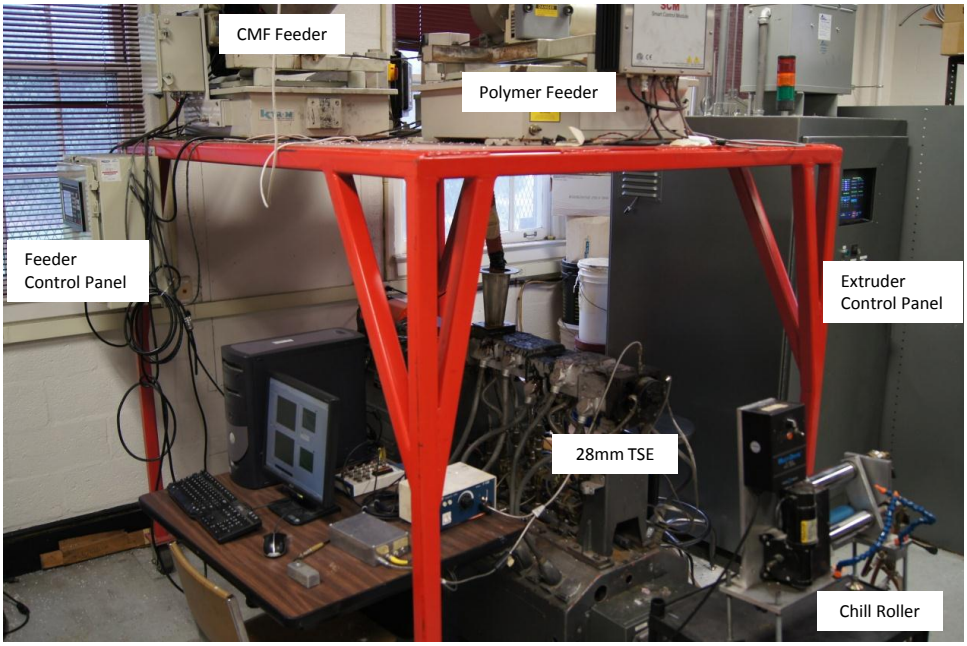

Figure 3.1: Experimental set-up for processing the polymer composites.

fully inter-meshing twin-screw extruder located in the Advanced Manufacturing Laboratory at the University of Maryland, shown in Figure 3.1. The screws have three flights and a 28mm diameter. The length to diameter ratio is 32.

The TSE consists of 8 sections: a feed port, 5 barrels, a connection block, and a die zone, as see in Figure 3.2. The PBT and pre-compounded PBT/MWCNT master-batch enter the extruder at the feed port. The barrels are electrically heated and can be water cooled in order to regulate the temperature for melt mixing the polymer composite. The CMFs enter the extruder at the mixing port, or the third barrel from left.

At barrel 5, just before the connection block, a Welch R1402 vacuum pump was used in the vacuum port as seen in Figure 3.3. The material was processed at a vacuum of 25 inches of mercury in order to remove any volatiles or air in the

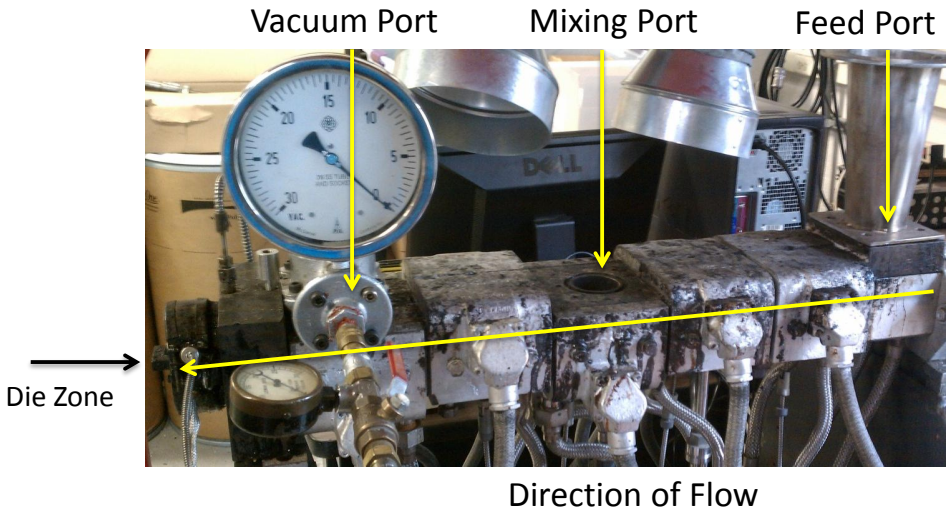

Figure 3.2: Coperion ZDSK-28mm twin-screw extruder.

material.

The connection block housed different instrumentation, such as a light probe, that were not used for this experiment. However, the instrumentation remained in the holes as to not let material escape through them. The die zone is what forms the material into the desired shape for collection. For these experiments, a slit die zone of 1mm thick and 2.5mm wide was used to form ribbon like material.

Inside the TSE are, as the name implies, two long screws that rotate to mix and move the material through the extruder. The extruder is characterized by the diameter and direction of the rotation of the screws. This extruder has two 28 mm screws, that are co-rotating, and fully inter-meshing.

The screws have several sections, or elements, along them that make up the threads of the screws. These elements can be re-arranged into different configurations, or geometries, to produce the desired degree of mixing for the process. This

Figure 3.3: Welch R1402 vacuum pump.

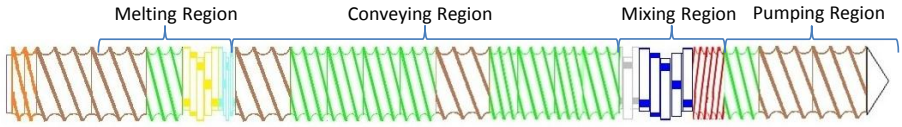

Color	Element Direction	Element Type	Axial Length (cm)	Axial Pitch (cm)
Orange	Forward	Conveying	1.0	1.0
Brown	Forward	Conveying	4.5	1.5
Green	Forward	Conveying	3.0	1.0
Yellow	Forward	Kneading Block	3.0	0.6
Light Blue	Reverse	Kneading Block	1.5	0.3
Grey	Forward	Kneading Block	1.5	0.3
Blue	Forward	Kneading Block	4.5	0.9
Red	Reverse	Conveying	3.0	1.0
White	Forward	Screw Tips	2.5	--

Figure 3.4: Screw geometry used for all experiments.

arrangement is very important for extrusion since it has the potential to change the properties of the extrudate. The seperate elements make extrusion a very flexible process, and therefore desirable. The screw geometry for this experiment was kept constant and is shown in Figure 3.4.

There are four regions of the screw: melting, conveying, mixing, and pumping. The polymer entered at the beginning of the melting region and the CMFs were added in the middle of the conveying region. The mixing section was where the pri-

Figure 3.5: Coperion ZDSK-28mm TSE control panel .

mary mixing the microsacle filler and the polymer or pre-compounded PBT/MWCNT mixture occurred. After the mixing, devolatalization took place to remove any contaminants from the material, and the material was pumped to the end of the screws. The screw tips are housed inside the die zone, and then the material exited the extruder through the slit.

Processing of the material involved several steps. The FACTS MI 101 control system with a digital touch-screen control panel pictured in Figure 3.5 controlled the extruder.

The control panel had both manual and digital controls. The digital controls were used for these experiments which could turn the extruder on and off, set screw speeds, set temperatures, monitor the motor amperage, turn on the lube oil pump, turn on the blower, and examine other menus that monitored other features. There is also an emergency stop button that can be used when conditions are in danger of

damaging the components.

On the control panel, various screw speeds can be set in order to increase the degree of mixing and break-up of the composite. For this motor, a maximum screw speed of 300 rpm can be achieved. More importantly, the amperage seen from the motor was not to exceed 15 amps so as to not cause damage to the machine. This was closely monitored when the screw geometry was being selected. When a too aggressive of a mixing section was selected, the CMFs would not move through the extruder fast enough, and the motor could not overcome this torque to turn the screws, increasing the amperage. This had a potential to damage the equipment, so the mixing section was reduced.

Furthermore, the temperature of the barrels were set with this panel, with a maximum temperature of 549°F. Although the melting temperature of PBT is 435°F, a processing temperature of 550°F can be used. The typical arrangement for barrel temperatures is shown in Table 3.2.

To regulate the flow rate at which the material entered the extruder, two laboratory scale twin screw feeders were used, one for pellets of PBT and MWCNTs, and one for the CMFs. The feeders were located on top of the movable platform so that the access to the extruder was not blocked. A K-Tron loss-in-weight feeder was used to feed the pellets, shown in Figure 3.6.

The pellet feeder was connected to the extruder feed port via flexible tubing and a steel funnel to ensure the pellets entered the feed port from the platform.

The feeder control panels were set to various flow rates since it had been shown that quality mixing depends screw speed, N, and specific throughput, Q/N [7].

Table 3.2: Temperature profile for barrels for TSE.

Barrel Number	Temperature (°F)
1	445
2	471
3	466
4	485
5	484
Die Zone	458

Figure 3.6: Laboratory scale K-Tron loss-in-weight twin screw pellet feeder.

Figure 3.7: K-Tron loss-in-weight pellet feeder control panel.

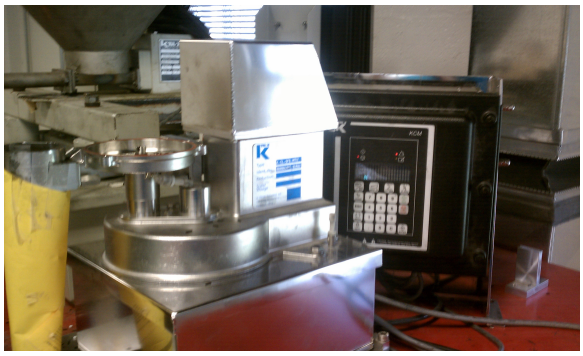

Figure 3.8: K-Tron Micro Feeder MT12 loss-in-weight model.

The pellet feeder control panel is shown in Figure 3.7. The pellet feeder had a maximum flow rate of about 10 lbs/hr.

The CMFs were fed in by a K-Tron Micro Feeder MT12 loss-in-weight model, shown in Figure 3.8. Although this is typically a powder feeder, the fibers were able to be regulated through the feeder without jamming the screws, unlike when pellets are put through powder feeders. The control panel, shown next to the feeder in Figure 3.8 controlled the feed rate of the micro fibers so that the weight percent of CMFs could be varied from 0% to 25%.

The fibers were fed from the feeder to the mixing port via a stainless steel pipe

Figure 3.9: Chill roller.

of 50mm in diameter, the same diameter as the mixing port hole. The maximum flow rate for the micro feeder is 1 lb/hr. This was a limiting constraint for the CMF loading that could be achieved. For example, if a maximum loading of 25 wt% CMF is desired, a maximum total flow rate could only be 4lbs/hr, with the micro feeder set to 1 lb/hr and the pellet feeder set to 3 lbs/hr.

When the material exited the die zone, it was collected in strips so that samples for various tests could be made later. To safely and effectively collect the strips, a chill roller was used, as shown in Figure 3.9.

The material exited the die zone and passed over the top roller. The material was then fed between the two bottom rollers, flattened, and rolled from there. There was also an option to turn on a water source to cool the two steel rollers and to turn on sprinklers on the sides; however, this material cooled fast enough that this

option was not necessary. The speed at which the rollers rotate was controlled by a Penta KB Power motor, and for best results, the rollers were set to a speed that matched that of the extrudate. The speed of the roller controlled the width and thickness of the extrudate.

3.2.2 Tensile Tests

To characterize the relationship between TSE mixing and the composition of the polymer composite, a small-scale tensile tester was built to determine mechanical properties using sub-scale ASTM standard dogbone specimens prepared from extruded strips of the micro and micro-nano composites processed in the TSE.

Tensile tests are a proven way to determine the yield and ultimate strength of materials, the percent elongation at yield and fracture, as well as the Young's Modulus. Tensile testing is when a specimen is pulled apart and the applied load and distance stretched are measured. Subsequent stress vs. strain curves can then be generated to obtain mechanical properties for comparison.

The tensile specimens used were dogbones. These are a standard specimen type used since they will consistently break in the middle of the dogbone. The dogbone was sketched on ProEngineer 5.0, and then imported into the laser cutter program. The dimensions of the dogbone are shown in Figure 3.10.

Since the thickness of the material was thinner than standard ASTM dogbones, the small scale dogbone was used. The smaller dogbone also allowed for several trials of tensile tests per material without needing to make copious amounts of material,

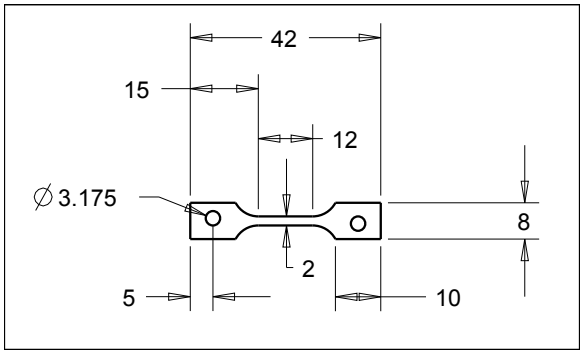

Figure 3.10: Sub-scale ASTM standard dogbone.

Figure 3.11: Versa laser cutter.

as in the case of injection molding the dogbones.

The dogbones were prepared using a Versa laser cutter, shown in Figure 3.11. The laser cutter cut the specified size dogbone using a power setting of 25-30% and speed at 100% as to not burn the composite.

When the samples were removed from the laser cutter, they were nearly ready to be tested, making this method of cutting dogbones advantageous for the experiment that required multiple trials for each material.

The set-up for the tensile tests is pictured in Figure 3.12. The tensile tester

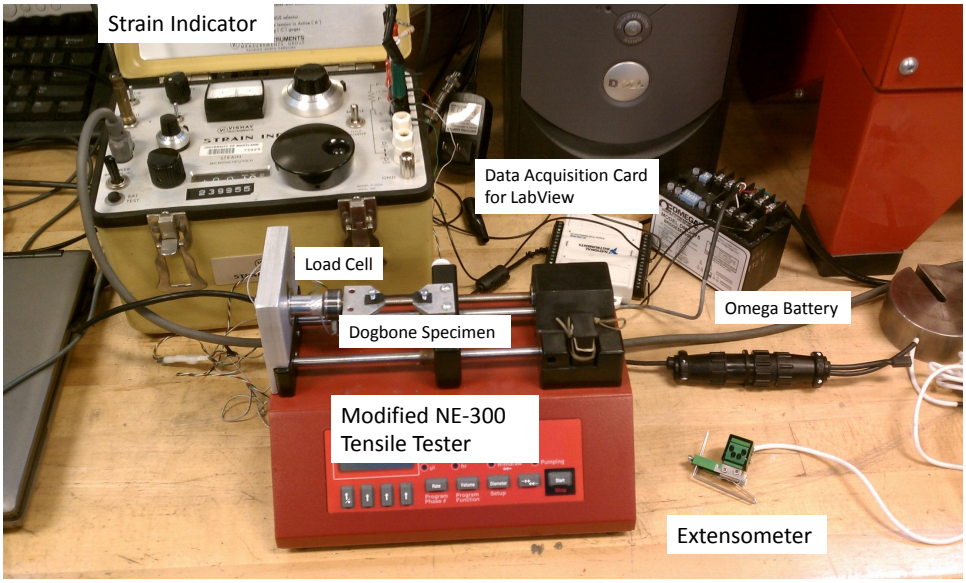

Figure 3.12: Tensile testing set-up.

was a modified NE-300 Just Infusion Syringe Pump [64]. It is screw-driven, and has a maximum load capacity of 30 lbs (13.6 kg) with strain rates ranging from 0.01/sec to 0.00001/sec. The aluminum grips and block were added to convert the syringe pump into the tensile tester. The grips were set about 30 mm apart, and a gauge length of approximately 12 mm was used.

A LPM-530 Miniature Load Cell along with a Vishay Instruments Strain Indicator were used to measure and record the load applied to the specimens. As the middle block moved away from the stationary aluminum block, a load was applied to the specimen and recorded via the load cell and data acquisition card (DAQ), and plotted in LabView.

Strains could be measured using a small-scale mechanical extensometer with a gauge length of 6.5 mm powered by an Omega Battery. Again, as the middle block moved away, the strain gauge spread further apart. This distance could be

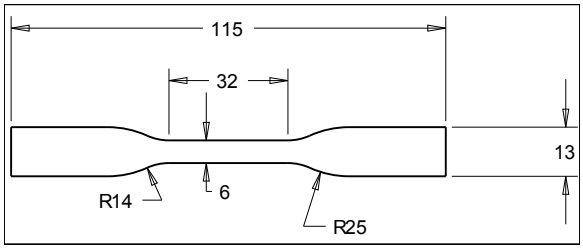

Figure 3.13: ASTM D638 type IV dogbone.

measured using a voltage to mm conversion factor. The extensometer was secured to the specimen via grips that come with the extensometer and rubber bands that were added to ensure there was nothing slipping.

There were several options for fixturing specimens onto the grips of the small-scale load frame. Since the load capacity is very low (30 lbs), it is possible to use fast-curing cyanoacrylate epoxy adhesive to attach the tabbed ends of the dogbone specimen. However, to achieve adequate shear strength to resist failure during testing, cure times of up to 12 hours were needed. Therefore, an alternate approach was pursued where the specimen is attached to the grips via screws. It was determined that holes as small as 3 mm could be used on the tabbed ends of the dogbone specimen without causing failure during testing. Thus, it was possible to more quickly fixture the specimens and test them then was permitted previously. Furthermore, a combination of adhesive and screws could be used, where the adhesive would be adequate with a much shorter cure time of approximately 5 minutes. The combination method proved to be the most reliable for consistent results.

The sub-scale sized dogbone was tested against an ASTM D638 type IV sample to validate the results [65]. The drawing of the dogbone is seen in Figure 3.13

The dogbones were prepared on the laser cutter as before and were tested on a Tinius Olsen load frame with a 25 KN load cell. The grips were approximately 60 mm apart, per the standard requirements, and the tests were conducted at 5 mm/min. The load and displacement data was once again converted to stress and strain data for analysis.

3.2.3 Thermal Tests

Thermal testing was explored by using a MicroFlash RT - Thermal Properties Measuring System. This type of testing could measure the thermal conductivity of the samples.

In order to perform the tests, the extruded strips needed to be chopped and injection molded. A Killion Extruders, Inc. pelletizer (Figure 3.14) was used to chop the extrudate into strips so that they could be injection molded. The pellitizer could take the strips directly and slice them as it passed through the slot about every 4 mm.

A Cincinnati Milarcron BabyPlast injection molder shown in Figure 3.15 was used to make the proper square sample sizes of 8mm by 8mm by 2mm. The injection molder has a digital display where the position and temperatures of the chambers, nozzle, and mold can be adjusted. The chambers are hydraulically controlled and the electrically heated.

The typical temperature profile for the injection molding machine is shown in Table 3.3.

Figure 3.14: Killion Extruders, Inc. pelletizer.

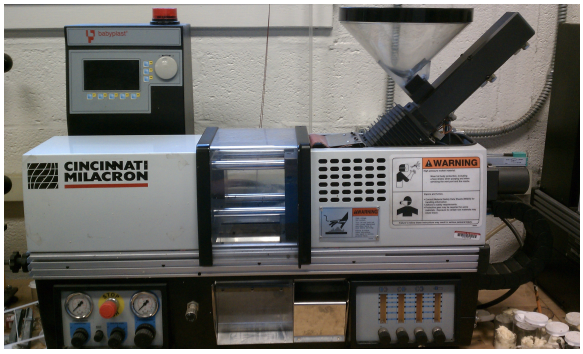

Figure 3.15: Cincinnati Milacron BabyPlast injection molder.

Table 3.3: Temperature profile for injection molds.

Element	Temperature (°C)
Plastification	292
Injection Chamber	295
Nozzle	260
Mold	23

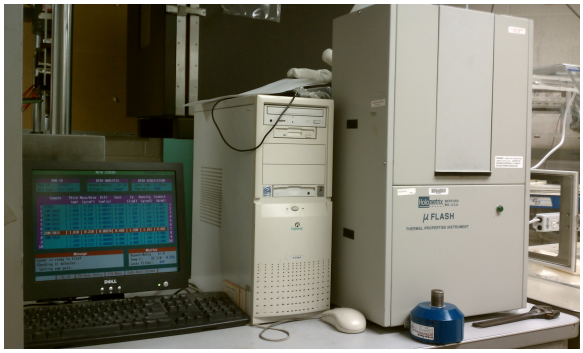

Figure 3.16: Holometrix MicroFlash RT - Thermal Properties Measuring System .

The Holometrix MicroFlash RT - Thermal Properties Measuring System was used to measure the thermal conductivity, k, and is shown in Figure 3.16.

Specific sample preparation guidelines were followed in order to properly prepare the samples [66]. The MicroFlash is cooled with liquid nitrogen and digitally controlled through a computer. The MicroFlash uses the laser flash sample methods and a series of calculations in order to determine the thermal conductivity of the sample. The small sample is subjected to a very short burst of high intensity

randiant energy from a laser. The resulting temperature rise of the rear surface of the sample is measured and thermal diffusivity is calculated based on the thickness and density of the sample, as shown in Equation 3.1 [67].

$$\alpha = \frac{0.139t^2}{\tau_{\frac{1}{2}}} \tag{3.1}$$

where t is the sample thickness, and $\tau_{\frac{1}{2}}$ is the time it takes for the temperature to rise to half of its maximum temperature on the back face of the sample not exposed to the laser. Once the thermal conductivity is calculated, the specific heat needs to be measured. Specific heat is the energy required to raise a unit of mass by one unit of temperature at constant pressure. The specific heat is measured with the laser flash by comparing the temperature rise between the sample and the reference sample of known specific heat [68]. In this case, the reference sample used was pyrex. The specific heat, C_p, is calculated according to Equation 3.2.

$$C_p\ sample = \frac{Q_e}{m\Delta T} = \frac{(mC_p\Delta T)_{ref}}{(m\Delta T)_{sample}} \tag{3.2}$$

where m is the mass of the sample, and ΔT is the change in temperature. After determining the thermal diffusivity, specific heat, and density, thermal conductivity can be calculated according to Equation 3.3

$$k = \alpha * \rho * C_p \tag{3.3}$$

where α is the thermal diffusivity, ρ is the density of the sample, and C_p is the specific heat. The thermal conductivity can then be recorded for each sample and

further analyzed.

3.2.4 Imaging

To qualitatively examine the mixing of the composite, optical and scanning electron microscope (SEM) images were obtained.

Optical images aid in determining the number and size of agglomerates present in the material. The black samples are set in a clear resin in order to obtain the desired view, either flat or cross-sectional. Ted Pella, Inc. PELCO Fast Curing Epoxy Hardener and Epoxy Resin, in a 48:100 ratio, respectively, were used to make the optical sample casing. After setting the samples in resin, they are polished using a Buehler Ecomet 3 Variable Speed Grinder Polisher to remove scratches from the surface of the sample.

The samples are then imaged on a Unitron Versamet - 2 optical microscope located in the Multi-Scale Measurements Laboratory at the University of Maryland, shown in Figure 3.17. The optical microscope is lit from the underneath, and magnifications of 5, 20, 40, and 100 can be used. The images are captured using an OptixCam computer program.

SEM images were used for a more in-depth look at the degree of mixing of the CMFs. A Hitachi SU-70 Schottky field emission gun scanning electron microscope located in the Nanoscale Imaging Spectroscopy and Properties Laboratory at the University of Maryland was used, shown in Figure 3.18. SEM images were taken of broken dogbone specimens and were used to visually assess the mixing.

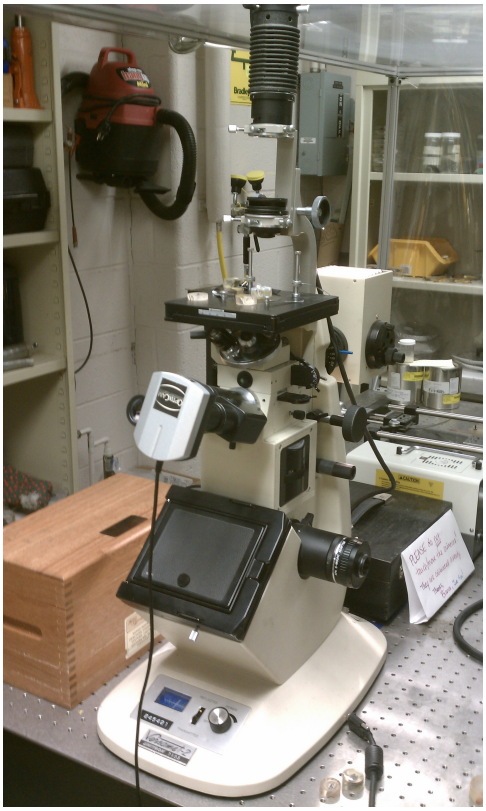

Figure 3.17: Unitron Versamet -2 optical microscope.

Figure 3.18: Hitachi SU-70 Schottky field emission gun SEM.

3.3 Procedure

3.3.1 Processing

The following procedure was used to process and test the polymer composite. First, the composite was made on the Coperion ZDSK-28mm co-rotating, fully intermeshing twin-screw extruder.

PBT was placed in ovens for 3 hours at 140°C in order to dry the polymer prior to processing it. The dried PBT was put in the polymer feeder. The feeder was purged using neat PBT in order to remove any remaining residue from the previous days work.

If only CMFs were being added to the composite, the dried PBT was left in the feeder to be used for processing. When MWCNTs were to also be used, the dried PBT was purged from the feeder into a container. The pre-compounded MWCNT pellets and PBT were then measured to specific amounts in order to obtain the correct weight percent of MWCNTs and CMFs. The pellets were mixed together in a bucket to create a master-batch of a given weight percent that was put in the polymer feeder. The Micro Feeder MT12 was set to a specific flow rate in order to achieve the desired weight percent of CMFs.

The operating conditions, including flow rate, screw speed, and barrel temperatures were set. The barrels would take approximately one hour to heat up to the desired temperatures. For this study Q/Ns of 0.136 mL/rev, 0.202 mL/rev, 0.267 mL/rev and 0.333 mL/rev were compared. To achieve the desired specific throughput, the screw speed was kept constant at 200 rpm, and the flow rate was varied

from 2.7 lbs/hr, 4 lbs/hr, 5.3 lbs/hr and 6.6 lbs/hr respectively. This produced the desired Q/Ns once geometric considerations were taken into account.

The screw speed would be set to 200 rpm, then time would be allowed for the fluctuations in screw speed to become minimal. As previously mentioned, during this time the amperage of the motor would be monitored in order to assure safe operating conditions for the equipment. The pellet feeder and the micro feeder were set to the appropriate feed rates. The pellet feeder was switched on first and once extrudate exited the die zone, the micro feeder would be turned on. The feed rates varied depending on the loading of the CMFs. The PBT or PBT/MWCNT masterbatch entered the extruder at the feed port. The CMFs were added at the mixing port.

The extruder mixed the polymer and fillers and the vacuum was used to removed any volatile organic compounds or voids from air entrainment that occur when using a TSE to process polymer composites. The effects of processing the material under vacuum of 25 inches of mercury, 5 inches of mercury, and without a vacuum were also observed.

As the pressure built up in the extruder, the extrudate exited the die zone, and the chill roller was used to collect all of the material strips in rolls. To determine when to start to collect the material, the time was recorded for when PBT with the varying amount of CMFs went from white, the original color of PBT to black, the color of the composite with CMFs. These times were then used as the minimum time needed between turning on the micro feeder and the beginning of collection for the given amount of CMFs. The width and thickness of the extruded strips

Q=4lbs/hr N=200 rpm	0% CMF	5% CMF	10% CMF	15% CMF	20% CMF	25% CMF
0% CNT	X	X	X	X	X	X
0.5% CNT			X	X	X	X
1% CNT				X		
1.5% CNT			X	X	X	
2% CNT				X		
2.5% CNT			X	X	X	
3% CNT				X		

Q=2.7, 5.3, 6.6 lbs/hr N=200 rpm	0% CMF	5% CMF	10% CMF	15% CMF	20% CMF	25% CMF
0% CNT			X	X		
0.5% CNT			X	X		

Figure 3.19: Summary of materials made and tested.

depended on the loading of the CNTs and CMFS, as well as the speed of the rollers. Attempts were made to keep the thickness and width constant, however this was very difficult, and thus the strips vary depending on who was collecting the material that day and the loading of the composite. All of the materials made and tested are summarized in Figure 3.19.

3.3.2 Tensile Tests

Once the material was processed and identified according to the weight percent of CMFs and CNTs, as well as the Q/N condition, the dogbone specimens were made on the Versa laser cutter. The sub-standard ASTM size dogbone results were compared to ASTM D638-IV dogbones to validate the results [65]. After this verification, the sub-standard dogbones continued to be use because of ease of fabrication and testing. However, some testing occurred on the ASTM size dogbones

for consistency of results since this testing equipment was more reliable.

To begin the tensile testing, the set-up was calibrated using a 1 kg weight to ensure the load cell was recording properly. Additionally, the extensometer was examined to ensure that the voltage was kept constant, meaning no wire connections had become loose since the last use.

To test the dogbones, the samples were glued and then screwed onto the grips of the tensile tester. The extensometer griped the dogbones at two points, and rubber bands were used to ensure the extensometer did not slip during testing. One of the blocks then moved away at a rate of 2.052 mm/min. The load cell and extensometer recorded the applied load and displacement respectively.

The data was read into LabView as voltages. This was processed in Matlab using the calibration factors of kg/V and mm/V for the load cell and extensometer, respectively. The ultimate goal was to yield stress versus strain curves for each specimen. The Matlab code imports the data as a text file. Stress is determined by Equation 3.4, thus the width and thickness of the middle of the dogbone was recorded prior to testing.

$$\sigma = F/A_c \tag{3.4}$$

The strain for each specimen is given by Equation 3.5

$$\epsilon = \Delta l/l_0 \tag{3.5}$$

Since the equipment records the load and distance in terms of voltage, various

factors to convert from volts to newtons and millimeters were needed. These factors came from manufactured specified values, and were confirmed with calibrations of the equipment. To determine the load cell conversion of volts to kilograms, a 1 kg weight was placed on the load cell and the change in voltage reading was recorded, thus the conversion factor could be calculated. Likewise, the extensometer would be moved by 1mm to determine the volts per mm conversion factor for strain.

With Equation 3.4, Equation 3.5 and the conversion factors determined from the calibration methods described above, the values for stress and strain could be determined and stress vs strain curves could be plotted. From here Young's modulus could be calculated for the specimen according to Equation 3.6 for the linear region of the stress versus strain curve.

$$E = \sigma/\epsilon \tag{3.6}$$

The broken dogbones were then observed under an optical microscope. The variation in the mechanical performance of dogbones could then be qualitatively described. Distribution, dispersion, Inter-particle distances, number of voids, and other metrics could be gathered from the images and related to the properties.

3.3.3 Thermal Tests

The thermal samples were prepared using the Cincinnati Milacron BabyPlast injection molding machine. The samples needed to be exactly 8mm by 8mm by 2mm squares, and with the chill roller and die zone not being able to accommodated this

specific and consistent thickness, the samples needed to be injection molded.

First, the extruded strips of material were chopped approximately every 4mm using the Killion Extruders Inc. pelletizer. Those strips were then fed into the injection molder feeder. The material was again heated up according to the previously specified temperatures, and filled into the injection chambers as liquid.

Before each run, PBT pellets were put directly into the injection mold chambers in order to purge old material. Furthermore, since PBT is white and the other materials are black, it was used to visually confirm when the material previously molded was out of the chambers and the new material was completely filled in the chambers. Since the liquid dripping from the nozzle would go from white, to grey, to black when the material had been fully changed to the next one, it could then be assumed that the new material was successfully filled in the chambers.

The mold was filled with the liquid, and cooled instantly, thus forming the necessary sample sizes. After making the molds, the samples had to be further prepared for the thermal tests.

The materials were prepared according to the standard operating procedures outlined [66]. Four layers of graphite had to be applied to each side of the sample. Additionally the exact length, width, thickness, and mass had to be measured. The MicroFlash RT - Thermal Properties Measuring System could then be used to calculate the thermal conductivity.

The MicroFlash first uses a pyrex sample to calibrate the laser. Since the density and thickness are given, and the specific heat and thermal diffusivity can be measured, the thermal conductivity can be calculated according to Equation 3.3.

The samples of the composite are placed in the machine, and the laser is used as an impulse of heat so that the temperature rise can be recorded as a function of time. From this, thermal diffusivity and specific heat could be calculated. The measurements from the system are then compared against various theoretical models to determine the thermal conductivity. If there is a good match between the experimental data and the theoretical values, the machine recorded it as one good trial. If the values did not match, the trial was repeated with a different laser intensity or time limit, and the values were again compared. Five good trials for each sample were obtained before switching samples, and several samples per loading of CMF and MWCNT were tested. The thermal conductivity results were normalized against pyrex to account for the changes in calibrations from day to day.

Since PBT was not conductive enough to use this method of testing thermal conductivity, the theoretical value was used for comparison. Once again, the thermal samples were then observed under the an optical microscope to qualitatively observe the degree of mixing after injection molding the material, and to also see if reasons for variance in thermal conductivity could be determined.

Chapter 4

Results and Discussion

Tensile tests and thermal tests were carried out to compare the performance of the material after processing the composite in various combinations of CMF and MWCNT loadings, and using different processing techniques. Optical pictures were taken to examine the difference in dispersion and distribution of the fibers under different conditions. The following sections discuss the results of these tests for each parameter variation.

4.1 Microstructure

The microstructure of the CMF, MWCNT, and PBT composite was examined in detail under an optical microscope, supplemented by SEM images. The quality of mixing, based on the distribution, dispersion, and attrition was observed.

4.1.1 Dispersion and Adhesion

First, the quality of dispersion was assessed. As previously mentioned, dispersion is a measure of how well the fibers are separated and the size and number of agglomerates present in the composite.

A cross-sectional view of the CMF and PBT composite is shown in Figure 4.1, over a range of 5 wt% to 25 wt% CMF.

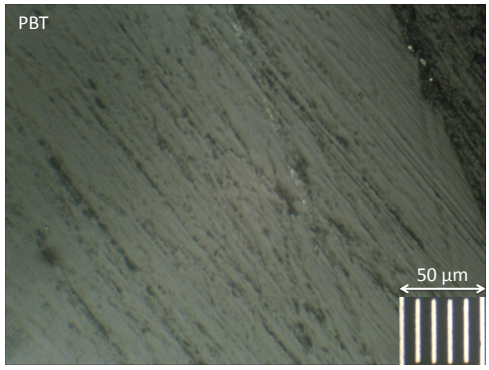

(a) 0 wt% CMF.

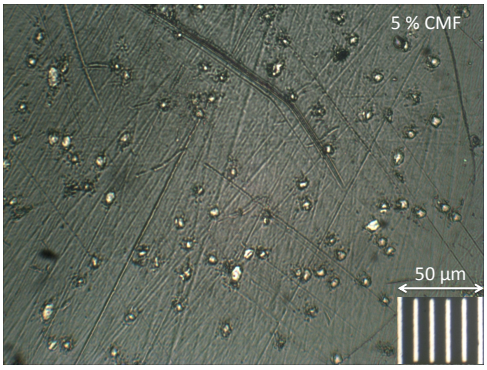

(b) 5 wt% CMF.

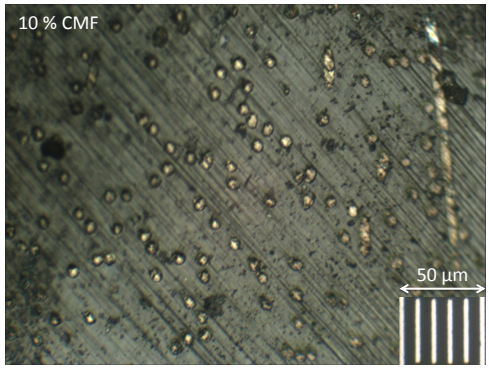

(c) 10 wt% CMF.

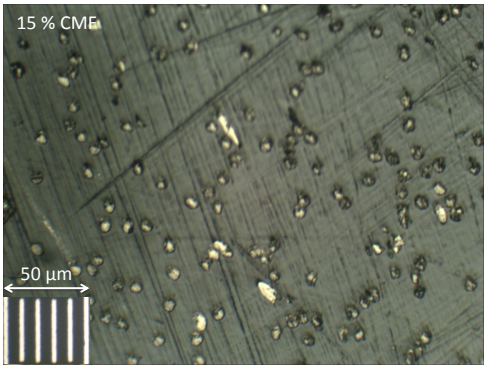

(d) 15 wt% CMF.

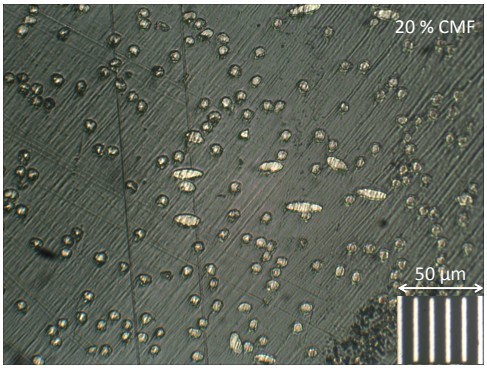

(e) 20 wt% CMF.

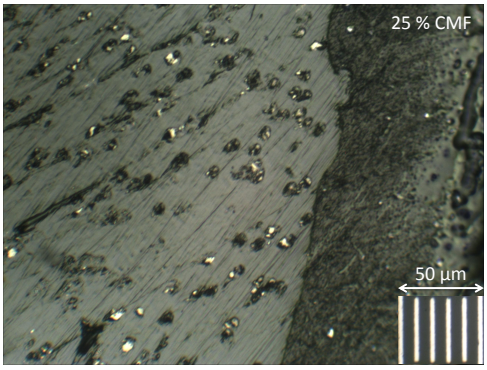

(f) 25 wt% CMF.

Figure 4.1: Optical images for varying wt% CMF at 20X magnification.

With the given scale, and knowing that the CMF diameter is 7μm, it was concluded that each circle shown is indeed one fiber surrounded by polymer. With each fiber being able to individually be seen, the dispersion of the fibers within the polymer matrix was confirmed.

The well dispersed fibers continues as the MWCNTs are added to the composite, as seen in Figure 4.2. Although the MWCNTs are not visible with an optical lens, the CMFs are still well dispersed within the PBT, and therefore the dispersion of the CMFs can be concluded. A closer look at the composite would reveal the quality of mixing of the MWCNTs, however this imaging was beyond the capabilities of the current laboratory set-up. Since the MWCNTs came in a pre-compounded mixture from the PolyOne Corporation, it was assumed that the MWCNTs have been previously dispersed within the polymer matrix, and remain that way throughout the extrusion process.

The adhesion of the fibers to the polymer matrix can be partly assessed with the amount of pull-out observed. Under 15 wt%, there appears to be very little pull-out. Since the optical specimens are the fractured dogbones from the tensile tests, if there is poor adhesion, the fibers would be separated around the area of fracture. Since the fibers remain within the polymer throughout the tensile test, it is concluded that there is little pull-out under 15 wt% CMF loading.

When the loading is increased above 15 wt%, some evidence of pull out can be seen. Figure 4.3 shows SEM images of the difference in pull-out between 10 wt% CMF and 20 wt% CMF. Although at this scale, the pull out at 10 wt% is noticeable, it is more consistent and there are less fibers pulled out when compared to the 20

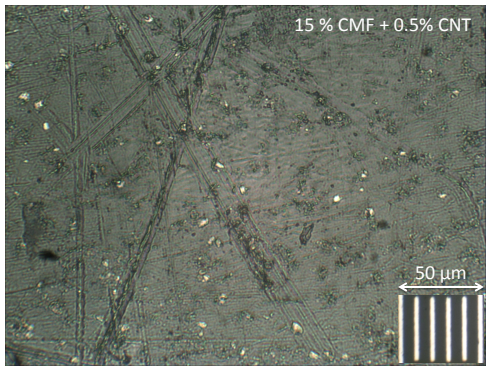

(a) 0.5 wt% MWCNT.

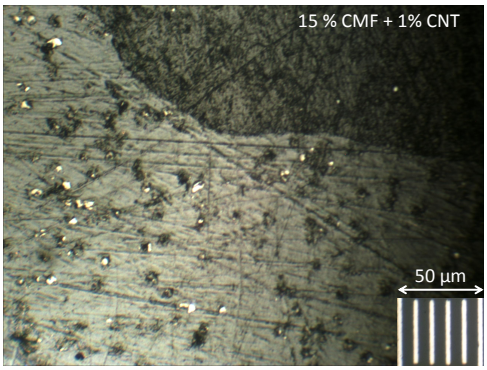

(b) 1 wt% MWCNT.

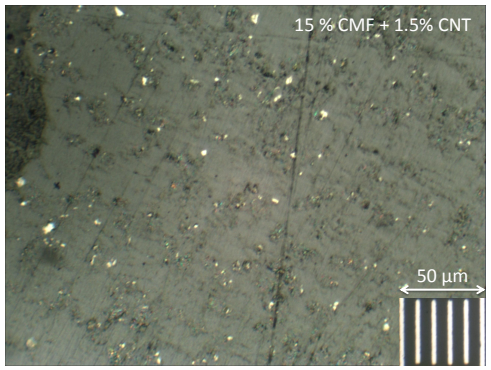

(c) 1.5 wt% MWCNT.

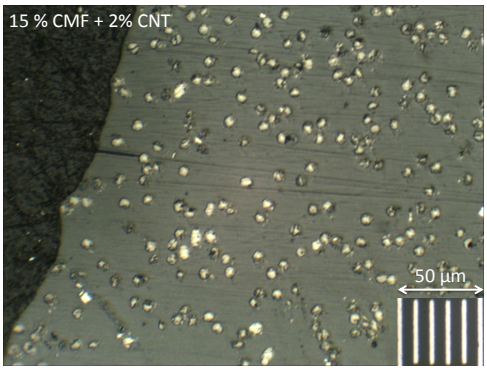

(d) 2 wt% MWCNT.

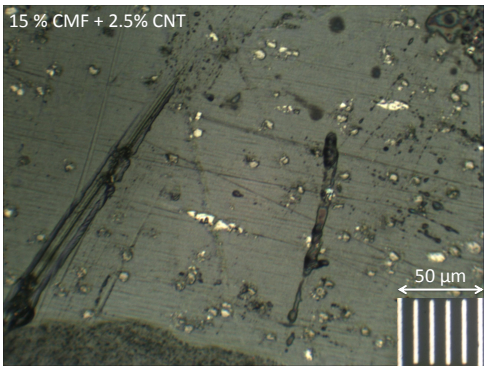

(e) 2.5 wt% MWCNT.

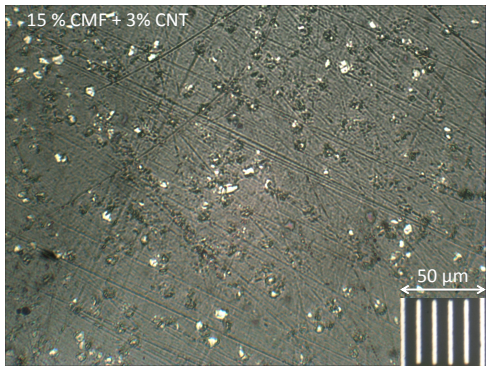

(f) 3 wt% MWCNT.

Figure 4.2: Optical images for 15 wt% CMF and varying wt% MWCNT at 20X magnification.

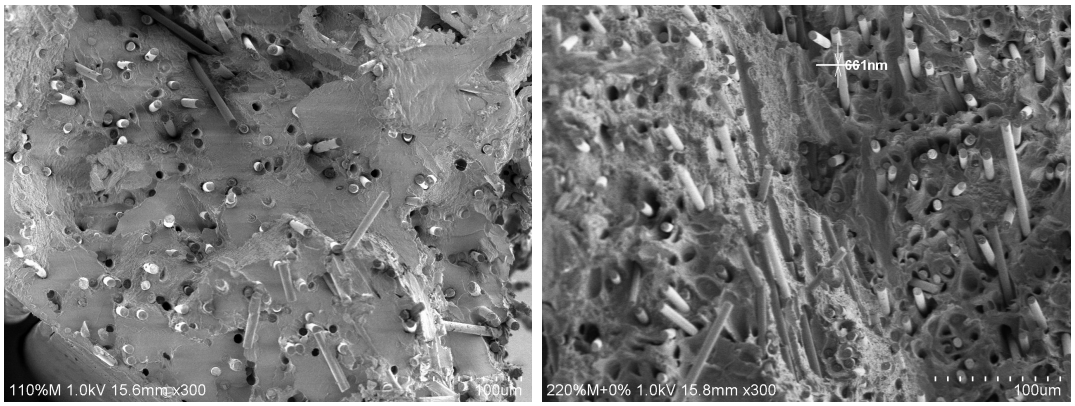

(a) 10 wt% CMF. (b) 20 wt% CMF.

Figure 4.3: SEM images for varying weight percent CMFs at 300X.

wt% CMF.

In both Figure 4.1 and Figure 4.3, there are clear voids in the polymer from where fibers had been previously inserted, however they have been pulled out during testing. This indicates that the adhesion strength between the polymer and matrix was weaker than the composite itself failing due to fracture and is not desirable. These holes are not thought to be air bubbles or other contaminants because of their uniform appearance and the differences when compared to the voids seen later in this section.

4.1.2 Distribution and Alignment

An even distribution of the fibers means that the fibers are evenly spaced throughout the polymer within a set grid. From Figure 4.4, it is clear that this is not the situation for this composite on an optical or SEM scale. However, it is not a completely random distribution either. The fibers tend to stay in a certain area

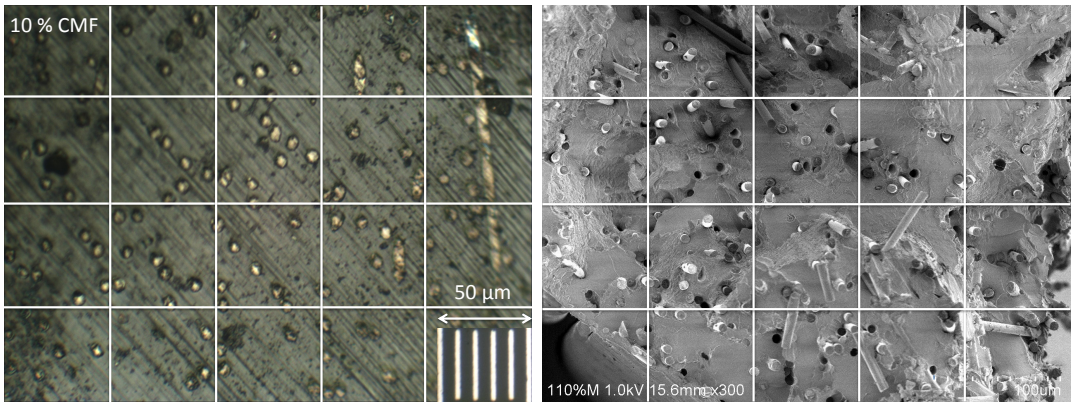

(a) Optical image at 20X. (b) SEM image at 300X.

Figure 4.4: Optical and SEM images for 10 wt% CMF.

without being agglomerates since they are still dispersed. Therefore non-uniform mixing is achieved.

The distribution of fibers is important to achieve consistent properties throughout the composite, however, as long as agglomerates are not formed and there are fibers relatively well distributed within the polymer, the properties seemed to remain consistent. As discussed, dispersion, adhesion, and alignment are the main factors that affect the performance of a composite. For this composite, the alignment of the fibers is predominantly in the direction of flow. This is due to the fact that the die zone used is a slit die that would orient the fibers as they are formed to that shape. The cross sectional view shows all of the fibers perpendicular to the cut. Figure 4.5 shows the axial view of the dogbone specimens, once again showing that the microfibers are predominantly aligned.

Since the extrudate was collected from the die zone in the direction of flow, and the samples were cut directly from these strips, the fibers were aligned and tested

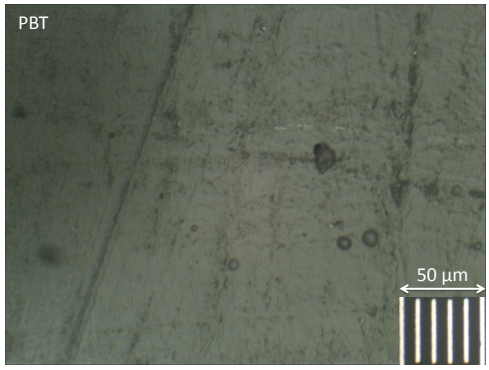

(a) 0 wt% CMF.

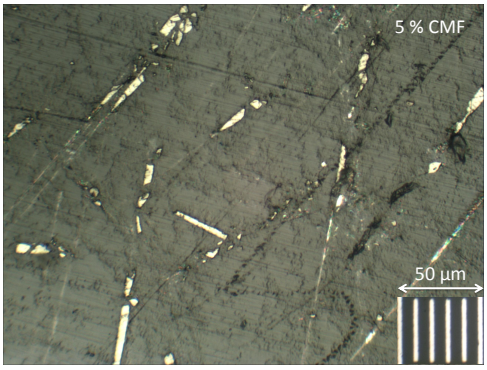

(b) 5 wt% CMF.

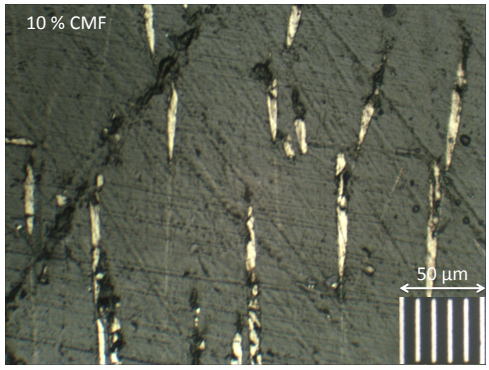

(c) 10 wt% CMF.

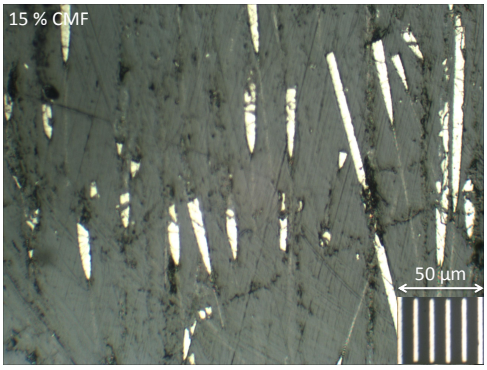

(d) 15 wt% CMF.

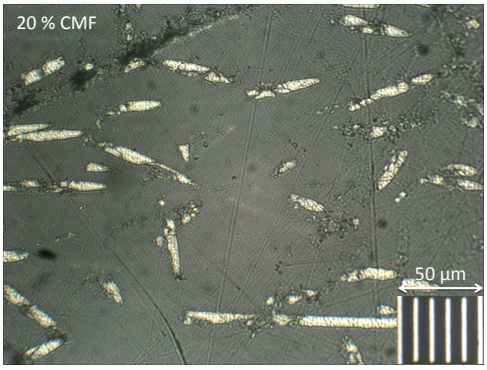

(e) 20 wt% CMF.

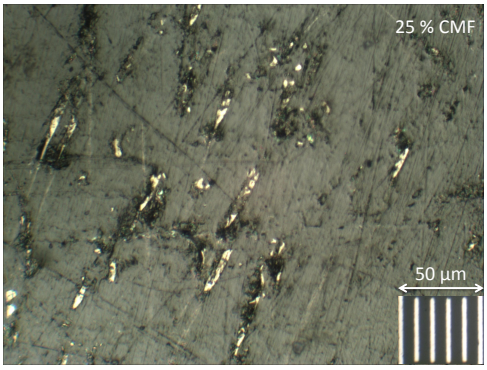

(f) 25 wt% CMF.

Figure 4.5: Axial view of optical images for varying wt% CMF at 20X magnification.

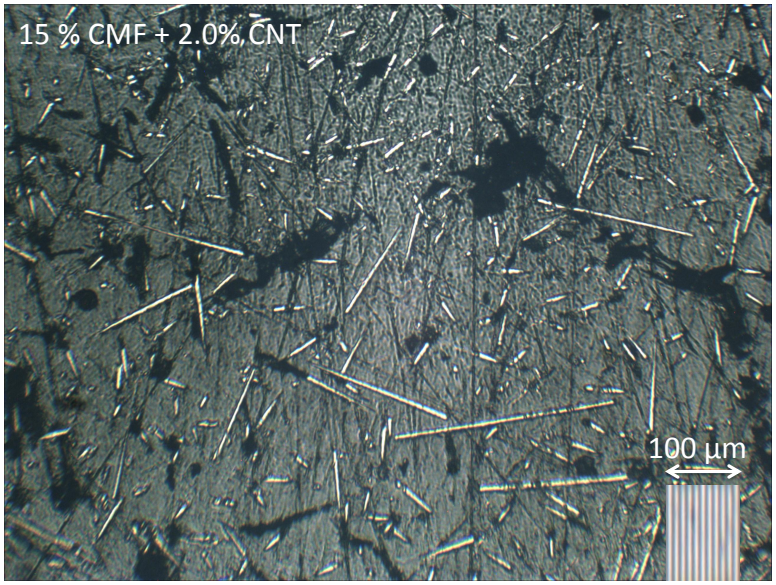

Figure 4.6: Optical image for 15 wt% CMF and 2.0 wt% MWCNT at 5X .

in the axial direction. The axial direction provides a great deal of load transfer and therefore typically shows a higher strength when compared to the transverse direction which pulls perpendicular to the direction of flow. However, as previously discussed, sometimes even the slightest misalignment in the composite can have a significant effect on the resulting properties.

When the samples are then taken and chopped into pieces and injection molded, the alignment of the samples decreases as seen in Figure 4.6.

This representative image shows that the alignment of the fibers in the direction of flow decreases. However, most fibers still seem to be oriented in the same, axial direction, and therefore when tested for thermal properties, the transverse direction is being tested. The fibers seem to be significantly more damaged after being pellitized and injection molded, which can have effects on the properties, as discussed in later sections.

4.1.3 Contaminants and Attrition

Often times when processing material in a twin screw extruder, a vacuum port is needed to remove air and other contaminants from the material. A vacuum pump was set up at the end of the extruder just before the die zone where the material exited and was collected. Previous work had shown that the closer to the die zone the vacuum port is placed, the better the reduction in air entrainement observed [3].

Optical images were obtained for material processed with no vacuum, vacuum at 5 inches of mercury (Hg), and vacuum at 25 inches of Hg and are shown in Figure 4.7. The images show clear voids when the vacuum is not used. When at 5 inches of Hg, there are some voids present around the fibers, but a majority of the voids and contaminants have been removed. When the suction of the vacuum was increased to 25 inches Hg, the voids virtually disappear. The reduction in defects is thought to improve the properties of the material and will be discussed further in this chapter. Although around the fibers there are still some voids, this is expected when processing in a TSE.

Attrition, or breaking of the fibers, is also evident at loadings above 15 wt% CMF. The fibers start to break apart, noticeable by the pieces that are smaller than the diameter of a fiber. It is also evident when examining the axial view in Figure 4.5. Once again the fibers seem to break up at a loading above 15 wt%. The axial view of the samples in Figure 4.5 shows that although the fibers remain clumped in a line, they are indeed broken since there is polymer sitting between the

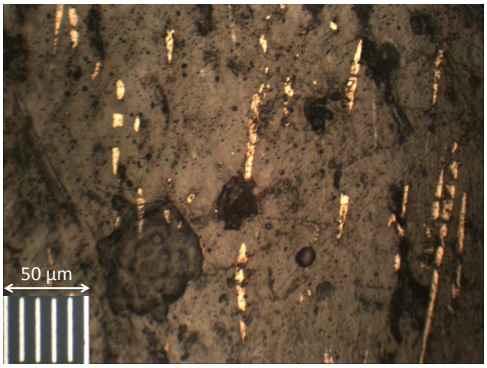

(a) 15 wt% CMF no vacuum.

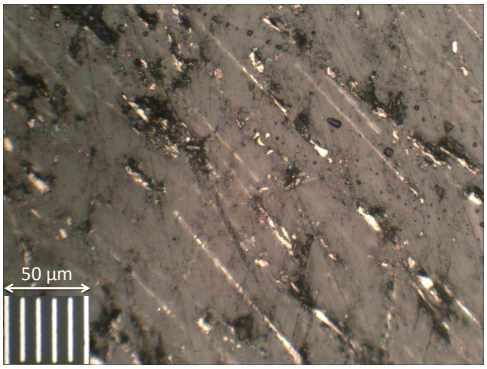

(b) 15 wt% CMF Vacuum at 5 in Hg.

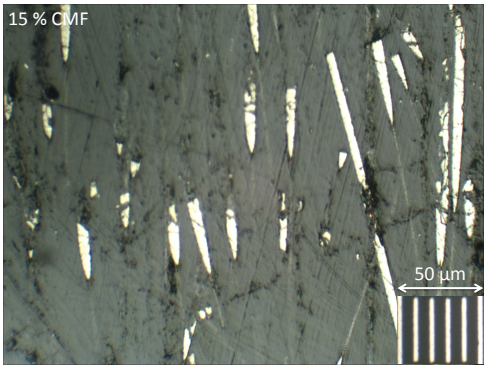

(c) 15 wt% CMF Vacuum at 25 in Hg.

Figure 4.7: Optical images for 15 wt% CMF with and without a vacuum at 20X magnification.

chunks of fibers.

The length of the fibers is also being significantly shortened when looking at the axial view of the composite. However, the fibers may be longer than appear in the images since they could be slightly angled down with a thin layer of polymer preventing the entire length of the fiber from showing in the optical images.

Although a relatively mild mixing section was used, the fibers are still experiencing damage at increased loadings. It is possible that the fibers start to damage each other and cannot mix with the polymer easily enough as to not cause attrition. However, a closer study of the polymer at various loadings and at a closer magnification may reveal more information.

4.2 Mechanical Properties

The tensile properties of the composite were tested for various processing conditions, loadings of CMFs and MWCNTs, and different sized specimens.

4.2.1 Processing with Devolatilization

Extrusion can often times introduce air and other contaminants when processing material, especially when there are fillers in a polymer matrix. Thus, the effects of these volatiles were studied by processing the composite with a vacuum present at the end port at 5 inches of Hg, 25 inches of Hg, and without the vacuum. Tensile tests were performed for neat PBT, 10 wt%, 15 wt%, and 20 wt% CMF for all vacuum conditions with a Q and N of 4 lbs/hr and 200 rpm, respectively. The

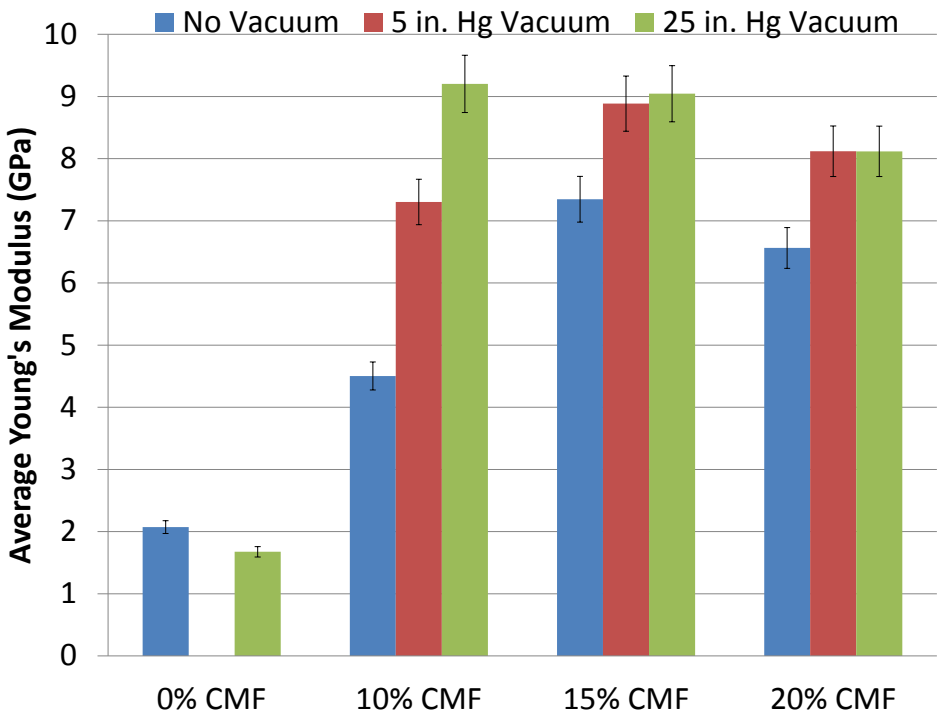

Figure 4.8: Mean young's modulus for vacuum vs. no vacuum.

young's modulus for the samples was calculated from the results of the tensile tests and is plotted in Figure 4.8.

The difference in mechanical performance under the various processing conditions was very evident. When there was no filler added, the vacuum did not change the resulting young's modulus significantly. However, when processing the material with a vacuum, the young's modulus was greatly improved. Not only did processing the material under vacuum give a much higher E value, but the consistency of the results was very noticeable as well.

The ultimate stress the composite reached also increased when using a vacuum at the end port. Figure 4.9 shows the results.

These results are consistent with what was expected after observing the differ-

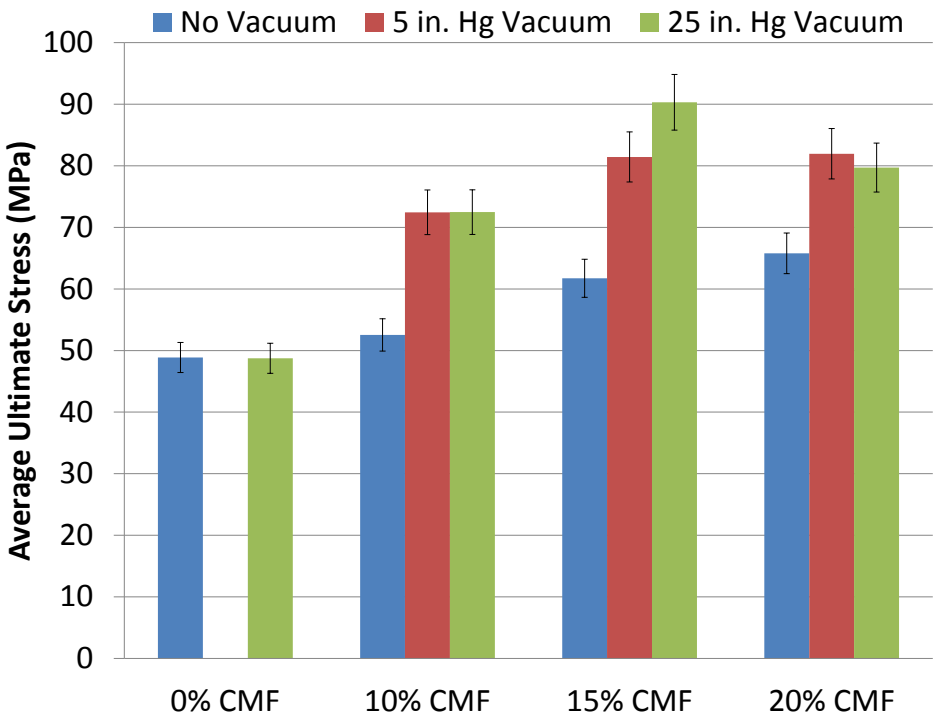

Figure 4.9: Mean ultimate stress for vacuum vs. no vacuum.

ent materials under an optical microscope. As predicted, when the voids, air, and defects were reduced, the mechanical properties were greatly enhanced. Even when the vacuum suction was only at 5 inches of Hg, that little bit of suction aided in removing the volatiles from the composite so that the properties could be further enhanced.

At 10 wt% CMF, the difference in vacuum suction made a difference for the young's modulus, however at higher loadings, this difference was negligible. This could be because higher loadings forced more air out by the nature of the mixing within a TSE. It is also reasonable that the two vacuum pressures showed similar results for both young's modulus and maximum stress because from the optical pictures in Figure 4.7, the difference in voids between material processed under

vacuum at 5 inches of Hg and 25 inches of Hg was minimal.

4.2.2 Varying Loading of CMF

First, the characterization of tensile properties for different weight percent of CMFs was performed. All of the following materials discussed were processed with vacuum suction of 25 inches of mercury at the end port, at 4 lbs/hr and 200 rpm. Tensile tests were performed for neat PBT, 5 wt%, 10 wt%, 15 wt%, 20 wt%, and 25 wt% CMF.

As mentioned before, the tensile tests were performed on sub-standard size dogbone specimens. This size specimen is compared to larger ASTM size specimen in a later section in order to validate the results. Several trials were performed for each specimen, with a minimum of five good trials recorded for each material. Results from representative tensile tests are shown in Figure 4.10.

From the stress versus strain curves, it is apparent that the the strength of the composite is significantly increased over PBT which tested at an average ultimate strength of 48.74 MPa ($\pm$ 2.07). This demonstrates that the processing of the material indeed achieved a high enough degree of adhesion and dispersion to support load transfer from the polymer matrix to the carbon fiber filler. Similarly, the elasticity of the composite decreases significantly when compared to plain PBT which tested at a strain typically around 12.1% ($\pm$ 2.90). This is expected since the fibers are far more brittle than the polymer, and therefore increase the stiffness of the composite.

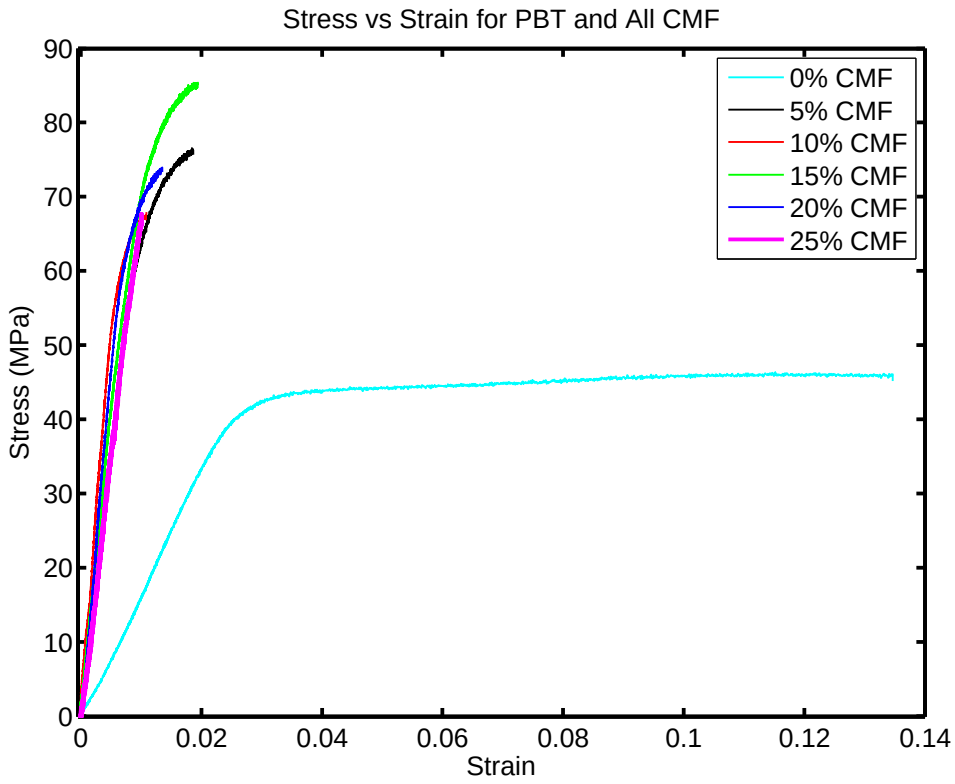

Figure 4.10: Stress vs. Strain for various weight percent CMF and PBT.

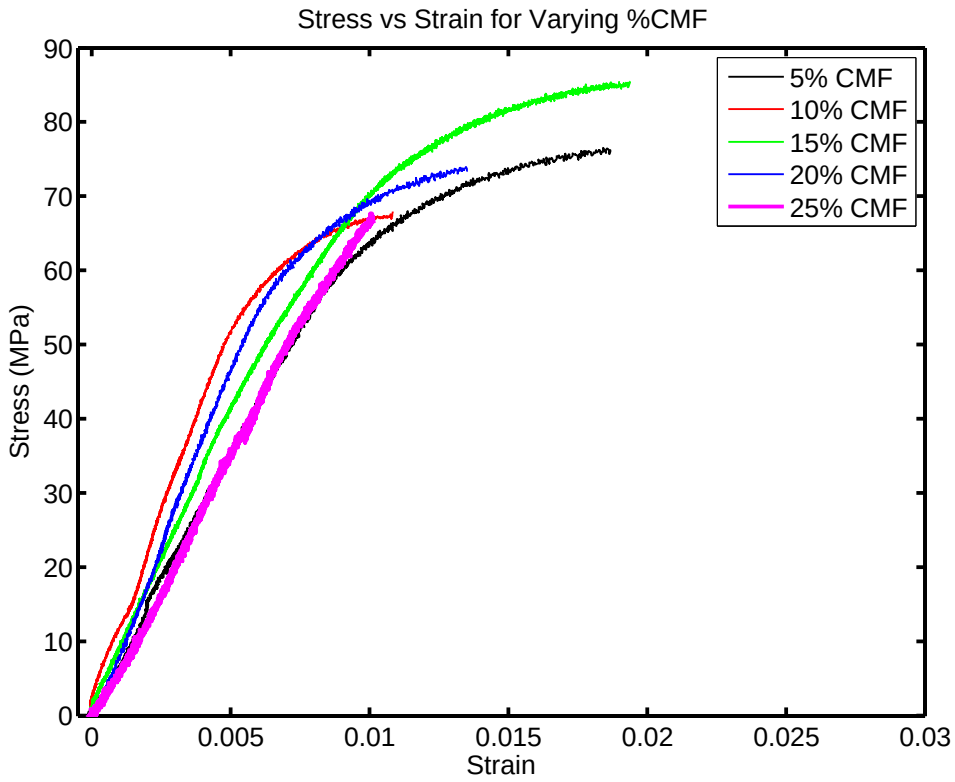

Figure 4.11: Stress vs. Strain for various weight percent CMF.

Once the clear difference between the neat resin and the composite was established, the difference in mechanical properties depending on the amount of filler was studied extensively. A closer look at the stress vs. strain curves with only the varying loadings of CMF is shown in Figure 4.11.

This shows that there is a dependence between the loading of CMF and the resulting mechanical properties. To further observe this pattern, young's modulus for the elastic region was calculated according to Equation 3.6 for each material. The average modulus value is plotted for neat PBT, 5 wt%, 10 wt%, 15 wt%, 20 wt%, and 25 wt% CMF, as shown in Figure 4.12.

The addition of CMFs increased the young's modulus significantly over neat

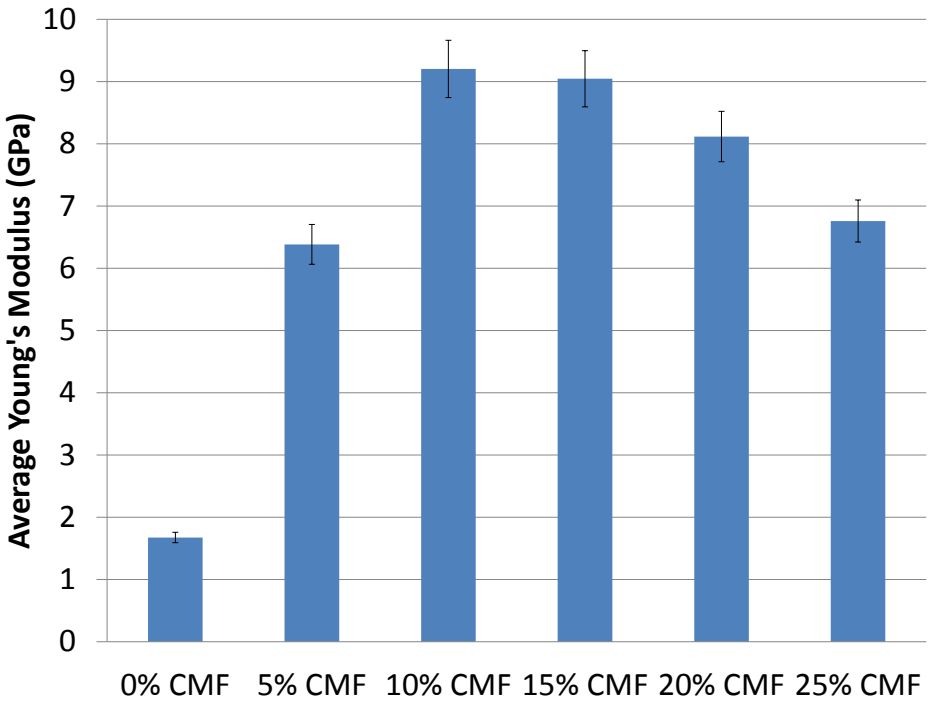

Figure 4.12: Mean young's modulus for various weight percent CMF.

PBT. Single-factor ANOVA was performed to determine statistical significance between the means at a 90% confidence level. All of the samples were statistically different from PBT, and there was statistical difference among 5 wt%, 10 wt%, 15 wt%, 20 wt%, and 25 wt% CMF.

At 5 wt% CMF, the young's modulus was increasing, but had not yet reached its maximum. Between 10 wt% and 15 wt% CMF, the maximum young's modulus is observed. At loadings above 15 wt% and below 25 wt%, the young's modulus started to decrease again. This is consistent with what was observed under the optical microscope. Around 15 wt% CMF, there seemed to be attrition of the fibers, which would decrease mechanical performance. The average ultimate stress was also recorded for the range of CMF loading and is shown in Figure 4.13

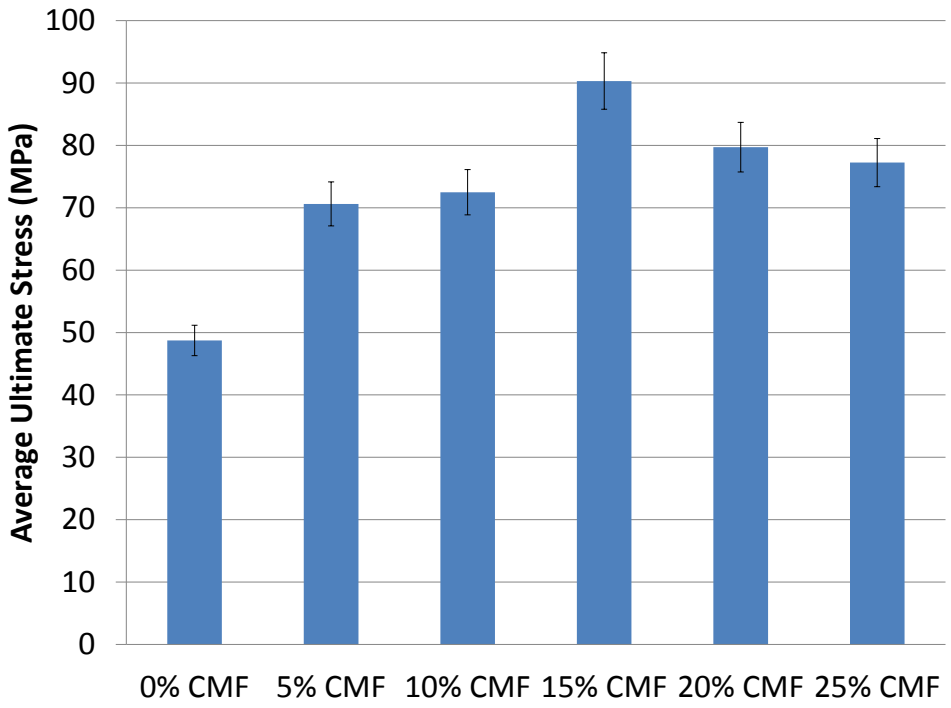

Figure 4.13: Mean ultimate stress for various weight percent CMF.

The average ultimate stress peaked around 15 wt% CMF, as seen with previous properties. This once again may be due to the fact that below 15 wt% CMF, the mechanical strength is still increasing and more load is continuing to be transferred to the fibers. At 15 wt% CMF, the maximum load is reached that benefits the mechanical strength. Between 15 wt% and 25 wt% CMF, the strength decreases which could be because the adhesion and attrition observed in the samples. Furthermore, there may be a threshold of microfiber that the polymer matrix can support without being broken down and where rheological effects start to take part. Repeated trials showed this trend of stiffening the material, with a peak of strength and stiffness at 15 wt% CMF.

4.2.3 Varying Loading of MWCNT

Initial results from varying the loading of CMF showed that between 10 wt% and 15 wt% CMF yielded the highest young's modulus. Thus a detailed study where the amount of MWCNT was varied within the composite was conducted with 15 wt% CMF to see if MWCNTs could further improve properties with a multi-scale composite with fillers in both the micro and nano scale lengths. Once again, all of the following materials discussed in the this section were processed at 4lbs/hr and 200rpm while pulling vacuum of 25 inches of Hg at the end port before the extrudate exited the extruder.

Tensile tests were performed on sub-standard size dogbones at 15 wt% CMF with 0 wt%, 0.5 wt%, 1.0 wt%, 1.5 wt%, 2.0 wt%, 2.5 wt%, and 3.0 wt% MWCNT. After repeated trials, with a minimum of five acceptable trials per material, the average young's modulus and ultimate stress was calculated. Stress vs. strain curves are shown in Figure 4.14 that represent typical results for these materials.

The addition of MWCNTs caused the material to become more brittle and stiffer. In some cases, the level of loading of MWCNTs caused a decrease in strength and ductility. To further examine the trends with both CMFs and MWCNTs, the average young's modulus was calculated for each composite and is shown in Figure 4.15.

Figure 4.15 shows that there may be a decrease in improvement as more MWCNTs are added until the loading of MWCNTs reaches a certain level, and then the MWCNTs aid in restoring the modulus to its original value. MWCNTs loading of

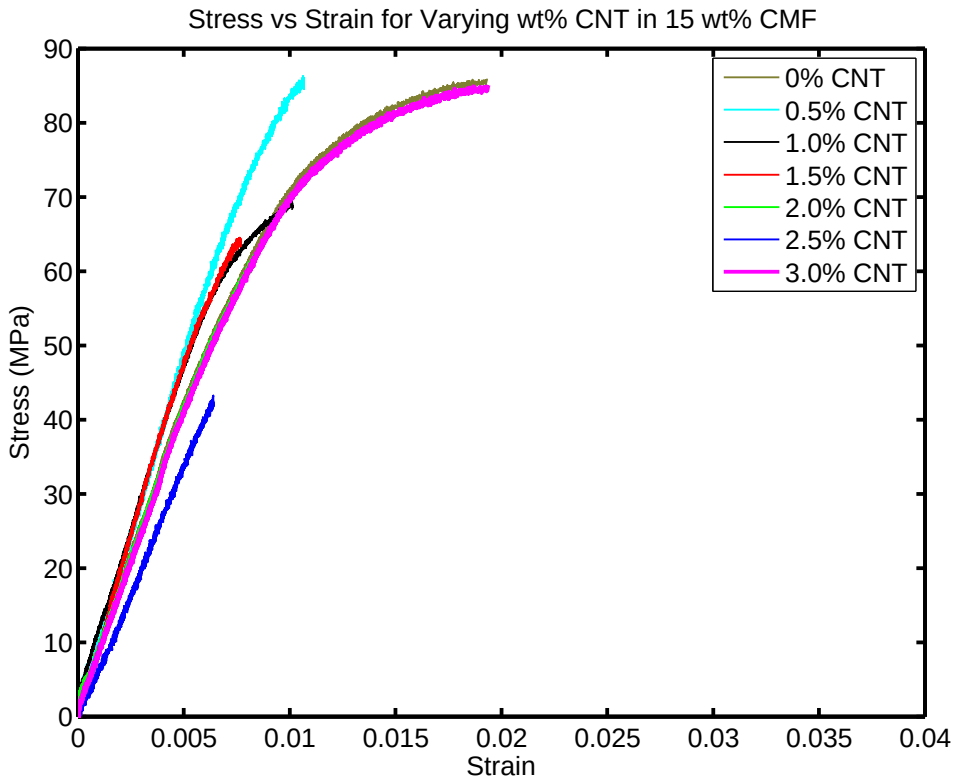

Figure 4.14: Stress vs. strain for 15 wt% CMF and varying weight percent MWCNT.

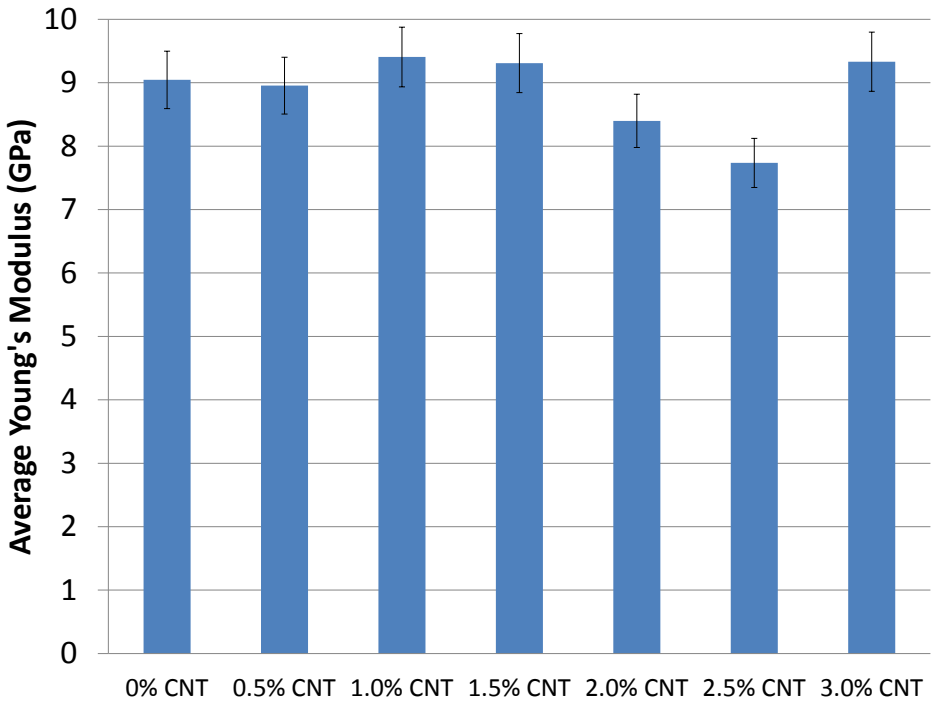

Figure 4.15: Mean young's modulus for 15 wt% CMF and varying wt% MWCNT.

0 wt% to 1.5 wt% show essentially the same value for young's modulus of around 9 GPa. This value starts to decrease to as MWCNT loadings approach 2.5 wt%, where the modulus decreases to 7.5 GPa. Then between 2.5 wt% MWCNT and 3.0 wt% MWCNT, the young's modulus once again approaches a value of 9 GPa. This may be explained because between 0 wt% and 1.5 wt% MWCNT, the nano particles do not alter the overall structure of the composite and the general stiffness of the composite remains constant. Furthermore, the presence of the MWCNTs may delay the attrition effects seen in the CMF only samples. At an optical level, there was no change in the structure from the nanotubes, and the attrition did not appear until after 2 wt% MWCNT, so this may be a valid assumption, however this would need confirmation with further studies, such as detailed SEM images. As the loading is

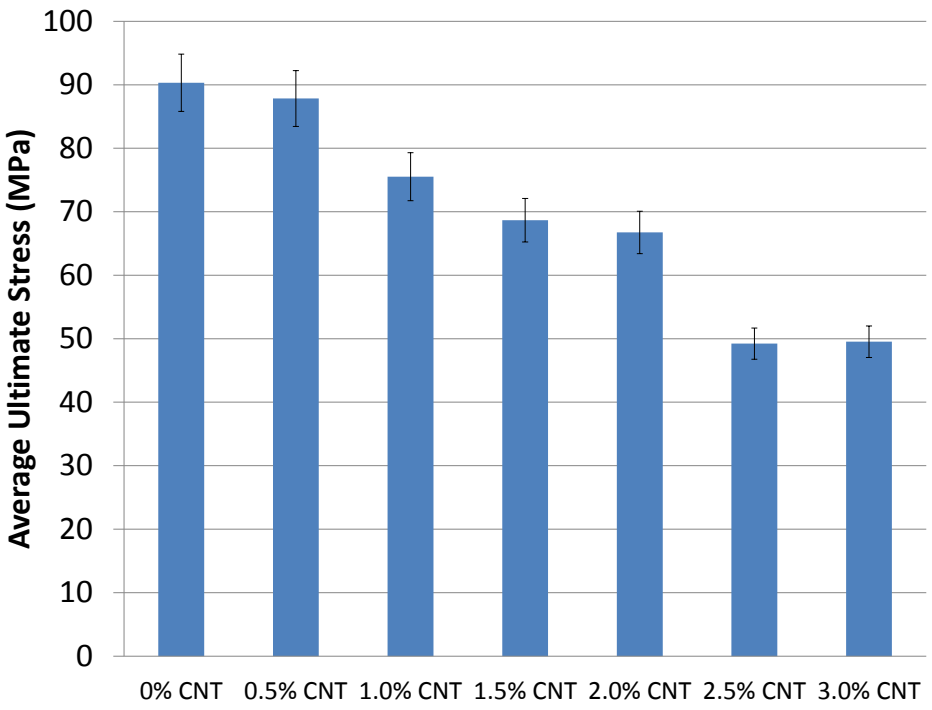

Figure 4.16: Mean ultimate stress for 15 wt% CMF and varying wt% MWCNT.

increased beyond a certain level, the stiffness is reduced because of possible agglomerates and attrition forming at this level of loading. The stiffness may then increase again since there are enough MWCNTs that even with some defects, the stiffness can increase because of the polymer, CMF, and MWCNT network that forms at this level. It may be something similar to a delayed percolation level sometimes seen with properties, especially with electrical properties.

To further characterize the tensile properties, the maximum stress for the samples was recorded and averaged at each loading, as seen in Figure 4.16.

The ultimate stress seen for each sample has a clear decreasing trend. At 0 wt% MWCNT, the maximum ultimate stress is observed, and this decreases as the loading of MWCNTs increases. This may be because agglomerates are forming in

the composite where the stiffness may not be greatly affected, however, the strength of a composite can be significantly affected with the presence of agglomerates and poor adhesion. Furthermore, the nano particles may cause more defects when processing the material, and thus the defects are showing as reductions in strength. The imaging of the MWCNT samples could not observe the MWCNTs since they were too small for the given capabilities, so once again, further examination in to the microstructure of the composite is necessary to help reveal more information about the decrease in strength.

It is seen that after the initial gain in strength with only CMF as the filler, the strength is reduced with the addition of MWCNTs. The trend when adding MWCNTs seems to also follow that as more MWCNTs are added, the stiffness and strength is generally reduced. While the addition of MWCNTs clearly increases the stiffness when compared to a PBT modulus of around 1.5 GPa, the ultimate stress is not improved when compared to PBT. At loadings above 2.0 wt% MWCNT, the maximum stress drops from over 60 MPa down to 49 GPa. The average maximum stress for neat PBT was seen around 48 GPa, therefore there is virtually no increase in strength at higher loadings of MWCNT. Thus, the optimal amount of MWCNTs would be from 0 wt% MWCNT to 0.5 wt% MWCNT since this maintains the same modulus and does not reduce the strength of the composite when compared to a CMF filled composite only.

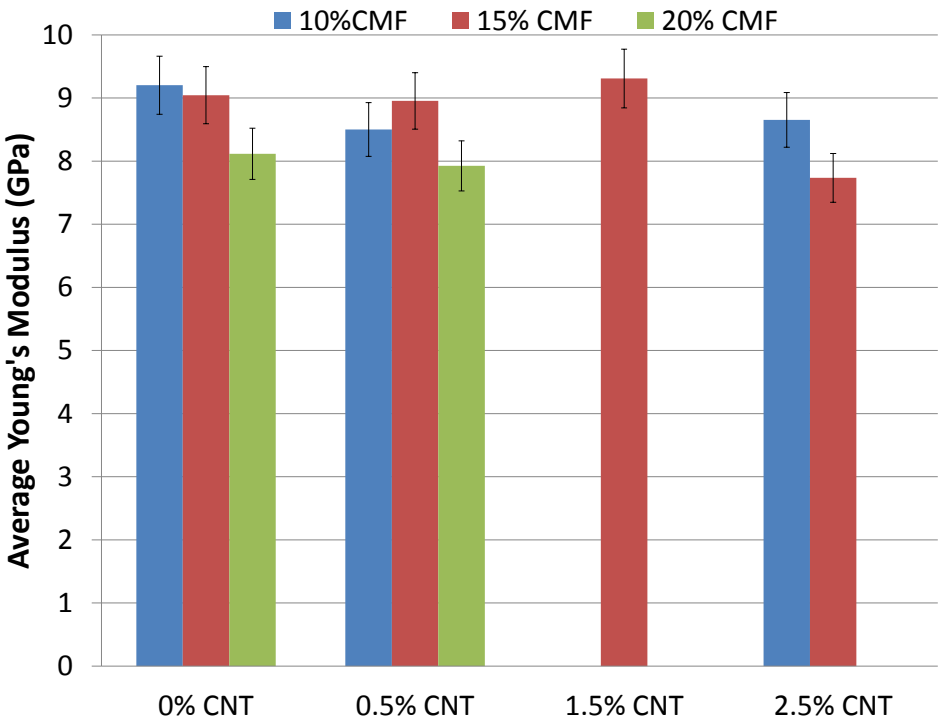

Figure 4.17: Mean young's modulus for varying wt% CMF and varying wt% MWCNT.

4.2.4 Varying CMF and MWCNT Loading

After observing the trends of varying the weight percent of MWCNTs within 15 wt% CMF, the wt% MWCNT was varied for 10 wt% CMF and 20 wt% CMF from 0.5 wt% MWCNT to 2.5 wt% MWCNT by 1.0 wt% MWCNT increments. All of the materials were processed at 4 lbs/hr and 200 rpm with a vacuum suction of 25 inches of Hg at the end port.

Tensile tests were performed on sub-scale specimens and the mean young's modulus and mean ultimate stress of a minimum of five samples are shown in Figure 4.17 and Figure 4.18, respectively. Due to equipment malfunction, the results for every condition are not presented.

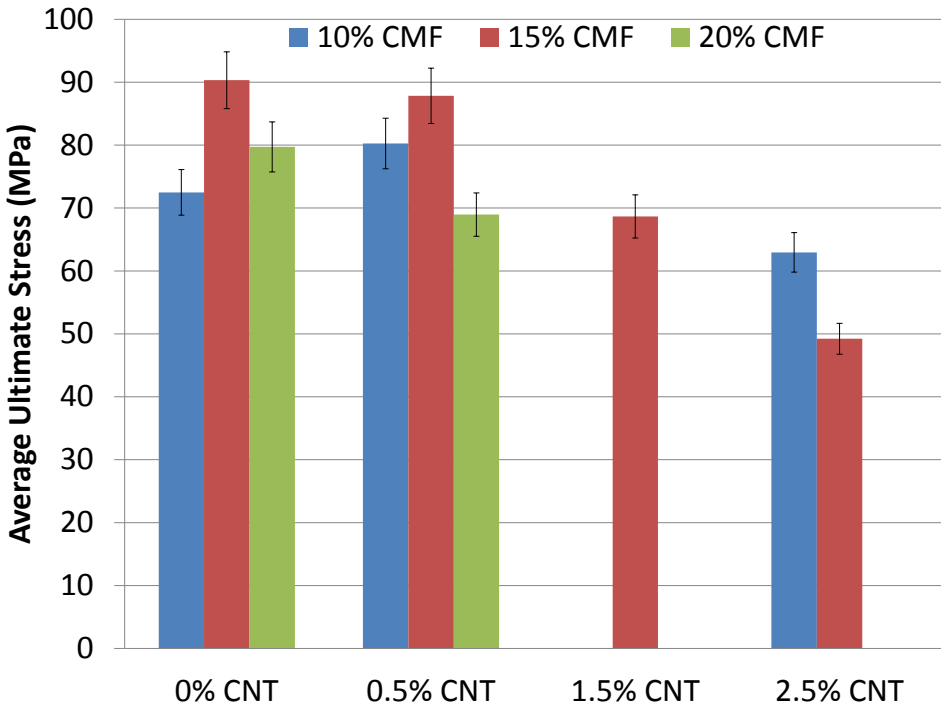

Figure 4.18: Mean ultimate stress for varying wt% CMF and varying wt% MWCNT.

The addition on MWCNTs in general did not improve the overall strength or stiffness of the composite, consistent with what was observed at 15 wt% CMF. With 10 wt% CMF, the MWCNTs did not reduce the stiffness significantly, however, the ultimate strength was greatly reduced at the higher loadings of MWCNTs. As previously mentioned, with 15 wt% CMF, the stiffness begins to drop off at loadings above 1.5 wt% MWCNT, and strength is reduced with the higher loadings of MWCNTs. Lastly, with 20 wt% CMF, this trend continues, where stiffness is maintained at low levels of MWCNT, but with 20 wt% CMF, the strength already beings to diminish even at low loadings of MWCNT of 0.5 wt% MWCNT. Thus, even with varying amounts of CMF, the overall trend of eventual reduction in stiffness and almost immediate reduction in strength with increasing amounts of MWCNTs

Table 4.1: Q/N values for the various flow rate and screw speed combinations.

Flow Rate (lbs/hr)	Screw Speed (rpm)	Specific Throughput (mL/rev)
2.7	200	0.136
4.0	200	0.202
5.3	200	0.267
6.6	200	0.333

is evident.

4.2.5 Varying Flow Rate

Previous studies showed that varying the specific throughput, Q/N, while processing composites can have a significant effect on the properties of the composite. For this study, the flow rate at which the material entered the extruder was varied while the screw speed was kept constant at 200 rpm. With a maximum CMF loading set at 15 wt% CMF, 6.6 lbs/hr was the maximum achievable flow rate through the extruder, thus this along with flow rates of 2.7 lbs/hr, 4 lbs/hr, and 5.3 lbs/hr were selected. Once geometric considerations are taken into account, the Q/Ns for the various flow rates were calculated [7] and are listed in Table 4.1. All of the materials were processed with a vacuum at the end port pulling 25 inches of Hg.

Tensile tests were performed on ASTM D638 type IV dogbone specimens for

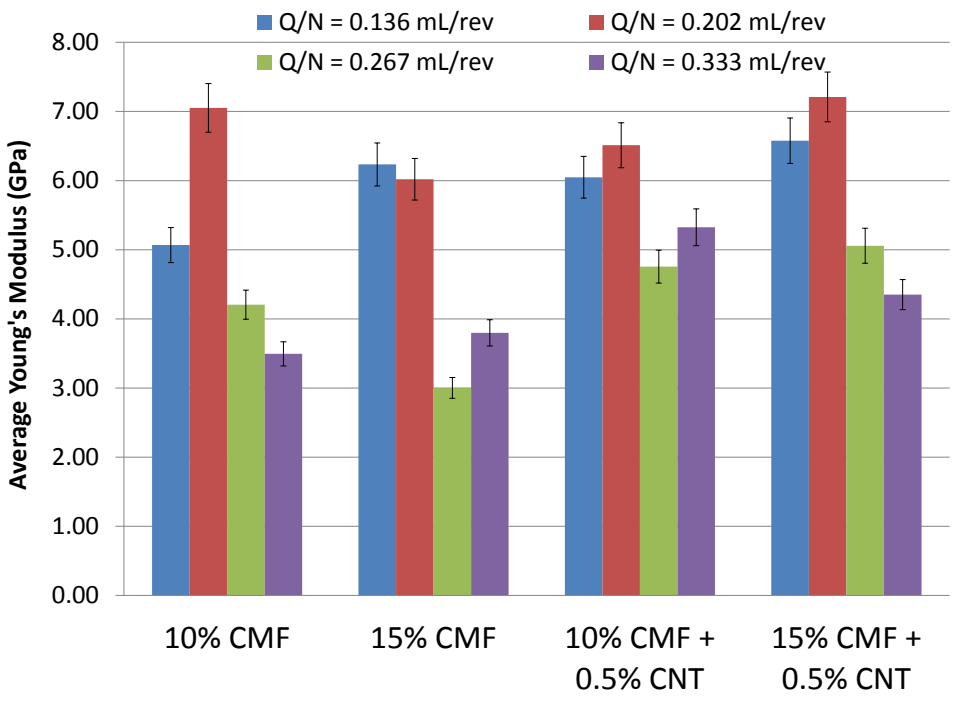

Figure 4.19: Mean young's modulus for various Q/N.

various amounts of CMF and MWCNT filler and the different specific throughputs. The average young's modulus was calculated for each material and is displayed in Figure 4.19.

Figure 4.19 shows that in general, material processed at a Q/N of 0.202 mL/rev yielded the highest young's modulus. Material processed at 0.136 mL/rev also showed a higher modulus when compared to those processed at higher Q/Ns of 0.267mL/rev and 0.33 mL/rev. While this trend may seem contrary to what would be expected, there are several possible explanations. Typically with a higher Q/N, more break up is observed in the filler. While this usually means that the agglomerates are more likely to break up and that the filler would be better dispersed, in this case the higher break up could be damaging the CMFs and MWCNTs.

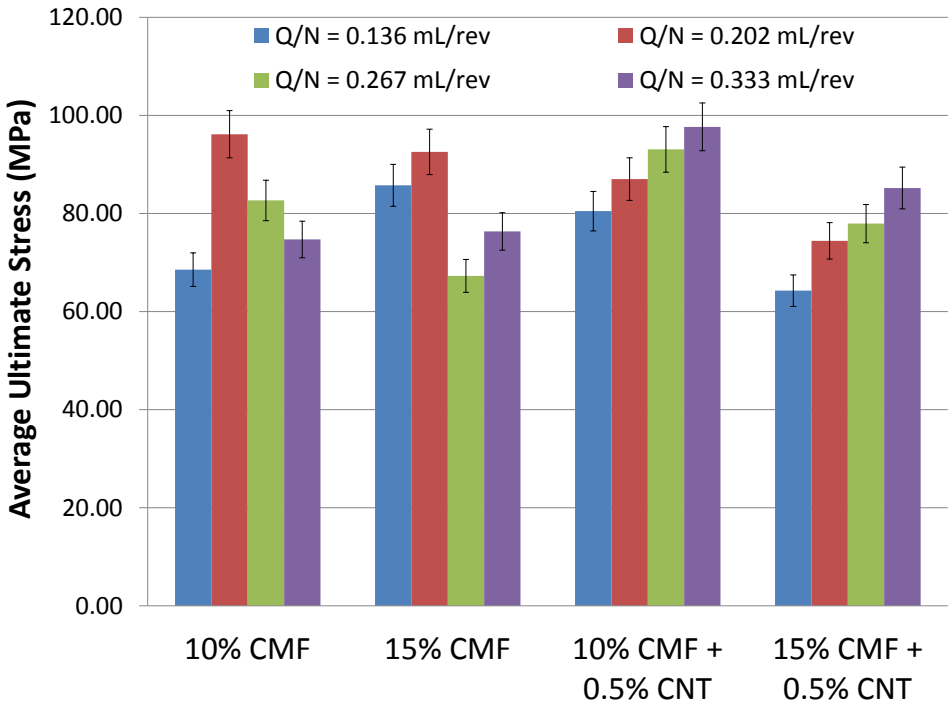

Figure 4.20: Mean ultimate stress for various Q/N.

Furthermore, two different phenomena may be occurring. From physical inspection, the material processed at 0.136 mL/rev seems to more ductile than the others. This ductility would be shown through a lower young's modulus. Then, as previously mentioned, the higher Q/N may be compromising the material, once again showing as reduced ductility. To further examine the possible phenomena occurring by varying the Q/N, the ultimate stress was recorded and averaged for a minimum of five samples per material, as shown in Figure 4.20.

Figure 4.20 shows that when there are MWCNTs in the composite, a higher Q/N yields a higher maximum stress. On the other hand, when there are only CMFs, a Q/N of 0.202 mL/rev produces the highest maximum stress at both 10 wt% and 15 wt% loading. The other Q/Ns produce similar results at 10 wt% CMF

loading, and the Q/N of 0.136 mL/rev has slightly higher ultimate stress at 15 wt% CMF. Using this knowledge and that from the young's modulus, certain conclusions can start to be drawn.

It seems that a higher Q/N helps break up the MWCNTs and disperses them within the polymer composite. MWCNTs generally make the material more brittle and stiffer, resulting in a higher modulus when compared to CMF only composites. This is indeed the case for the higher Q/Ns. Since the MWCNTs are not forming agglomerates and are being better mixed with the polymer, they can also transfer more load and increase the strength. Therefore, it may be expected that with increased loading of MWCNTs and increased Q/Ns, the resulting composite improves on its mechanical properties.

With the CMF loading it seems that the higher Q/Ns may be damaging the CMFs more than aiding in mixing them since as the wt% CMF increase, the modulus and strength both decrease overall. 0.136 mL/rev is the exception to the previous statement, which further supports it. At the lowest Q/N, agglomerates may still be present because there is not enough stress to separate the bundles of CMF, thus reducing mechanical properties at this level and allowing the properties to be improved at a slightly higher Q/N. At the lower-end Q/N, less attrition is occurring, and thus the added CMFs are transferring more load and improving the properties of the material. Therefore overall, it may be concluded that for composites with nano scale ingredients, higher Q/Ns improve mechanical properties, however composites with micro scale ingredients should use lower Q/Ns to avoid damage. Thus, with a multi-scale composite, a compromise must be selected, which seems to be, for this

material, around 0.202 mL/rev.

4.2.6 Inherent Variability with Extrusion

Extrusion presents an inherent variability within in the material. The free volume in an extruder can be calculated, and with the free volume a characteristic length can be determined [69]. The characteristic length is supposedly a length of material that has consistent properties. To test this, the characteristic length was determined from Equation 4.1.

$$\lambda = \frac{Free\ Volume}{Cross\ Sectional\ Area\ of\ Collected\ Strip} \tag{4.1}$$

The cross sectional area of the collected strip was directly measured for the 15 wt% CMF strip collected. The free volume for the given mixing section of one wide kneading block and one narrow kneading block is shown in Equation 4.2. It is important to note that the free volume is the same throughout the extruder and does not depend on the element type, therefore the free volume and dimensions of wide and narrow conveying elements can be related to the free volume for wide and narrow kneading blocks.

$$FreeVolume = n * c * l_w * h + n * c * l_n * h \tag{4.2}$$

In Equation 4.2, n is the number of screws, in this case 2, l_w and l_n are the widths of the wide and narrow kneading block channels, approximately 7 mm and 4 mm respectively. c is the circumference of the screws, in this case π * 28 mm since the screw diameter is specified as 28 mm, and h is the height of the channel, which is

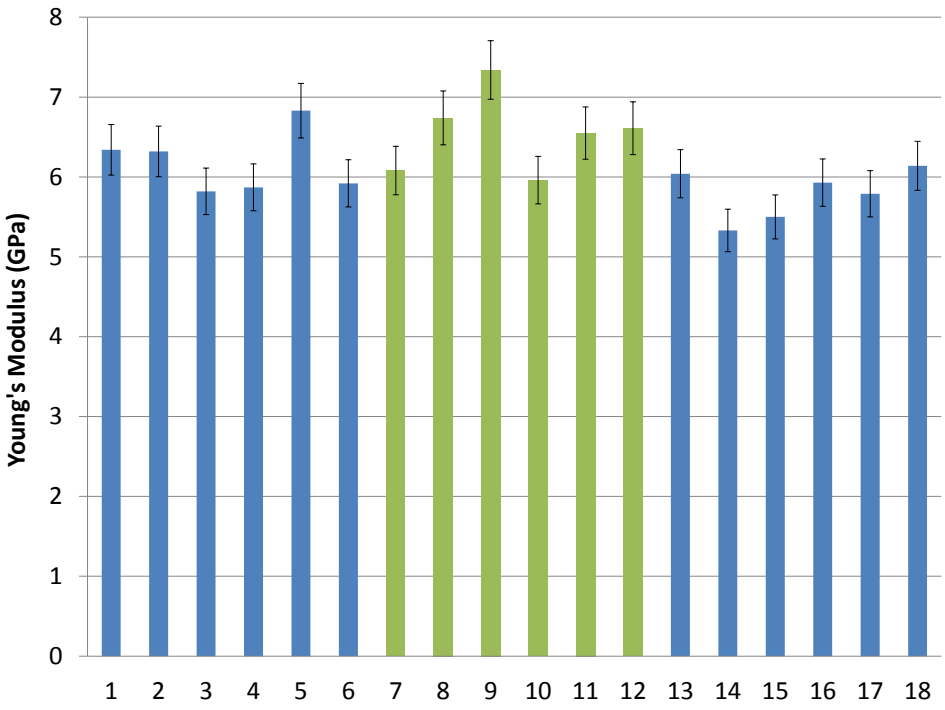

Figure 4.21: Young's modulus for 3 characteristic lengths at 15 wt% CMF.

approximately 5 mm for these elements. Using the given values and equations for the current screw configuration, the characteristic length was calculated to be 763.4 mm.

After the calculation of the characteristic length was completed, strips of 763.4 mm were cut and kept in sequential order for 15 wt% CMF. For this study, larger specimens of ASTM D638 type IV were used, since the consistency with the equipment to test these size dogbones was more reliable and the sequential order of the specimens could be maintained. Thus, within 763.4 mm, 6 dogbone specimens could be cut. The length was taken for 3 consecutive 763.4 mm section. The young's modulus and ultimate stress are shown in Figure 4.21 and Figure 4.22 for each specimen. The position of the dogbone is shown along the x-axis primarily to reinforce that

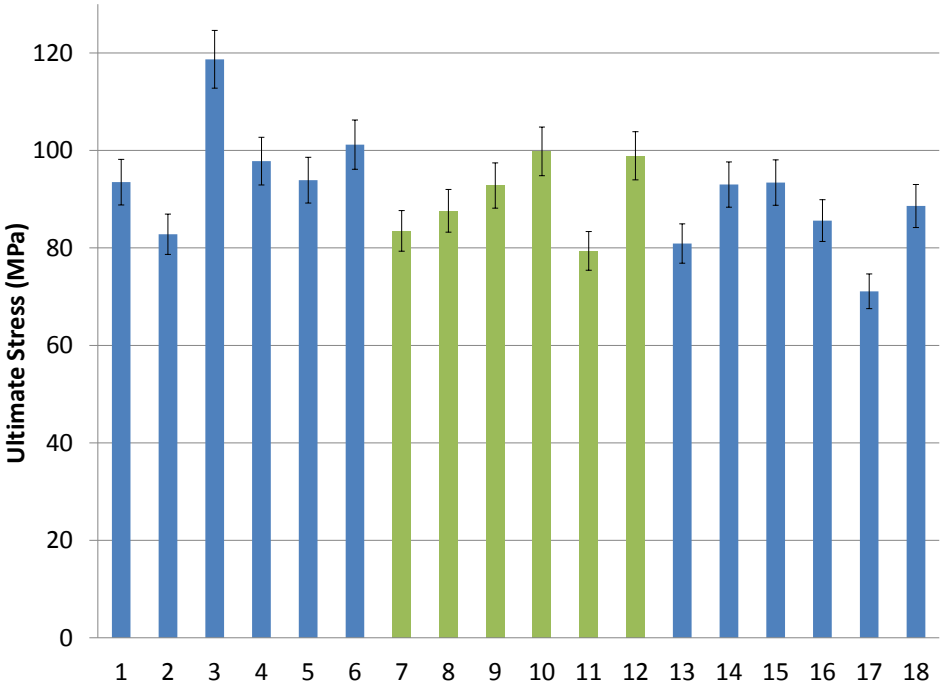

Figure 4.22: Ultimate stress for 3 characteristic lengths at 15 wt% CMF.

these specimens are taken in sequential order along the 15 wt% CMF strip processed at 4 lbs/hr and 200 rpm with a vacuum port at the end pulling 25 inches of Hg. The modulus and ultimate stress vary considerably between each sample. However, the average values for the length of the 763.4 mm are relatively close. These averages are summarized in Table 4.2.

There seems to be some variability in the samples within the characteristic length since the averages are not the same for all three groups. However, the averages are very close, and therefore an overall average for each sample can be taken within reason.

Overall, there seems to be inherent variability with extrusion of this polymer composite. However, it does not seem to follow the characteristic length assumption

Table 4.2: Average modulus and ultimate stress values for the characteristic length for 15 wt% CMF.

Position (Specimen No.)	Mean Young's Modulus (GPa)	Mean Ultimate Stress (MPa)
1-6	6.18	97.98
7-12	6.55	90.33
13-18	5.79	85.43

made for the TSE. There seems to be a constant peak and valley pattern throughout the length of the strip. This means that it is important to have several trials of the material in order to capture the true average of the sample. From Figure 4.21 and Figure 4.22, it seems that the pattern repeats between every 3 to 5 specimens. Since for this study the larger ASTM D638 type IV specimens were used, more specimens would have to be tested for the sub-scale specimens in order to capture the true average. In general, every material had between 30 and 50 samples tested at the sub-scale level, however not every specimen produced reasonable results due to fluctuations in the equipment and quality of cutting. Since the specimens were tested and results were recorded along more than the characteristic length of the strip, it seems that the true average of the sample would have been captured. Since the tests performed with the larger dogbones had a minimum of five samples tested, it seems that the true averages for those tests were also captured.

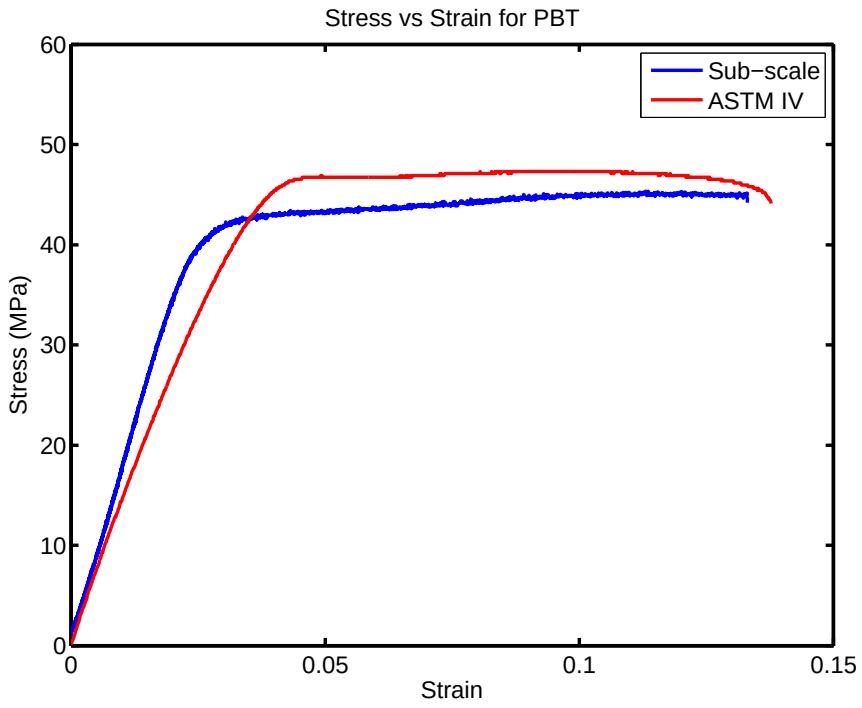

Figure 4.23: Stress vs. Strain for PBT for large and small dogbones.

4.2.7 Validation of Tensile Specimen Sizes

To validate the results from the sub-scale dogbone specimens, tensile results were compared between those specimens and ASTM D638 type IV specimens. The stress vs. strain curve from neat PBT is shown in Figure 4.23.

For neat PBT, the small and large dogbones gave virtually the same results, including the shape of the stress vs. strain curve. From these results, it could be concluded that the values obtained from the sub-scale specimens were valid. The next validations occurred for the CMF filled composite. Stress vs. strain curves for 10 wt% CMF, 15 wt% CMF and 20 wt% CMF are shown in Figure 4.24, Figure 4.25, and Figure 4.26, respectively.

From these curves, it was hard to assert that the values obtained from the

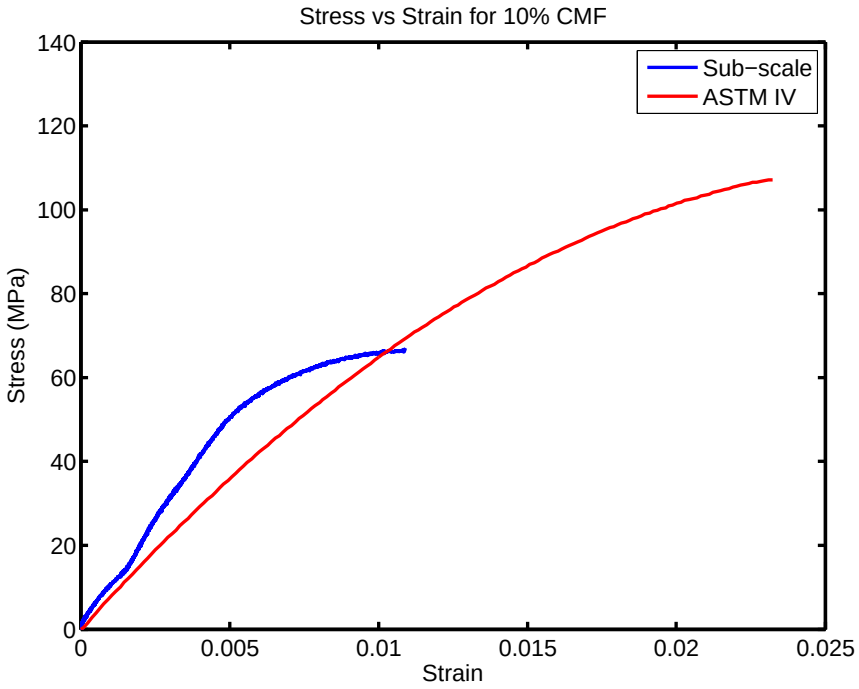

Figure 4.24: Stress vs. Strain for 10 wt% CMF for large and small dogbones.

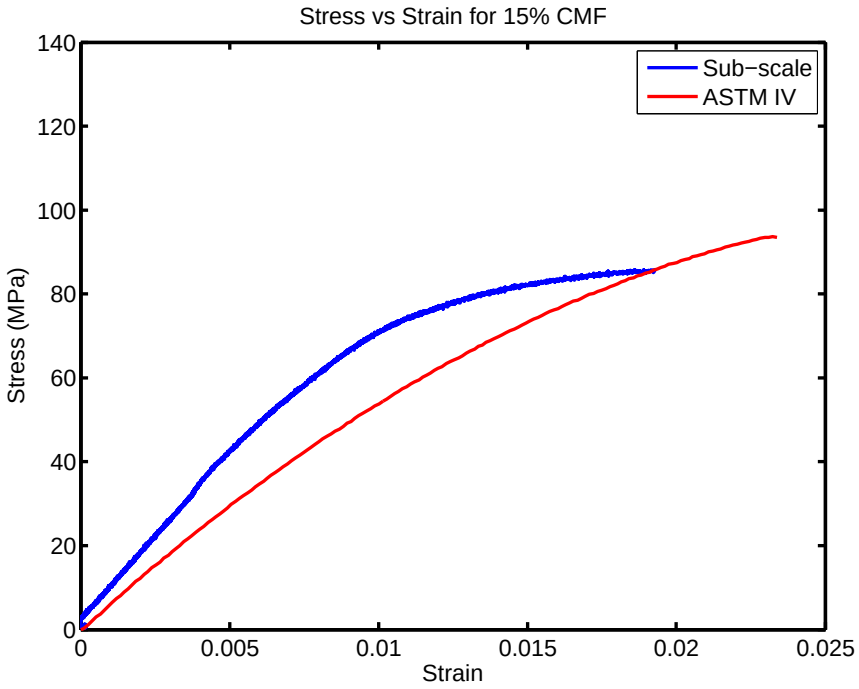

Figure 4.25: Stress vs. Strain for 15 wt% CMF for large and small dogbones.

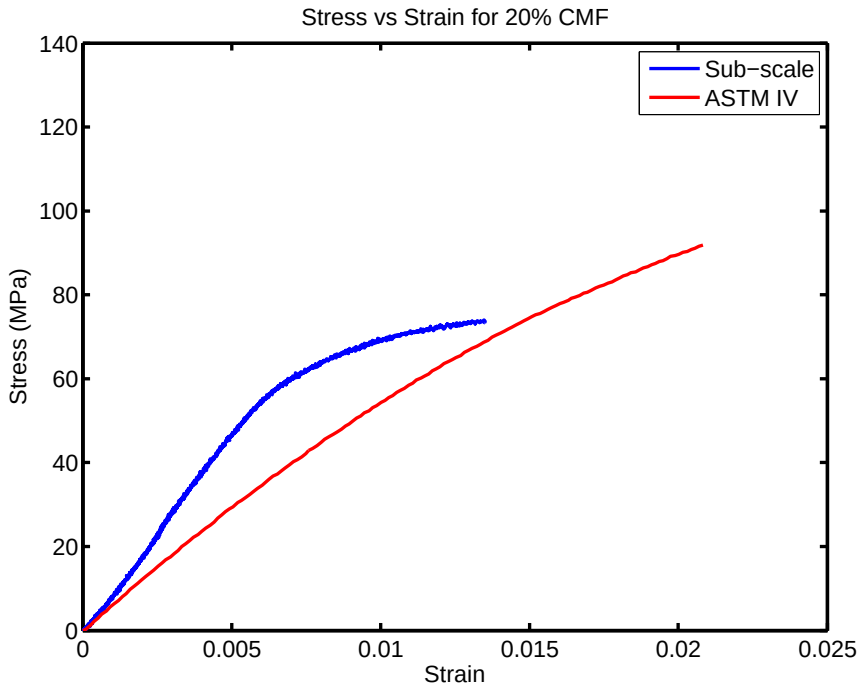

Figure 4.26: Stress vs. Strain for 20 wt% CMF for large and small dogbones.

sub-scale specimens were valid. Therefore the mean young's modulus and average maximum strength were taken to see if the trends observed at both scales matched. The results are shown in Figure 4.27 and Figure 4.28.

For both the modulus and strength, the general trends of the composite are maintained. They both show a clear improvement over neat PBT. Furthermore, there is still a peak in strength and stiffness between 10 wt% CMF and 15 wt% CMF, and the properties decrease in value at higher loadings.

The difference in results may also be due to the difference in equipment used to measure the strain of the specimen. For the sub-scale specimen, an extensometer was used to record the strain, however for the ASTM sized dogbone, the displacement between the grips was used to measure the strain. In general, the extensometer

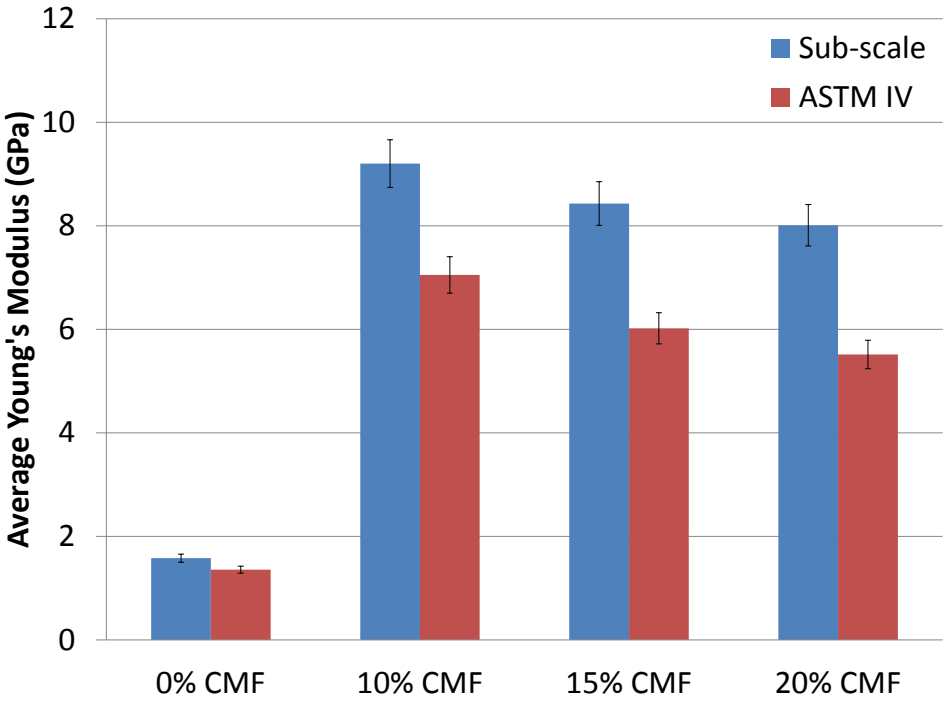

Figure 4.27: Mean young's modulus for large and small dogbones.

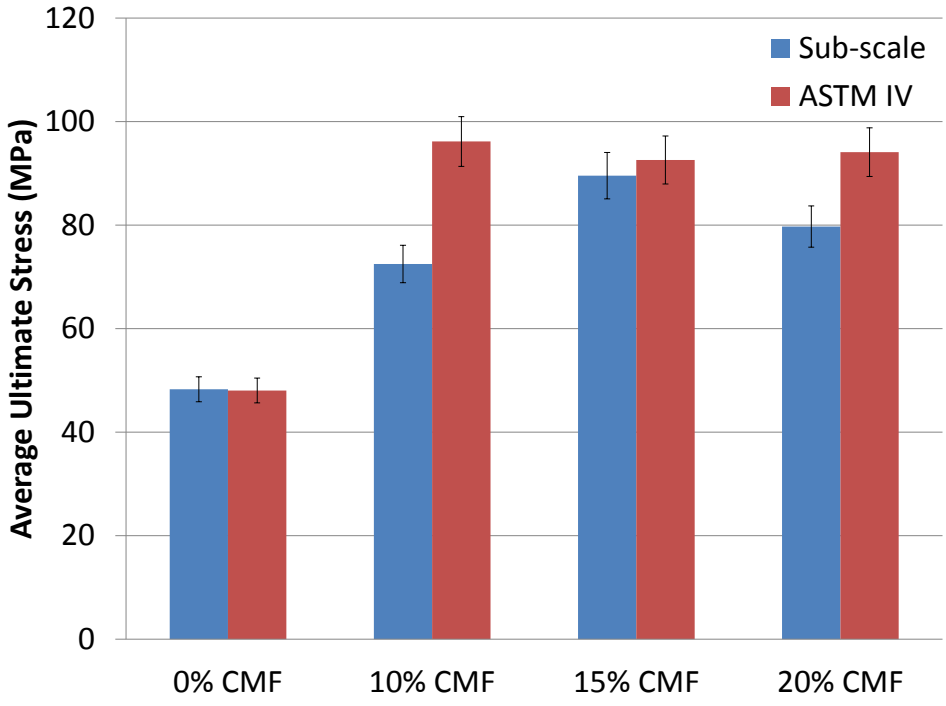

Figure 4.28: Mean ultimate stress for large and small dogbones.

measures lower values than the displacement method, thus resulting in a higher value for young's modulus. Furthermore, the sub-scale specimens will be more susceptible to defects, and so the larger, more defect tolerant, specimens will measure a higher stress.

With the general trends of the composite confirmed between the ASTM sized and sub-standard sized dogbones, the results were qualitatively validated. Although quantitatively the exact values for the modulus and ultimate stress may have to be further verified when sub-scale specimens were used, the trends and general conclusions are valid.

4.2.8 Benchmarking Against Theoretical Values

Theoretical calculations of young's modulus were performed in order to see if theoretical predictions matched the results from the experiments. Three models to predict the the theoretical young's modulus were considered: Voigt, Reuss, and Cox.

The Voigt model assumes the fibers are in parallel arrangement subjected to the same strain [70]. Voigt proposed the effective elastic modulus of the composite as:

$$E_c = E_f v_f + E_m v_m \tag{4.3}$$

with $v_f + v_m = 1$ and where E_f is the elastic modulus of the filler, E_m is the elastic modulus of matrix, v_f is the volume fraction of filler, and v_m is the volume fraction of matrix. This mixing rule is for the iso-strain state.

The volume fraction of the filler was determined for the composite from Equation 4.4.

$$v_1 = \frac{W}{W + (1 - W)\frac{\rho_f}{\rho_m}} \tag{4.4}$$

where W is the weight fraction of the filler used, and ρ_f and ρ_m are the density of the filler and matrix, respectively. For the condition of isostress, Reuss [71] proposed a formula for the effective elastic modulus as:

$$E_c = \frac{E_f E_m}{E_f v_m + E_m v_f} \tag{4.5}$$

Upadhyay et al. explained that for real materials, the iso-stress and iso-strain assumptions are not valid [72]. Therefore there have been several people who have made modified young's modulus prediction equation based on combinations of these two basic equations using the rule of mixtures and other laws [73, 74].

The modified Cox model, which combines Cox's original model and Krenchel's expression, is widely used as an alternative to Reuss and Voigt [28, 58, 75, 76]. Cox's shear lag model was developed for aligned discontinuous elastic fibers in an elastic matrix. The applied load is transferred from the matrix to the fiber via interfacial shear stresses. As the fiber length increases, the efficiency of stress transfer increases, however it can never reach 100% because the maximum tensile stress along the length of the fiber can never exceed the tensile stress in the matrix [77].

The Cox model uses Equation 4.6 to predict the composite modulus.

$$E_c = v_m E_m + q(1 - \frac{tanh\beta}{\beta}) v_f E_f \tag{4.6}$$

where

$$\beta = \frac{l}{d}\sqrt{\frac{E_m}{(1+\nu)E_f * ln(\frac{\pi}{4v_f})}} \tag{4.7}$$

ν is Poisson's ratio for the matrix, in this case $\nu = 0.44$. The Cox model also uses a factor, q, to determine the orientation of the filler. A value of q=1 means the fibers are aligned, q=1/2 means the fibers are in the same plane, but randomly oriented, and a value of q=1/6 means the fibers are randomly oriented in all three dimensions [58]. For this study, previous imaging showed the alignment to be fairly uniform, however all three values were compared since it had been shown that even slight misalignment can have a significant effect on the resulting modulus.

Figure 4.29 shows the resulting composite modulus predictions for the three models with various loadings of CMF compared to experimental results from tensile tests on the sub-scale dogbones.

The Cox and Voigt model yielded very similar results when the fibers were assumed to be aligned, and are much higher than experimental values. The Reuss model is almost invariant when the CMF loading is altered since it is being considered in the isostress condition, resulting in values lower than experimental data. For this model, the fibers are not aiding the polymer matrix significantly since it assuming there is not significant load transfer from the polymer to the matrix to increase the maximum stress. When the Cox model varies the degree of alignment, the effect on the modulus is significant. The random in plane model is close to experimental values for 5 wt% CMF and 10 wt% CMF. The random orientation in the three dimensions model is closer to the values for 20 wt% CMF and 25 wt%

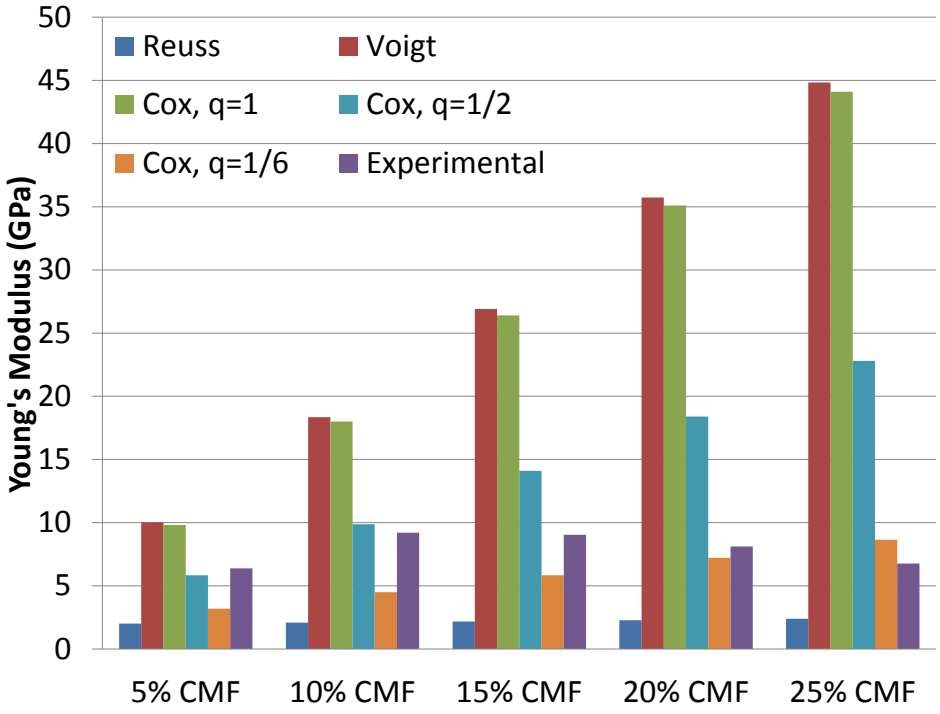

Figure 4.29: Predicted values for young's modulus compared to experimental results for varying wt% CMF.

CMF. 15 wt% CMF seems to be between these two models. Overall, the theoretical values were unmatched when compared to experimental data.

The experimental results showed a peak in performance whereas these model show that increased loading should yield increased performance. This peak is because when actually processing the composite, at higher loadings the fibers are experiencing degradation. Furthermore, there is a complex interplay between PBT and processing because of its polyester base.

While the fibers showed strong alignment in the direction of flow from the extruder, there was some misalignment, but it does not seem to be to that the fibers were completely random in two or three dimension. However, this slight misalignment can have significant effects on the resulting modulus and thus a further investigation into the alignment of the fibers would have to be conducted to determine the proper modeling tool for the modulus of the composite. Furthermore, more complex models that take the exact shape of the filler and other factors into account might yield more accurate results. Since the theoretical values were not matched by experimental results, no modeling for the three phase material of PBT, CMFs, and MWCNTs was conducted.

4.3 Thermal Conductivity

Thermal conductivity tests were performed to further characterize the properties of the multi-scale composite. The thermal tests were performed using the MicroFlash system that measured thermal diffusivity through the sample, and given

density and thickness, could calculate thermal conductivity. The samples for these tests were injection molded, partially altering the alignment of the fibers. All materials tested for thermal properties were processed at 4 lbs/hr and 200 rpm, with a vacuum pulling 25 inches of Hg at the end port.

The direction of heat flow for these thermal tests was perpendicular to the fibers. The thermal conductivity in the transverse tends to be lower when compared to the axial direction, however with the available equipment, this was the only direction that could be tested. The following sections describe the trends when the weight percent of CMFs and MWCNTs are altered.

4.3.1 Varying Loading of CMF

The CMF loading was varied between 5 wt% and 25 wt% by 5 wt% increments to observe the changes in thermal conductivity. The average thermal conductivity was calculated for each loading level for approximately 15 trials per material. Since PBT is not thermally conductive and usually used as an insulator, the added thermal conductivity can be assumed to come solely from the fibers. However, since neat PBT was not thermally conductive, it could not be used in the MicroFlash, and therefore a theoretical value was used for comparison. The average thermal conductivity observed for each sample is plotted in Figure 4.30.

All combinations of wt% CMF were statistically different from PBT within a 95% confidence. The trend in thermal conductivity for increased CMF loading shows that as the loading is increased, the thermal conductivity also increases until

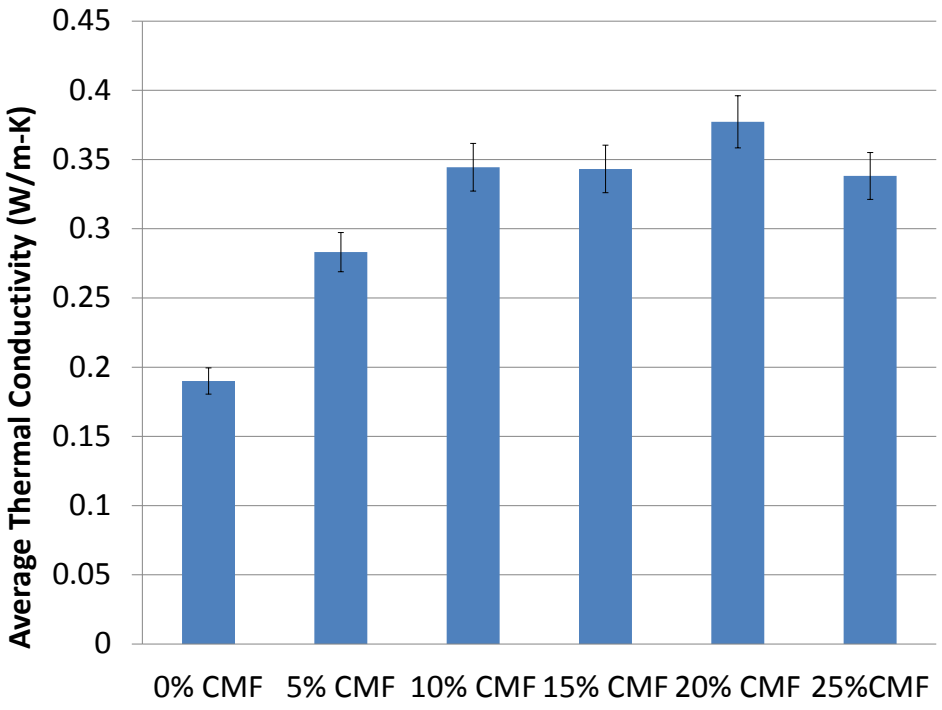

Figure 4.30: Mean thermal conductivity for varying wt% CMF.

it hits a maximum at 20 wt% CMF. Higher loadings of CMF would be expected to yield higher thermal conductivity, however microstructure effects may have started to affect properties again. Thermal conductivity depends on a strong network of fibers and contacts, so with attrition showing at higher loadings, this may be causing the decrease in thermal conductivity because the network is not as strong and resistances between the polymer and the fibers may be starting play a role. Further studies at higher loading of CMF would need to take place to determine if this trend continues to decrease, or if with the higher loadings, the attrition makes less of an impact because the fibers are still able to create this network. However, for this characterization of the CMF only composite, it seems that thermal properties track with mechanical properties in that there is a peak in performance in both.

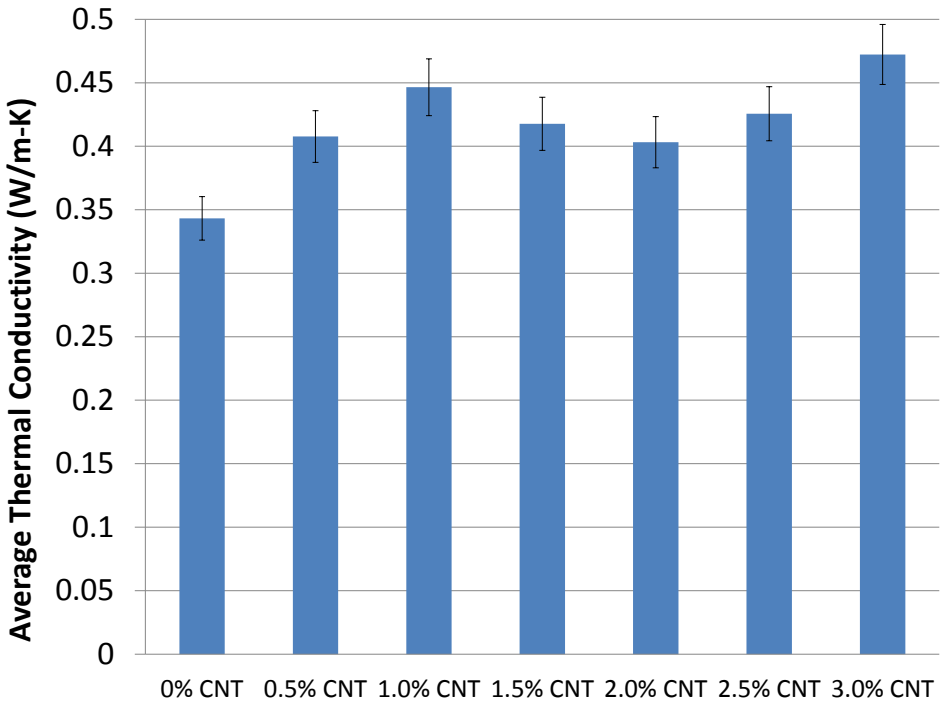

Figure 4.31: Mean thermal conductivity for 15 wt% CMF and varying wt% MWCNT.

4.3.2 Varying Loading of MWCNT

MWCNTs are known more for their enhanced thermal properties [33], thus thermal tests were performed on the multi-scale composite to see if there are added benefits when MWCNTs are used in addition to CMFs when observing thermal conductivity. Figure 4.31 shows the average thermal conductivity for each sample.

With the addition of MWCNTs, thermal properties were enhanced. All loadings of MWCNTs yielded higher thermal conductivity when compared to the composite with only CMFs. Again, there may be evidence of a peak and valley pattern as the loading increases from 0 wt% MWCNT to 3 wt% MWCNT. The results agree with theoretical predictions that the presence of MWCNTs would aid in creating

the network between the fibers to improve thermal conductivity. Since the attrition at 15 wt% CMF was not always observed, especially with the addition of MWCNTs, it makes sense that the CMFs create a core network and the MWCNTs help in the connections between the fibers, creating a stronger network and minimizing the effects of the resistance presented from the polymer.

4.3.3 Varying CMF and MWCNT Loading

To further explore the potential of the multi-scale composite and thermal conductivity improvements, composites with 10 wt% CMF to 25 wt% CMF and 0 wt% MWCNT to 0.5 wt% MWCNT were tested. Again, the average thermal conductivity is plotted in Figure 4.32.

For every weight percent of CMF, the addition of MWCNTs improved the thermal conductivity. The improvement is especially noticeable for the cases where the CMF only composite did not yield the highest thermal conductivity. At 10 wt% CMF, the loading of CMFs was too little to create a strong network of fibers, however by adding the MWCNTs, the network is significantly improved and the thermal conductivity increases. This same phenomena occurs for a loading of 15 wt% CMF. For 20 wt% CMF, the network was already adequate, and thus the addition of MWCNTs does not alter the thermal conductivity by a significant amount. With 25 wt% CMF, the thermal conductivity is greatly improved with the MWCNTs. This supports the idea that at this loading of CMF, attrition is starting to take place and thus reduces the thermal conductivity. When the MWCNTs are added, the network

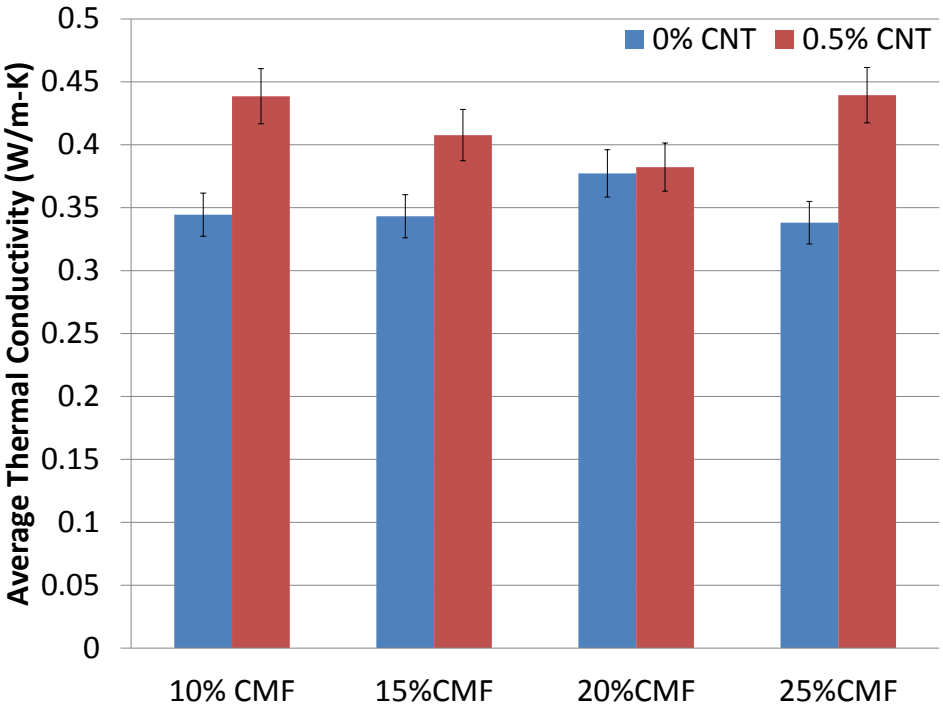

Figure 4.32: Mean thermal conductivity for varying wt% CMF and varying wt% MWCNT.

is once again restored. Since there are more CMF fibers than the other composites, the thermal conductivity can increase even more because even the broken fibers can be conductive.

Overall, it seems that the thermal properties are strongly dependent on the quality of the mixing of the composite. When there are enough fibers without attrition, the thermal conductivity is greatly improved. When the MWCNTs are added, the connections between the fibers are even further improved, which improves the thermal conductivity even more. The thermal conductivity, however, does not track with the mechanical properties. When the MWCNTs are added, the mechanical properties tend to be reduced, while thermal properties are improved.

4.3.4 Comparison to Theoretical Values

For this experiment, thermal conductivity was predicted using a two-phase model for the composite with various loadings of carbon microfibers. There are several models that can be used to predict thermal conductivity [78]. The various models use different aspects of heat conduction, convection, and radiation equations, along with temperature gradients and the shape of the filler.

The Nielsen model was selected to predict thermal conductivity for this material. The Nielsen model modifies the Halpin-Tsai equation to include the effect of the shape and the orientation of the particles [78]. The Nielsen model is unique in that the arrangement of the fibers within the polymer and the orientation of the heat flow can be adjusted to match what is observed in the samples [79]. The

thermal conductivity of the composite is determined from Equation 4.8.

$$k = k_1 \frac{1 + ABv_2}{1 - B\psi v_2} \tag{4.8}$$

where v_2 is the volume fraction of the filler and k_1 is the thermal conductivity of the matrix. A, B, and ψ are given by separate equations, shown in Equation 4.9, Equation 4.10, and Equation 4.11, respectively.

$$A = k_e - 1 \tag{4.9}$$

where k_e is the Einstein coefficient. Pre-calculated values for A are also calculated in a table in Nielsen's original paper [79].

$$B = \frac{\frac{k_2}{k_1} - 1}{\frac{k_2}{k_1} + A} \tag{4.10}$$

where k_2 is the thermal conductivity of the filler.

$$\psi = 1 + \frac{1 - \phi_m}{\phi_m^2} v_f \tag{4.11}$$

where ϕ_m is the maximum packing fraction. Again, common values for ϕ_m are given in a table in the original paper [79].

These equations are used to determine the theoretical thermal conductivity that is expected with uniaxially oriented fibers with heat flow perpendicular to the fibers, and a uniaxial random maximum packing factor. The volume fraction was again calculated for the weight percents from Equation 4.4.

The predictions from the Nielsen model are shown in Figure 4.33, along with

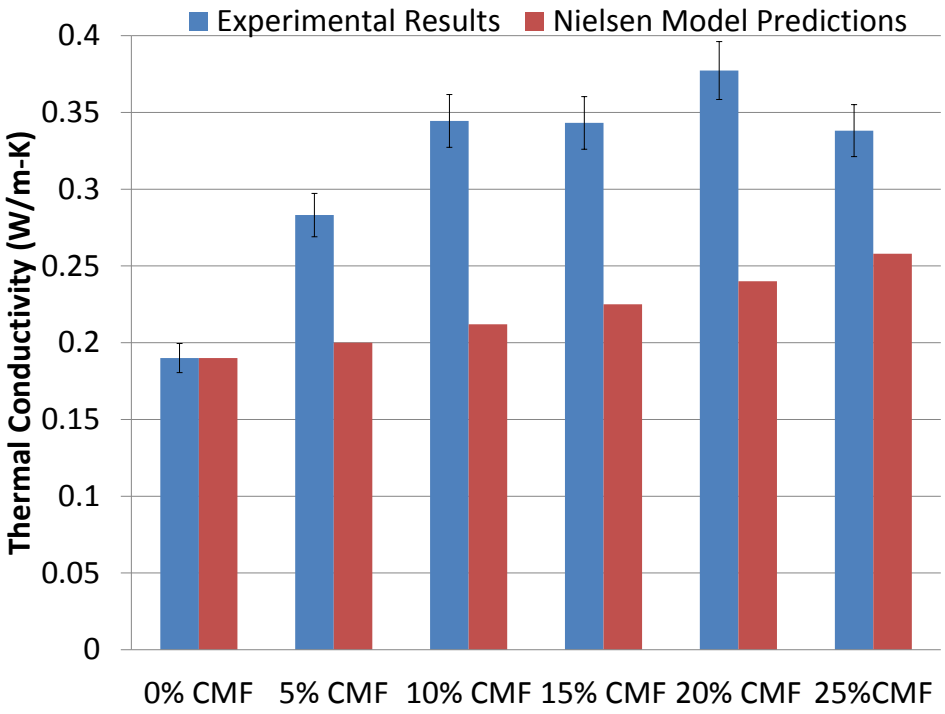

Figure 4.33: Comparison between experimental and theoretical thermal conductivity.

the average values obtained from testing. The predicted values for the composite are lower than what was seen experimentally. This is somewhat expected, however, because when the Nielsen model uses the calculated values for the A factor, they tend to be low. The values of A listed in the table in Nielsen's model are for elastic moduli, whereas for predicting thermal conductivity, the A values would need to be slightly higher.

Overall, the experimental values are not matched by the theoretical values from the Nielsen model. There are several factors that could contribute to this, including inherently low predictions from Nielsen. Furthermore, the theoretical trend is to show continually increasing thermal conductivity, however this was not

the observed trend. At some points, the increase in loading did not necessarily improve the thermal conductivity. Since the theoretical values for the two-phase composite was not matched, no further modeling took place.

4.4 Microstructure-Property Relationship

To further characterize the relationship between the microstructure and the mechanical properties, mapping between the two occurred. As with most materials, there are good and bad tensile tests as a result of defects and other variability within the material. This section looks at a good tensile test and a bad tensile test for each loading of CMF at 4 lbs/hr, 200 rpm, and pulling vacuum at 25 inches of mercury. The fractured dogbone specimens were then observed under an optical microscope in order to qualitatively see if there is a difference in the microstructure.

Figures 4.34 to Figures 4.39 show the results of the good and bad tensile tests, with the stress vs strain curve shown under the optical images.

Upon examining the optical images and the resulting stress vs strain curve, it is obvious that the quality of mixing plays a significant role in mechanical performance. When there is no filler, the results vary slightly. There are no visible defects in the neat polymer, and the mechanical properties reflect this with similar results. As mentioned before, there is inherent variability when processing on a TSE, thus this may be reflecting that variability.

Figure 4.40 shows the recorded young's modulus from the previous stress strain curves and Figure 4.41 shows the ultimate stress for the good and bad samples at

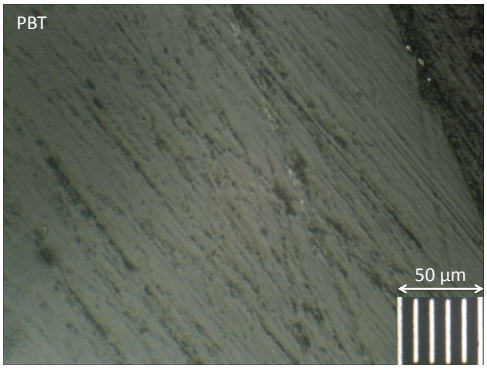

(a) 0 wt% CMF good sample.

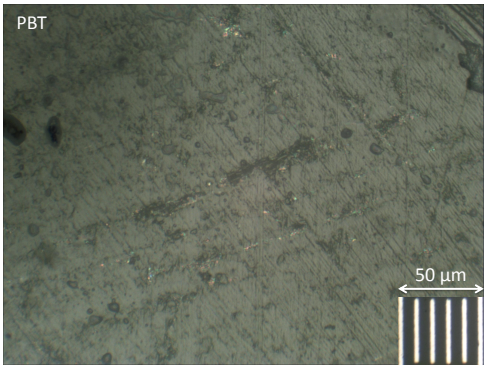

(b) 0 wt% CMF bad sample.

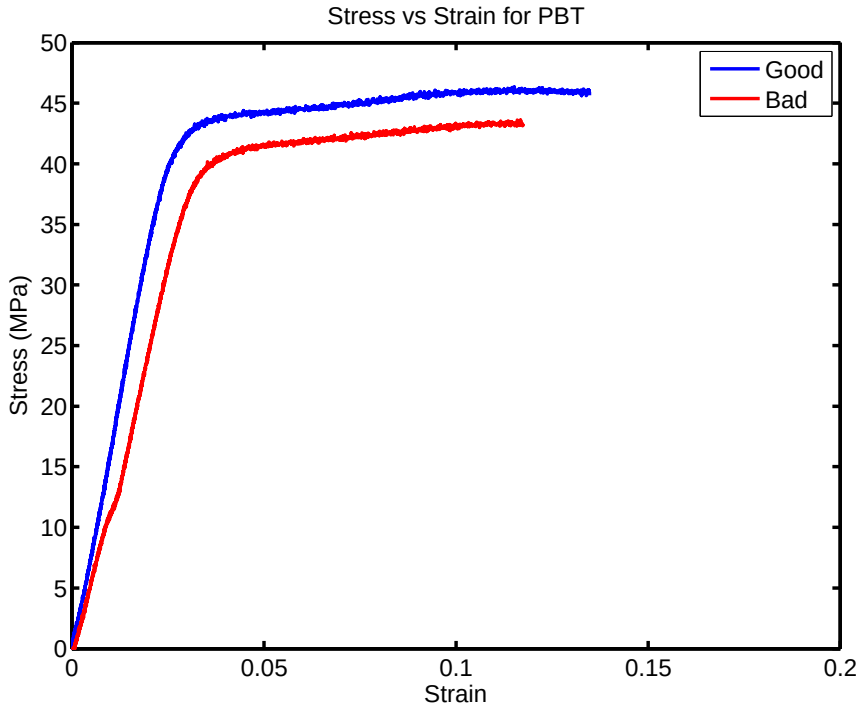

(c) 0 wt% CMF tensile results.

Figure 4.34: Optical images and tensile results for 0 wt% CMF for good and bad samples.

the various CMF loadings.

As filler is added, the changes in quality of mixing and product significantly alters the mechanical properties. The maximum stress is reduced by a considerable

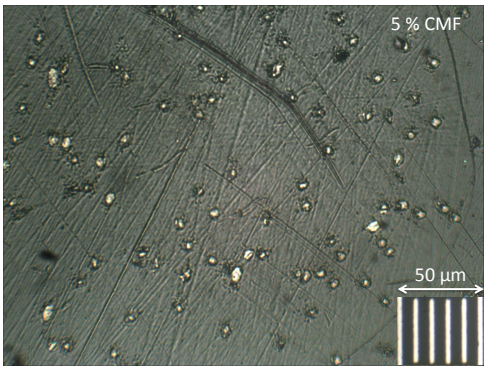

(a) 5 wt% CMF good sample.

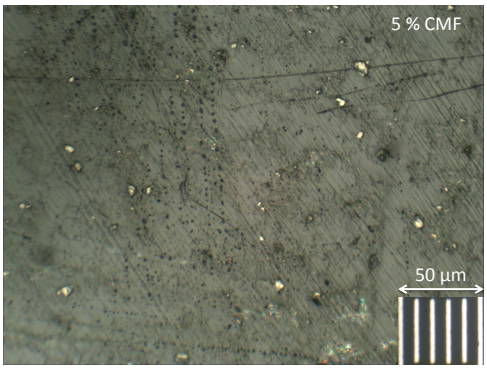

(b) 5 wt% CMF bad sample.

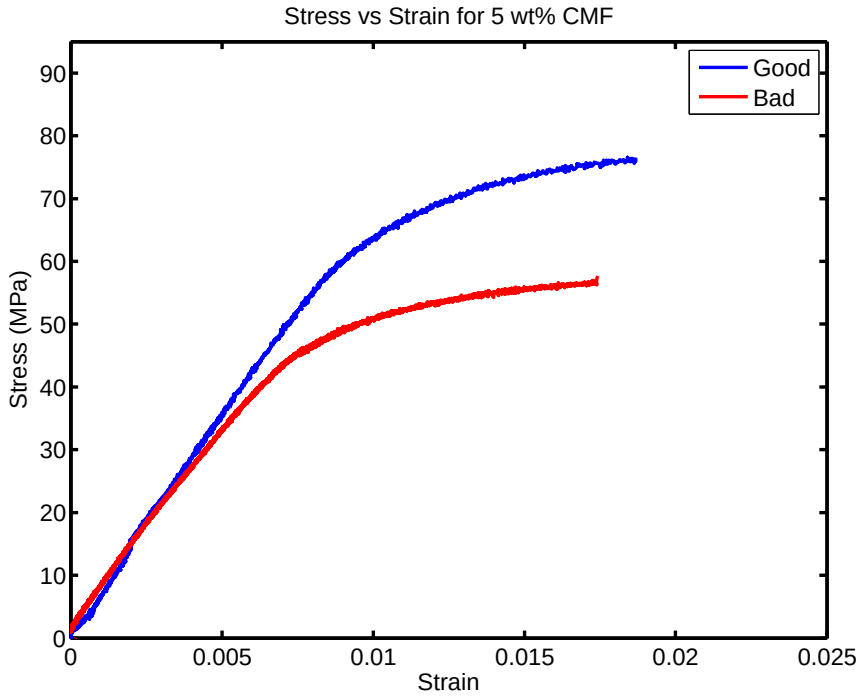

(c) 5 wt% CMF tensile results.

Figure 4.35: Optical images and tensile results for 5 wt% CMF for good and bad samples.

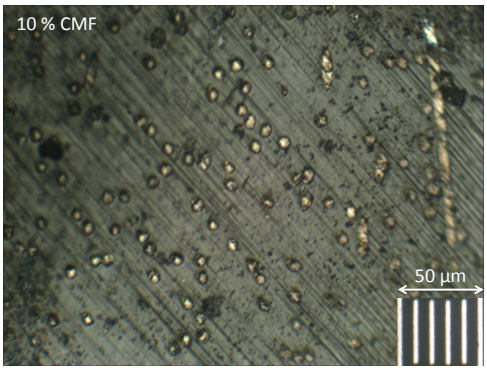

(a) 10 wt% CMF good sample.

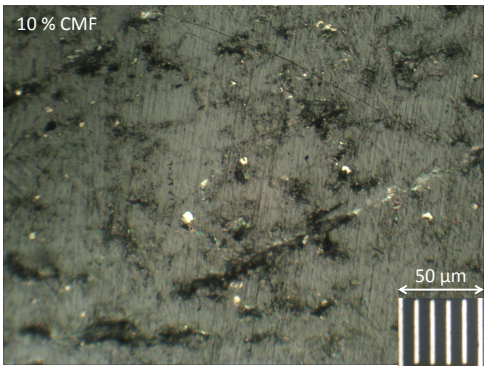

(b) 10 wt% CMF bad sample.

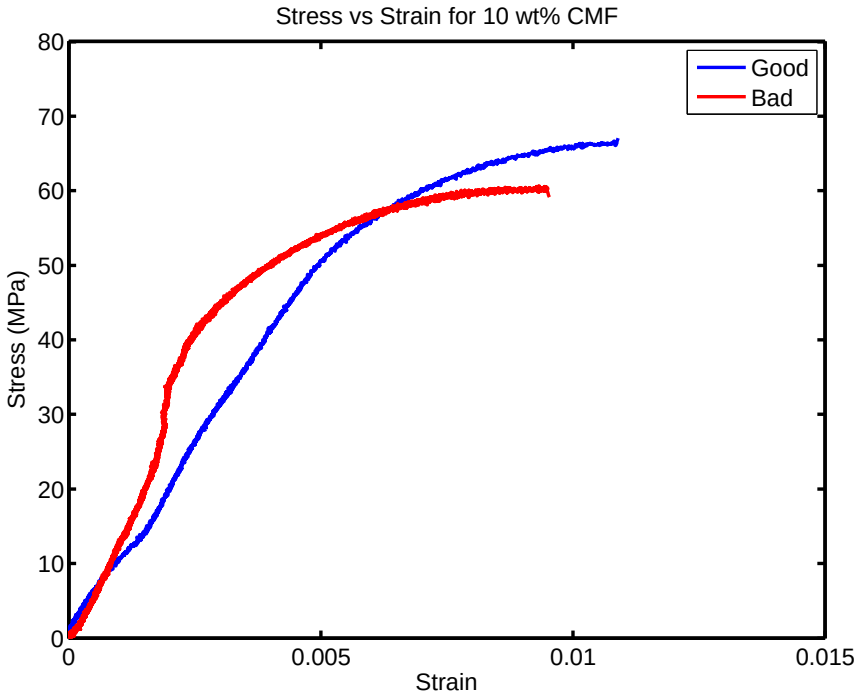

(c) 10 wt% CMF tensile results.

Figure 4.36: Optical images and tensile results for 10 wt% CMF for good and bad samples.

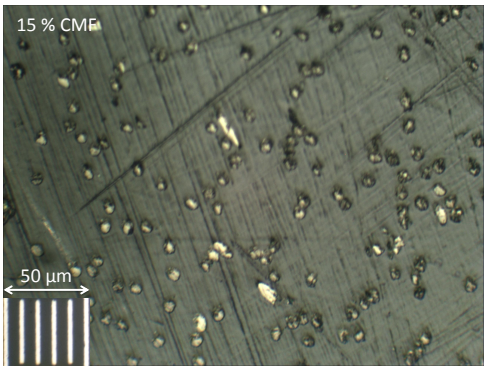

(a) 15 wt% CMF good sample.

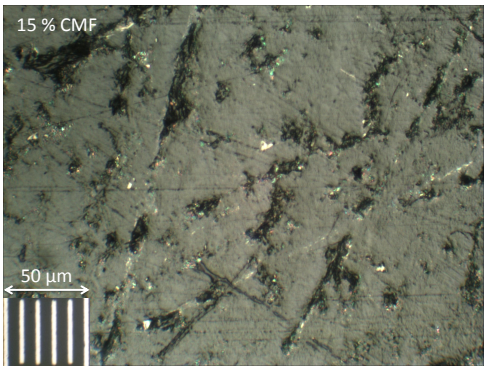

(b) 15 wt% CMF bad sample.

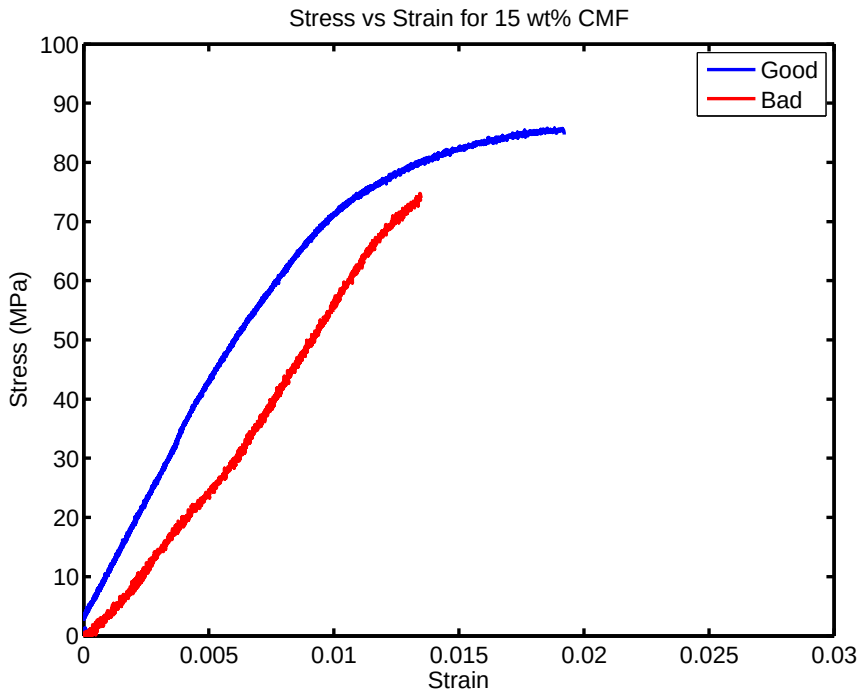

(c) 15 wt% CMF tensile results.

Figure 4.37: Optical images and tensile results for 15 wt% CMF for good and bad samples.

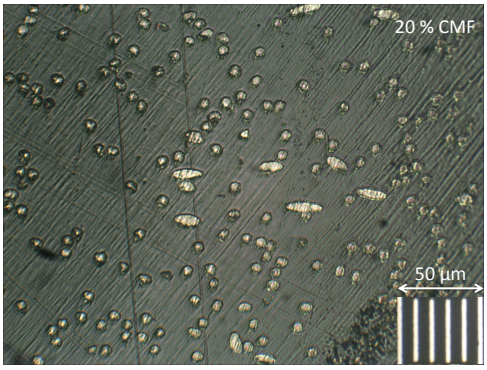

(a) 20 wt% CMF good sample.

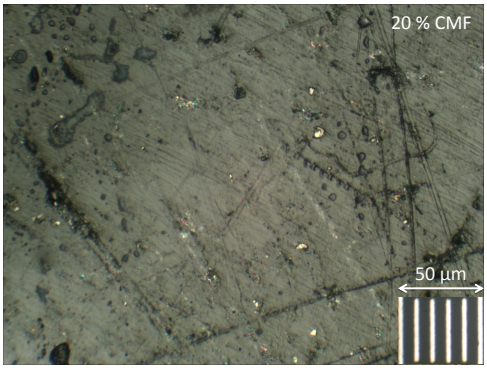

(b) 20 wt% CMF bad sample.

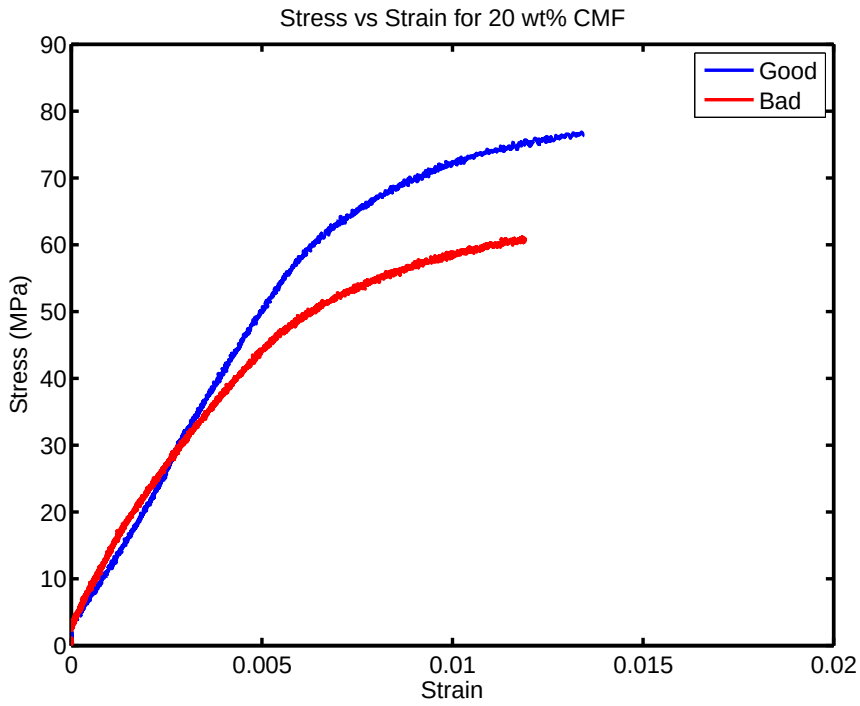

(c) 20 wt% CMF tensile results.

Figure 4.38: Optical images and tensile results for 20 wt% CMF for good and bad samples.

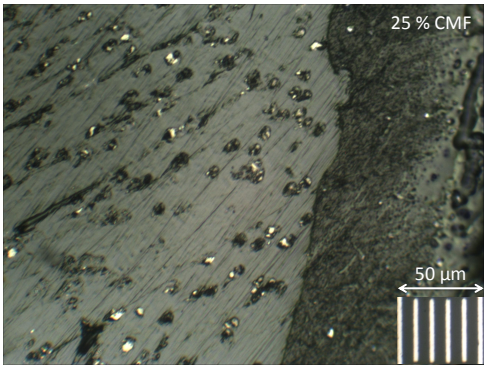

(a) 25 wt% CMF good sample.

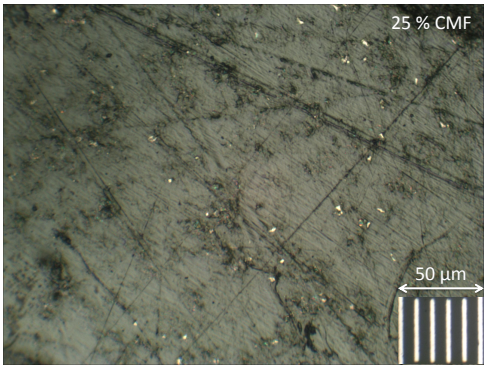

(b) 25 wt% CMF bad sample.

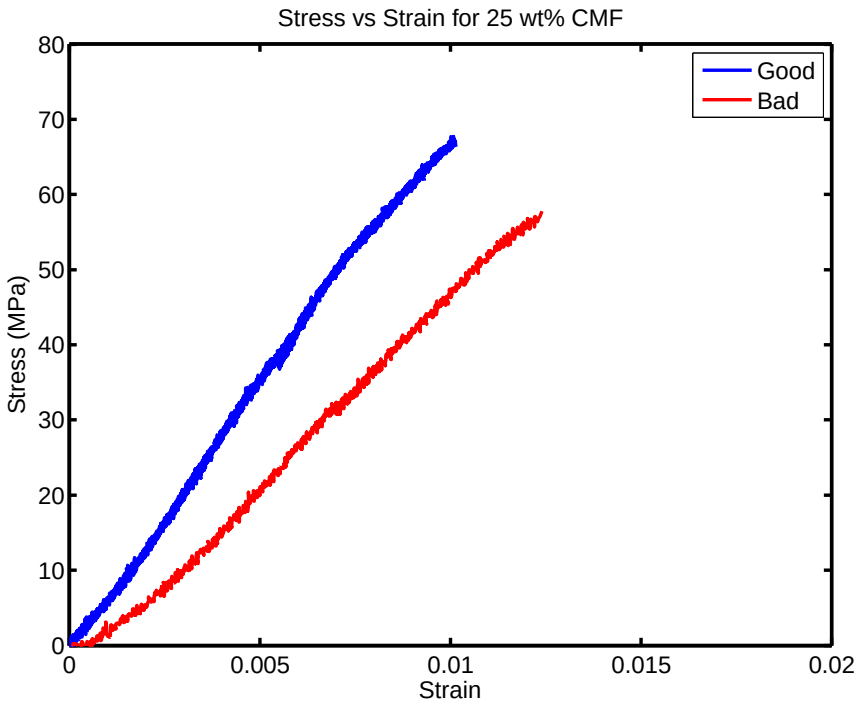

(c) 25 wt% CMF tensile results.

Figure 4.39: Optical images and tensile results for 25 wt% CMF for good and bad samples.

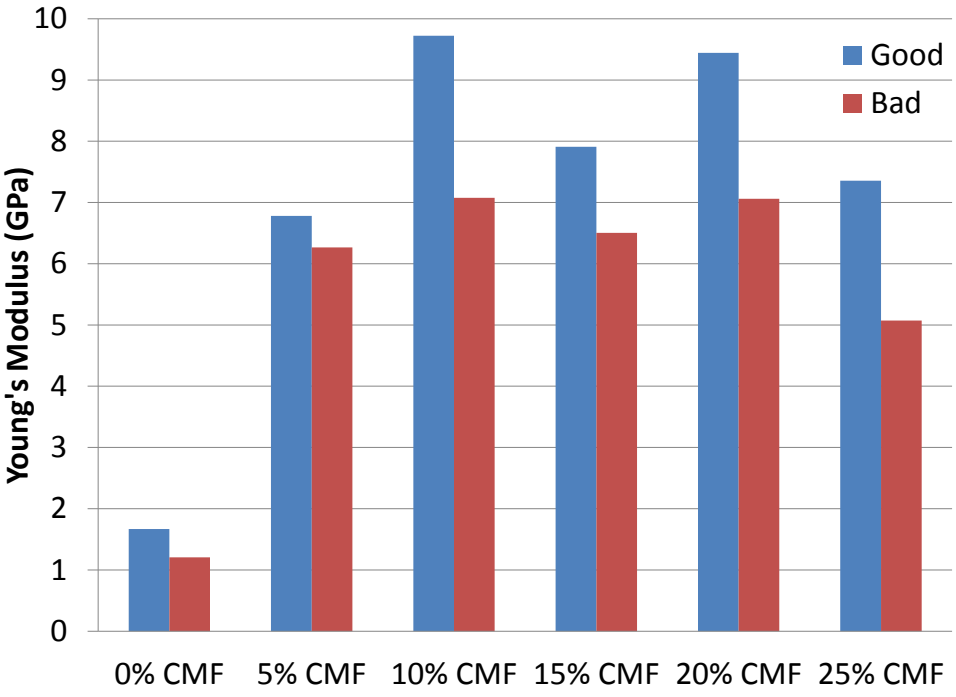

Figure 4.40: Young's modulus for good and bad tensile tests for varying wt% CMF.

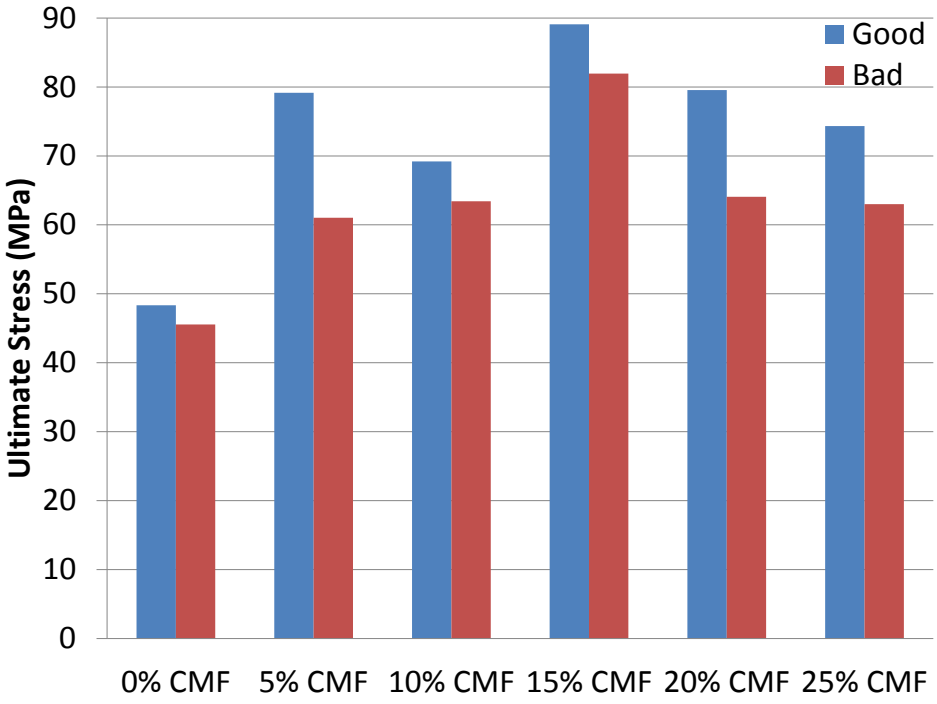

Figure 4.41: Ultimate stress for good and bad tensile tests for varying wt% CMF.

amount when defects and agglomerates are present, and the tendency is for the material to become weaker and show reduced stiffness.

The stiffness and strength are reduced with poor mixing because the dispersion and adhesion are not adequate for proper load transfer between the polymer matrix and the fibers. There are also clear voids in the samples that produced lower mechanical properties. The material is stiffer when the fibers are well mixed, as expected. The reduced strength may be due to pull out of the fibers and agglomerates that were not broken up in that section of the composite. Again, the variations may be due to inherent variability when processing with a TSE, however other factors with the quality of mixing are also playing a role when it comes to variations in stiffness and strength.

Chapter 5

Conclusions

Polymer composites with carbon microfiber and carbon nanotube fillers have been widely explored. However, there has been little reports of the properties of the composite when using a combination of both scales of filler in one multi-scale composite. Thus, a characterization of multi-scale polymer composites processed on a co-rotating twin screw extruder has begun. The effects on a processing-structure-property relationship have been closely observed, and the following sections look at key intellectual contributions, summarize the findings, and look to future work for each of these aspects.

5.1 Important Contributions and Findings

Upon examination of processing conditions, structure, and properties of a multi-scale polymer composite, new insight about the behavior of this composite has been gained.

5.1.1 Processing Polymer Composites

Various extrusion processing techniques were used to create a multi-scale composite. First, it was determined that pulling vacuum from the end port, just before the die zone where the extrudate exists the extruder, is significant in obtaining more

consistent results and better mechanical performance. The effects of the vacuum were visibly quantified with optical images that showed less voids in the polymer matrix. Furthermore, the tensile properties had a dramatic improvement, especially when processing polymers with fillers.

A specific throughput comparison between 0.136 mL/rev, 0.202 mL/rev, 0.267 mL/rev, and 0.333 mL/rev initially showed that at 0.202 mL/rev, peak mechanical performance is observed across loading of 10 wt% CMF and 15 wt% CMF and 0 wt% MWCNT and 0.5 wt% MWCNT. The variation of the processing conditions yielded a very different material. However, filler size and loading must be considered when selecting processing conditions.

When only CMFs are being used in the composite, the higher Q/Ns are damaging the fibers, thus the young's modulus and ultimate stress are reduced. When MWCNTs are added to the composite, the higher Q/Ns help disperse the MWCNTs within the composite, and thus the mechanical properties are restored to a level as if the CMFs were undamaged. Thus, with the added benefit of dispersed MWCNTs at higher Q/Ns, and less attrition occurring for the CMFs at lower Q/Ns, the optimal processing condition would be 0.202 mL/rev, or a flow rate of 4 lbs/hr and a screw speed of 200 rpm, for this experimental set-up.

Lastly, processing the composite in a TSE showed that there is inherent variability within the collected extrudate. However, as long as several specimens over the entire characteristic length for the extruder are tested, the average values should be representative of the true composite properties.

5.1.2 Structure of Polymer Composites

The structure of the composite proved to be a very influential element when it came to properties and determining proper processing techniques. The structure revealed that proper dispersion and adhesion were being achieved at a CMF loading below 15 wt%. Above this loading of CMF, attrition and other defects were being observed. Furthermore, the addition of MWCNTs seemed to delay the attrition effects since very little attrition was observed when MWCNTs were added to 15 wt% CMF.

Likewise, the effects of processing conditions could be qualitatively observed with optical images. Without pulling vacuum from the end port of the extruder, voids and air entrainment were clearly visible in the composite.

5.1.3 Properties of Composites

Mechanical and thermal properties were both improved from the addition of CMF and MWCNT fillers within the PBT polymer matrix. Upon examining various weight percentages of CMF, initial trends indicate that there may be a threshold for the amount of micro carbon fiber that improves the mechanical properties of the material within the ranges studied. Above 15 wt% CMF, damage to the fibers began to occur under processing conditions of 4 lbs/hr, 200 rpm, and a vacuum pulling 25 inches of mercury just before the composite exited the extruder. The thermal conductivity of the polymer was improved by a minimum of 49.0% and a maximum of 98.6% with the addition of CMFs.

The role of MWCNTs was studied by varying the amount of MWCNTs from 0.5 wt% to 3.0 wt% in 15 wt% CMF, as well as studying various amounts of MWCNTs in 10 wt% CMF and 20 wt% CMF. For tensile properties at 15 wt% CMF, the addition of MWCNTs stiffened the material slightly at loading below 2.0 wt% MWCNT, then there was a dip in stiffness and the stiffness was restored at a loading of 3.0 wt% MWCNT. When the weight percent of the CMF was altered, the results still showed consistent trends, although some of the values for when the changes occur differed. Overall, the addition of MWCNTs showed a reduction in ultimate stress. This could possibly be due to agglomerates, because as the processing condition was altered to a more aggressive Q/N, the MWCNTs improved the strength and stiffness, which could be due to the added dispersion of the MWCNTs.

When the measured modulus was compared to the aligned Cox model, the experimental values were much lower. Furthermore, it seems that perhaps the modulus is somewhat insensitive to the variations in loading since the change in value for different loadings was not nearly the same as the change predicted by theory. Other reports of comparison to the aligned Cox model have also shown lower experimental values [20, 28]. Further exploration into the orientation of the filler, degradation of the fibers, and fundamental changes occurring in the polyester based matrix would have to be explored in order to produce a proper model for the composite.

The thermal conductivity of the composite increased greatly when the MWCNTs were added. A minimum of 101.2% and a maximum of 148.6% improvement over neat PBT was observed with all combination of CMF and MWCNT loadings. When compared to a composite with only CMF, there was an average improvement

of 23.2% ±9.

Overall, the characterization of multi-scale composites has begun and initial trends indicate that a multi-scale composite with 15 wt% CMF and 0.5 wt% MWCNT processed at 4 lbs/hr and 200 rpm, with a vacuum pulling 25 inches of mercury at the end port, yields the best combination of thermal conductivity, stiffness, and strength.

5.2 Future Work

Characterization of a multi-scale composite has provided great insight to the relationships of CMFs, MWCNTs, and PBT with regards to structure, processing in a COTSE, and properties. However, there are further areas of investigation that could improve the understanding of the processing-structure-property relationship for the multi-scale composite.

1. *Microstructure* Further observations of the microstructure, particularly the structure with visible MWCNTs, can be explored. By an intensive investigation into the microstructure of this polymer, interactions between the two length scale fillers and the polymer can be quantified.

2. *Mechanical Properties* Tensile tests of the composites have been thoroughly investigated. However, there needs to be further exploration of the size specimen that produces quantitative results. In addition to adjusting tensile testing, other mechanical properties, such as hardness and impact, can be characterized.

3. *Thermal Properties* The thermal conductivity in the transverse direction has been recorded, but measurements of axial thermal conductivity need to take place. This may also lead to a broader range of applications for the composite since thermal conductivity in the directions of the fibers is generally higher than perpendicular to the fibers.

4. *Filler Loading* Although a wide range of filler loadings have been tested, higher loadings should be explored. This will especially aid in determining if the trends of valleys and peaks with mechanical and thermal properties continue. A different matrix could also be used to determine if there are potential effects from the selected polymer base.

5. *Specific Throughput* A constant screw speed and variation in flow rate experiment was conducted to observe effects from changes in specific throughput. A more extensive investigation could look at a more expansive range of filler loadings at various Q/Ns. Furthermore, a study of constant flow rate and various screw speeds, and varying flow rate and screw speed simultaneously, would give even further insight into the effects of percent fill and percent break up on the polymer composite.

Bibliography

[1] S.V. Joshi, L.T. Drzal, A.K. Mohanty, and S. Arora. Are natural fiber composites environmentally superior to glass fiber reinforced composites? *Composites Part A: applied science and manufacturing*, 35(3):371–376, March 2004.

[2] T. Lan and T.J. Pinnavaia. Clay-reinfroced epoxy nanocomposites. *Chemistry of Materials*, 6(12):2216–2219, July 1994.

[3] A. Kota. *Processing-Structure-Microstructure-Property Relationships in Polymer Nanocomposites*. PhD Thesis, University of Maryland, College Park, MD, December 2007.

[4] J. Coleman, U. Khan, W. Blau, and Y. Gun'ko. Small but strong: A review of the mechanical properties of carbon nanotube polymer composites. *Carbon*, 44(9):1624–1652, August 2006.

[5] T. Villmow, P. Potschke, S. Pegel, L. Haussler, and B. Kretzchmar. Influence of twin-screw extrusion conditions on the dispersion of multi-walled carbon nanotubes in poly(lactic acid) matrix. *Polymer*, 49(16):3500–3509, June 2008.

[6] S. Levy and J.F. Carley. *Plastics extrusion technology handbook*. Industrial Press Inc., Maryland, 1989.

[7] W. Pappas. Characterization and Comparison of Stress History in Various Sized Twin-Screw Extruders Using Residence Stress Distribututions. MS Thesis, University of Maryland, College Park, MD, December 2011.

[8] F. Li, H. Cheng, S. Bai, G. Su, and M. S. Dresselhaus. Tensile strength of single-walled carbon nanotubes directly measured from their macroscopic ropes. *Applied Physics Letters*, 77(20):3161–3163, November 2000.

[9] D. A. Walters, L. M. Ericson, M. Casavant, J. Liu, D. T. Colbert, K. A. Smith, and R. E. Smalley. Elastic strain of freely suspended single-wall carbon nanotube ropes. *Applied Physics Letters*, 74(25):3803–3805, June 1999.

[10] Y. Li. Effect of addition of carbon nanofibers and carbon nanotubes on properties of thermoplastic biopolymers. *Polymer*, 52(10):2310–2318, May 2011.

[11] J. P. Salvetat, J. M. Bonnard, N.H. Thomson, A.J. Kuklik, L. Forro, W. Benoit, and L. Zuppiroli. Mechanical properties of carbon nanotubes. *Applied Physics A Materials Science and Processing*, 69(3):255–260, July 1999.

[12] M. Sanchez-Garcia, J. Lagaron, and S. Hoa. Effect of addition of carbon nanofibers and carbon nanotubes on properties of thermoplastic biopolymers. *Composites Science and Technology*, 70(7):1095–1105, July 2010.

[13] Z. Spitalsky, D. Tasis, K. Papagelis, and C. Galiotis. Carbon nanotubepolymer composites: Chemistry, processing, mechanical and electrical properties. *Progress in Polymer Science*, 35(3):357–401, March 2010.

[14] M. Moniruzzaman and K. Winey. Polymer nanocomposites containing carbon nanotubes. *Macromolecules*, 39(16):5194–5205, July 2006.

[15] J. Salvetat, A. Kulik, J. Bonard, G. Briggs, T. Stockli, K. Metenier, S. Bonnamy, F. Beguin, N. Burnham, and L. Forro. Elastic modulus of ordered and disordered multiwalled carbon nanotubes. *Advanced Materials*, 11(2):161–165, 1999.

[16] A. Kothari, K. Jian, J. Rankin, and B. Sheldon. Comparison between carbon nanotube and carbon nanofiber reinforcements in amorphous silicon nitride coatings. *Journal of the American Ceramic Society*, 91(8):2743–2746, August 2008.

[17] R. Andrews, D. Jacques, M. Minot, and T. Rantell. Fabrication of carbon multiwall nanotube/polymer composites by shear mixing. *Macromolecular Materials and Engineering*, 287(6):395–403, 2002.

[18] D. Tasis, N. Tagmatarchis, V. Georgakilas, and M. Prato. Soluble carbon nanotubes. *Chemistry-A European Journal*, 9(17):4000–4008, September 2003.

[19] D. Tasis, N. Tagmatarchis, A. Bianco, and M. Prato. Chemistry of carbon nanotube. *Chemical Reviews*, 106:1105–1136, 2006.

[20] J. Sandler, P. Werner, M. Shaffer, V. Demchuck, V. Altsadt, and A. Windle. Carbon-nanofibre-reinforced poly(ether ether ketone) composites. *Composites Part A: Applied Science and Manufacturing*, 33(8):1033–1039, August 2002.

[21] T. Kashiwagi, E. Grulke, J. Hilding, R. Harris, W. Awad, and J. Douglas. Thermal degradation and flammability properties of poly(propylene)/carbon nanotube composites. *Macromolecular Rapid Communication*, 23(13):761–765, September 2002.

[22] J. Cho and D. Paul. Nylon 6 nanocomposites by melt mixing. *Polymer*, 42(3):1083–1094, February 2001.

[23] O. Carneiro, J. Covas, C. Bernardo, G. Caldeira, D. Hattum, J. Ting, R. Alig, and M. Lake. Production and assessment of polycarbonate composites reinforced with vapour-grown carbon fibres. *Composites Science and Technology*, 58(3–4):401–407, March-April 1998.

[24] E. Bekyarova, E. Thostenson, A. Yu, H. Kim, J. Gao, J. Tang, H. Hahn, T. Chou, M. Itkis, and R. Haddon. Multiscale carbon nanotube-carbon fiber reinforcement for advanced epoxy composites. *Langmuir*, 23(7):3970–3974, February 2007.

[25] K. Lozano and E. V. Barrera. Nanofiber-reinforced thermoplastic composites. I. thermoanalytical and mechanical analyses. *Journal of Applied Polymer Science*, 79(1):125–133, January 2001.

[26] S. Lee, O. Choi, W. Lee, J. Yi, B. Kim, J. Byun, M. Yoon, H. Fong, E. Thostenson, and T. Chou. Processing and characterization of multi-scale hybrid composites reinforced with nanoscale carbon reinforcements and carbon fibers. *Composites Part A: Applied Science and Manufacturing*, 42(4):337–344, April 2011.

[27] G. Broza, M. Kwiatkowska, Z. Roslaniec, and K. Schulte. Processing and assessment of poly(butylene terephthalate) nanocomposites reinforced with oxidized single wall carbon nanotubes. *Polymer*, 46(16):5860–5867, July 2005.

[28] J. Zeng, B. Saltysiak, W. Johnson, D. Schiraldi, and S. Kumar. Processing and properties of poly(methyl methacrylate)/carbon nano fiber composites. *Composites Part B: Engineering*, 35(2):173–178, March 2004.

[29] S. Yesil, O. Koysuren, and G. Bayram. Effect of microfiber reinforcement on the morphology, electrical, and mechanical properties of the polyethylene/poly(ethylene terephthalate)/carbon nanotube composites. *Polymer Engineering & Science*, 50(11):2093–2105, November 2010.

[30] D. Zhang, D. Arola, and M. Luo. Characterization of mechanical properties on the meso-scale with digital image correlation. In *2004 SEM X International Congress and Exposition on Experimental and Applied Mechanics*. Society for Experimental Mechanics, 2004.

[31] A. Gershon and H. Bruck. Multiscale mechanical behavior of hierarchically-structured polymer composites. In *SEM Annual Conference*, Albuquerque, New Mexico, June 2009. Society for Experimental Mechanics.

[32] H. Bruck and A. Gershon. Dynamic and static mechancial behavior of hierarchically-structured and nano-structured polymer composites. In *XIth International Congress and Exposition*, Orlando, Florida, June 2008. Society for Experimental Mechanics.

[33] S. Berber, Y. Kwon, and D. Tomanek. Unusually high thermal conductivity of carbon nanotubes. *Physical Review Letters*, 84(20):4613–4616, May 2000.

[34] J. Che, T. Cagin, and W. Goddard. Thermal conductivity of carbon nanotubes. *Nanotechnology*, 11(2):65–69, June 2000.

[35] F. Incropera, D. Dewitt, T. Bergman, and A. Lavine. *Fundametals of Heat and Mass Transfer*. John Wiley Sons, Inc., Danvers, MA, 2007.

[36] M. Bratcher, B. Gersten, H. Ji, and J. Mays. Study in the dispersion of carbon nanotubes. *Materials Research Society Proceedings*, 706, 2001.

[37] M.Bryning, D. Milkie, M. Islam, J. Kikkawa, and A. Yodh. Thermal conductivity and interfacial resistance in single-wall carbon nanotube epoxy composites. *Applied Physics Letters*, 87(16):16909–1–16909–3, October 2003.

[38] J. Hone, M. C. Llaguno, A. T. Johnson, B. Batlogg, Z. Benes, and J.E. Fischer. Thermal properties of carbon nanotubes and nanotube-based materials. *Applied Physics A Materials Science and Processing*, 74(3):339–343, June 2002.

[39] J. Hone, M. Whitney, C. Piskoti, and A. Zettl. Thermal conductivity of single-walled carbon nanotubes. *Physical Review B*, 59(4):2514–2516, January 1999.

[40] S. Agarwal, M. Masud, K. Khan, and R. Gupta. Thermal conductivity of polymer nanocomposites made with carbon nanofibers. *Polymer Engineering and Science*, 48(12):2474–2481, October 2008.

[41] S. Frusteri, V. Leonardi, S. Vasta, and G. Restuccia. Thermal conductivity measurement of a pcm based storage system containing carbon fibers. *Applied Thermal Engineering*, 25(11–12):1623–1633, August 2005.

[42] T. Zhou, X. Wang, G. Mingyuan, and X. Liu. Study of the thermal conduction mechanism of nano-sic/dgeba/emi-2,4 composites. *Polymer*, 49(21):4666–4672, October 2008.

[43] F. Gojny, M. Wichmann, B. Fiedler, I. Kinloch, W. Bauhofer, A. Windle, and K. Schulte. Evaluation and identification of electrical and thermal conduction mechanisms in carbon nanotube/epoxy composites. *Polymer*, 47(6):2036–2045, March 2006.

[44] Y. Kim, S. Kamio, T. Tajiri, T. Hayashi, S. Song, M. Endo, M. Terrones, and M. S. Dresselhaus. Enhanced thermal conductivity of carbon fiber/phenolic resin composites by the introduction of carbon nanotubes. *Applied Physics Letters*, 90(9):093125–1–093125–3, March 2007.

[45] C. Guthy, F. Du, S. Brand, K. Winey, and J. Fischer. Thermal conductivity of single-walled carbon nanotube/pmma nanocomposites. *Journal of Heat Transfer*, 129(8):1096–1099, August 2007.

[46] O. Shenderovaa, T. Tyler, G. Cunningham, M. Raya J. Walsh, M. Casulli, S. Hens, G. McGuire, V. Kuznetsov, and S. Lipa. Nanodiamond and onion-like carbon polymer nanocomposites. *Diamond and Related Materials*, 16(4–7):1213–1217, April-July 2007.

[47] L. Pedroni, M. Soto-Oviedo, J. Rosolen, M. Felisberti, and A. Nogueira. Conductivity and mechanical properties of composites based on mwcnts and styrene-butadiene-styrene block copolymers. *Journal of Applied Polymer Science*, 112(6):3241–3248, June 2009.

[48] J. Bai and A. Allaoui. Effect of the length and the aggregate size of mwnts on the improvement efficiency of the mechanical and electrical properties of nanocomposites experimental investigation. *Composites Part A: Applied Science and Manufacturing*, 34(8):689–694, August 2003.

[49] G. Chen, Y. Li, and H. Shimizu. Ultrahigh-shear processing for the preparation of polymer/carbon nanotube composites. *Carbon*, 45(12):2334–2340, October 2007.

[50] J. Vera-Agullo, A. Glria-Pereira, H. Varela-Rizo, J. Gonzalez, and I. Martin-Gullon. Comparative study of the dispersion and functional properties of multiwall carbon nanotubes and helical-ribbon carbon nanofibers in polyester nanocomposites. *Composites Science and Technology*, 69(10):1521–1532, August 2009.

[51] J. Gao, G. Walsh, D. Bigio, R. Briber, and M. Wetzel. Residence time distributions model for twin-screw extruders. *AIChE Journal*, 45(12):2541–2549, December 1999.

[52] J. Gao, G. Walsh, D. Bigio, R. Briber, and M. Wetzel. Mean residence time analysis for twin-screw extruders. *Polymer Engineering and Science*, 40(1):227–237, January 2000.

[53] M. Rong, M. Zhang, Y. Zheng, H. Zeng, R. Walter, and K. Friedrich. Structure-property relationships of irradiation grafted nano-inorganic particle filled polypropylene composites nanotube composites. *Polymer*, 42(1):167–183, January 2001.

[54] X. Gong, J. Liu, S. Baskaran, R. Voise, and J. Young. Surfactant-assisted processing of carbon nanotube/ polymer composites. *Chemistry of Materials*, 12(4):1049–1052, March 2000.

[55] R. Ruoff and D. Lorents. Elastic modulus of ordered and disordered multiwalled carbon nanotubes. *Carbon*, 33(7):925–930, February 1995.

[56] F. Du, J. Fischer, and K. Winey. Coagulation method for preparing single-walled carbon nanotube/poly(methyl methacrylate) composites and their modulus, electrical conductivity, and thermal stability. *Journal of Polymer Science: Part B: Polymer Physics*, 41(24):3333–3338, November 2003.

[57] E. Thostenson and T. Chou. Aligned multi-walled carbon nanotube-reinforced composites: processing and mechanical characterization. *Journal of Physics D: Applied Physics*, 35(16):L77–L80, August 2002.

[58] R. Kuriger, M. Alam, D. Anderson, and R. Jacobsen. Processing and characterization of aligned vapor grown carbon fiber reinforced polypropylene. *Composites Part A: Applied Science and Manufacturing*, 33(1):53–62, January 2002.

[59] P. Potschke, A. Bhattacharyya, and A. Janke. Carbon nanotube-filled polycarbonate composites produced by melt mixing and their use in blends with polyethylene. *Carbon*, 42(5–6):965–969, January 2004.

[60] D. Acierno, P. Scarfato, E. Amendola, G. Nocerino, and G. Costa. Preparation and characterization of pbt nanocomposites compounded with different montmorillonites. *Polymer Engineering & Science*, 44(6):1012–1018, June 2004.

[61] A. Arostegui and J. Nazabal. Compatibilization of a poly(butylene terephthalate)/poly(ethylene octene) copolymer blends with different amounts of an epoxy resin. *Journal of Applied Polymer Science*, 91(1):260–269, January 2004.

[62] N. Manabe and Y. Yokota. The method for analyzing anhydride formed in poly(butylene terephthalate) (pbt) during thermal and photo-degradation processes and applications for evaluation of the extent of degradation. *Journal of Applied Polymer Science*, 69(2):183–190, July 2000.

[63] Steinwall Inc. *Beginning guide to thermoplastic injection molding*. Steinwall Scientific, Minneapolis, MN, 2009.

[64] New Era Pump Systems Inc. *NE-1000 Family of Programmable Syringe Pumps*. New Era Pump Systems Inc., Farmingdale, NY, 12 v3.9 edition, 2011.

[65] ASTM Standard D638. *Standard Test Method for Tensile Properties of Plastics*. The American Society for Testing and Materials, West Conshohocken, PA, 2010.

[66] CALCE Electronic Products and Systems Center Standard Operating Procedures. *MicroFlash RT-Thermal Properties Measure System*. The Center for Advanced Life Cycle Engineering, College Park, MD, 2007.

[67] H. Lee. *Theraml Diffusivity in Layered And Dispersed Composites*. PhD Thesis, Purdue University, West Lafayette, IN, May 1975.

[68] Holometrix, Bedford, MA. *Operation Manual Holometrix Model Microflash*.

[69] H. Giles Jr., J. Wagner Jr., and E. Mount III. *Extrusion: The Definitive Processing Guide and Handbook*. William Andrews, Inc., Norwich, NY, 2005.

[70] W. Voigt. Uber die beziehung zwischen den beiden elastizitatskonstanten isotroper korper. *Annalen der Physik*, 274(12):573–587, 1889.

[71] A. Reuss and Z. Angrew. Berechnung der fliessgrenze von mischkristallen auf grund der plastizitatsbedingung fur einkristalle. *ZAMM Journal of Applied Mathematics and Mechanics*, 9(1):49–58, 1929.

[72] A. Upadhyay and R. Singh. Prediction of effective elastic modulus of biphasic composite materials. *Modern Mechanical Engineering*, 2(1):6–13, February 2012.

[73] C. Wong and R. Bollampally. Thermal conductivity, elastic modulus, and coefficient of thermal expansion of polymer composites filled with ceramic particles for electronic packaging. *Journal of Applied Polymer Science*, 74(14):3396–3403, December 1999.

[74] G. Kalaprasad, K. Joseph, S. Thomas, and C. Pavithran. Theoretical modelling of tensile properties of short sisal fibre-reinforced low-density polyethylene composites. *Journal of Material Science*, 32(16):4261–4267, 1997.

[75] H.L. Cox. The elasticity and strength of paper and other fibrous materials. *British Journal of Applied Physics*, 3(3):72–79, March 1952.

[76] H. Krenchel. *Fibre Reinforcement*. Akademisk Forlag, Copenhagen, 1964.

[77] J. Thomason and M. Vlug. Influence of fibre length and concentration on the properties of glass fibre-reinforced polypropylene: 1. tensile and flexural modulus. *Composites Part A: Applied Science and Manufacturing*, 27(6):477–484, 1996.

[78] R. Progelhof, J. Throne, and R. Ruetsch. Methods for predicting the thermal conductivity of composite systems: A review. *Polymer Engineering and Science*, 16(9):615–625, September 1976.

[79] L.E. Nielsen. The thermal and electrical conductivity of two-phase systems. *Industrial Engineering Chemical Fundamentals*, 13(1):17–20, February 1974.